

# TOOLS FOR PREDICTION OF ENVIRONMENTAL PROPERTIES OF CHEMICALS BY QSAR/QSPR WITHIN REACH

AN APPLICABILITY DOMAIN PERSPECTIVE

---

PhD dissertation by:

SAHIGARA FAIZAN ABDULRAZAK



DEPARTMENT OF ENVIRONMENTAL SCIENCES  
UNIVERSITY OF MILANO-BICOCCA

ACADEMIC YEAR: 2012/2013  
PHD ENROLMENT CYCLE: XXV



*TOOLS FOR PREDICTION OF ENVIRONMENTAL  
PROPERTIES OF CHEMICALS BY QSAR/QSPR WITHIN REACH*

*AN APPLICABILITY DOMAIN PERSPECTIVE*

SAHIGARA FAIZAN ABDULRAZAK

TUTOR: PROF. ROBERTO TODESCHINI

CO-TUTORS: DR. VIVIANA CONSONNI  
DR. DAVIDE BALLABIO



# Preface

This research was funded within the Marie Curie Initial Training Network - Environmental ChemOinformatics (ECO-ITN). Aimed at developing the careers for Environmental Cheminformatians, this Initial Training Network (ITN) has been mainly implemented to provide advanced training in both environmental and computational approaches. This ITN is functioning within several research groups located in 5 EU countries over a period of four years until September 2013. Additionally, external collaborations with other research networks and industrial partners open doors to new future opportunities for the ECO participants. Internal trainings at other ECO partner groups facilitate a better way of knowledge exchange within the training network while the flexibility to opt for external collaborators allow participants to take their research a step ahead on a global level.

One of the important considerations within the new European legislation on chemicals and their safe use REACH (Registration, Evaluation, Authorization and restriction of CHemicals) is to minimize the number of animal testing by replacing them with suitable alternatives such as in-silico methods, wherever possible. The primary goals of ECO-ITN can be fits well with these considerations since the trainees within this project are exposed to several state-of-the-art computational approaches which can then be applied to towards the development of novel automated strategies for risk assessment of chemicals.

## *Thesis outline*

As the title suggests, this work is mainly focussed at providing an Applicability Domain (AD) perspective towards the QSAR/QSPR models predicting environmental properties relevant to REACH regulations. A well-defined AD is one of the prerequisites for a predictive model before it is

considered as validated for regulatory purposes. The main idea behind compiling this thesis is to provide the reader with all the major insights towards defining a model's AD where it can reliably predict the modelled endpoint for new test samples.

The thesis contents are divided into three major parts summarized as follows:

The first section is an introductory part which guides through the scope of validated QSARs within REACH. A regulatory insight is presented towards the consideration of QSAR methodologies as one of the alternatives to animal testing and the possibility to use its reliable predictions directly or include them as supplementary information within a Weight of Evidence approach. The major principles towards QSAR validation are briefly discussed with a particular attention towards the prerequisite to have a well-defined AD for reliable predictions.

The second section initially discusses several classical approaches proposed in the existing literature towards defining the AD of QSAR models in its descriptor space. In theory, all these approaches attempted to characterize the interpolation space where a model is capable of making reliable predictions. The major highlights for each approach include a) the basic strategy followed to characterize the interpolation space and b) the major advantages and/or limitations in addressing the model's AD. Later, a novel AD approach based on the classical  $k$ -Nearest Neighbours principle is introduced which also features the major highlight of the thesis. This discussion includes the motivation behind proposing the new approach followed by the description of the underlying algorithm. Finally, an AD perspective is provided towards the application of a novel pseudo-distance called *Locally-centred Mahalanobis distance* for outlier detection. The results derived from this newly proposed outlier detection approach provides an excellent platform to better understand the impact of extreme training outliers on the defined AD using different AD approaches as well as to verify if the test samples detected as outliers in the training space could hint for them being unreliably predicted and thus, likely to get excluded from the model's AD.

The final section of this thesis work discusses the results derived implementing previously introduced classical and two novel AD approaches on several QSAR models from the existing literature. Some of these models predicting significant environmental properties were intended to contribute towards REACH implementation and thus, served as ideal case studies to better evaluate for their AD. The performance of both the novel AD approaches was evaluated with respect to the classical methodologies. Moreover, presence of consensus test samples excluded from the model's AD with different approaches, further allowed to reflect upon the similar trends within the underlying algorithms and also added to the confidence in rendering those test samples being unreliably predicted.

Last but not the least, general conclusions and future prospects for this thesis work were briefly discussed. All the relevant research articles accepted by the scientific journals were listed and reported in the appendix.

# Acknowledgements

Big thanks to the entire Milano Chemometrics and QSAR Research group. Undoubtedly, first of all I would like to thank Prof. Roberto Todeschini for believing in my abilities and making me a part of his research group. There was so much I learnt from you in the past three years and there is much more beyond this to explore. At this point, I would like extend my thanks to Dr. Viviana Consonni and Dr. Davide Ballabio, my co-tutors who always made sure that my research was being carried out in a right direction. Viviana, thanks for looking after all the bureaucratic aspects and other issues at the university allowing me to focus on my research tasks. Davide, your valuable suggestions and hints made my life easier at work. Andrea and Alberto, thanks for always being there for me whenever I needed your assistance and suggestions. Kamel, it had been a pleasure working with you, sharing the same lab as well as the project. Matteo, your friendly nature and passion to help was very much appreciated. Francesca, the newest and youngest member in the group, you had been more like a friend than a colleague to me. Thanks to the administrative staff at the University of Milano-Bicocca for looking after my reimbursements and other financial matters.

I would like to take this opportunity to thank the Marie Curie Actions for funding my research within the Environmental Chemoinformatics Initial Training Network. ECO project manager Eva Schlosser, thanks for keeping us always updated and for your support and guidance whenever needed. A big thanks to the research groups of Dr. Igor Tetko and Prof. Ian Nicholls for their wonderful hospitality during my internships. My special thanks to the entire CEHTRA family, most importantly Dr. Paul Thomas who gave wings to my career life. Carine, Carole, Rija and Julien, it had been a great pleasure working with you as a part of my industrial training in Lyon and keeping in touch since then. Special thanks to Andrew Worth for his valuable suggestions and guidance. Your work on applicability domain helped me throughout my doctoral research. Prof. Marco Vighi, it was a pleasure to know your ideas and opinions about QSARs. I appreciated your guidance whenever needed. Stefan Brandmaier, you had been an amazing colleague,



collaborator and a fantastic friend! Thanks for making me a part of your research article.

My special thanks to Primina Monga and the Brignolis for their wonderful hospitality and affection. In the past three years, I never felt I was away from home. Let me take this opportunity to thank the Lombardos for their unconditional love and help in improving on my Italian skills. Gianfranco, learning Golf from you was so much fun. You and your entire family, especially Anna Maria always made me feel so proud.

Eva or shall I say Evanthia, you had been the biggest support as a colleague and as a friend, through most of my doctoral degree. Despite of the several disagreements and meaningless fights we had, our friendship never changed. My best friends Shruti and Vinaya, your presence in my life makes me feel complete and precious. Domenico, officially my first Italian friend, thanks to you and your family for making me feel at home since the day I arrived in Milan. Frantonio, Pierangela and Emmanuelle, thanks for your support and guidance. I thoroughly enjoyed your company and the good times we spent together. Alberto, thanks for dragging me along to the most amazing restaurants and gelato shops I have ever visited in town. Giorgio, discovering the city of Milan could not be as interesting without your company. I really enjoyed visiting several interesting places and always appreciated your valuable suggestions. Aggeliki, you had been a big support in all good and bad times.

Ivan and Manuela, since the day I met both of you, lunch hours had been amongst the most amazing moments at the university campus. Anu, it had been a pleasure to meet you. Thanks for always motivating me to accomplish my thesis goals. Paola, Simone and Ivan, thanks for your company in making the weekends so much fun. Jessica and Jessica, Cesare and Matteo, thanks for your company, it means a lot to me.

# Contents

<b>PART I. BACKGROUND</b>	<b>Page</b>
<b>1. Introduction</b>	
1.1 Scope of QSARs within REACH framework.....	1
1.2 QSAR predictions may be reliable yet restricted.....	2
1.3 Validated QSARs for their regulatory acceptance.....	4
1.4 Applicability domain for reliable predictions.....	6
 <b>PART II. THEORY</b>	
<b>2. Classical ways of characterizing the interpolation space</b>	
2.1 An introduction to the AD methodologies.....	9
2.2 Range-based and Geometric methods.....	11
2.3 Distance-based methods.....	14
2.4 Probability Density Function methods.....	21
 <b>3. A novel k-Nearest Neighbours based Applicability Domain evaluation</b>	
3.1 Background and Motivation.....	32
3.2 Methodology.....	34
 <b>4. Outlier detection from an Applicability Domain perspective</b>	
4.1 Introduction and the scope of this study.....	45
4.3 Definition of the Locally-Centred Mahalanobis distance.....	48
4.4 Remoteness and Isolation degree plot .....	51
4.5 Implementing the novel approach towards AD evaluation.....	55
 <b>PART III. APPLICATIONS</b>	
<b>5. Case studies</b>	
5.1 An overview of the case studies.....	59
5.2 Assessing reliability in derived results.....	60
5.3 CAESAR Bioconcentration Factor models.....	63
5.4 QSAR model for soil adsorption coefficient <i>K<sub>oc</sub></i> .....	73

# Contents

<i>5.5 OH tropospheric degradation model.....</i>	<i>79</i>
<i>5.6 Ready biodegradability of chemicals.....</i>	<i>86</i>
<b>General conclusions and future prospects.....</b>	<b>102</b>
<b>List of Figures.....</b>	<b>104</b>
<b>List of Tables.....</b>	<b>107</b>
<b>Bibliography.....</b>	<b>109</b>
<b>List of Publications.....</b>	<b>114</b>
<b>Appendix</b>	

*PART I*



*BACKGROUND*

# Chapter 1

## *Introduction*

As an alternative to animal testing, provisions for Quantitative Structure Activity Relationship (QSAR) predictions towards regulatory purposes are well-discussed and documented within the framework of a new European Community regulation for the safe use of chemicals – REACH. This chapter discusses the regulatory perspective towards the acceptance of QSARs and introduces the major principles for their validation, paying particular attention towards defining their Applicability Domain in order to differentiate the reliable predictions from extrapolations.

### *1.1 Scope of QSARs within REACH framework*

REACH is a European legislation on chemicals that came into force in 2007. It is mainly focussed on the risk assessment of chemicals for their safe use [1]. As a part of this regulation, a major responsibility lies on the industry towards risk management by providing all the necessary information about the chemicals and their properties. The outcome of REACH is mainly aimed at enhancing the human health protection and minimizing the environmental hazards by the safer handling of chemicals as well as replacement of hazardous chemicals with suitable alternatives [2,3].

One of the major objectives of implementing REACH is to minimize the animal testing. To achieve this, usefulness of non-testing approaches has been highlighted and as a result, REACH encourages the use of cost-effective methods like QSARs, Read-Across approaches and expert systems.

The possibility to train QSARs based on high quality and reliable data can allow evaluation of several physicochemical and biological properties for various chemicals relevant to REACH. Moreover, the results derived from QSARs can also be used as a part of Weight of Evidence (WoE) approach. Thus, QSARs and other relevant approaches can be significant for REACH in filling the data gaps prevailing towards the evaluation of several chemical properties. Depending on the reliability in their predictions, the QSAR models can directly replace the test data otherwise can be used as supplementary information to improve the transparency in evaluations [2,3].

QSARs are based on the principle that similar chemical structures can lead to similar biological activities. In general, QSARs can be thought as a combination of data analysis and statistical methods that are aimed towards finding a trend within the descriptor values of chemicals, which in turn can explain the corresponding trend in their biological activities [4]. A basic workflow of a QSAR includes data collection and pretreatment, followed by implementation of a model development technique (for instance, Linear Regression, Artificial Neural Network and so on) and finally evaluating the model performance through internal and external validation.

Enormous experimentally derived data for several significant endpoints is readily available from the existing literature. This data collection can be an excellent input to train models towards predicting several physicochemical and biological activities for new test compounds. This idea was realised in the past decades and consequently, several QSAR models emerged since then predicting different endpoints. From time to time, more efficient algorithms were proposed towards model development, thus a range of different methodologies were in place from a Simple Linear Regression to Artificial Neural Networks.

### *1.2 QSAR predictions may be reliable yet restricted*

In theory, applicability of QSAR models irrespective of their predictive reliability is limited. These limitations of a model can be referred to its structural domain and the response space which defines the scope of that model [5]. Usually, the predictive models are trained using a limited set of

chemical structures. The level of structural diversity reflected within a training set strongly relies on the information contained for instance, functional groups present, chemical categories covered and so on. For instance, a QSAR model trained using only aromatic structures may not be useful in predicting a test set of aliphatic structures. The resulting predictions will be unreliable as they will be beyond the scope of that model. Thus, it is reasonable to expect that the scope of local models is limited, though it shouldn't be confused with their predictive ability.

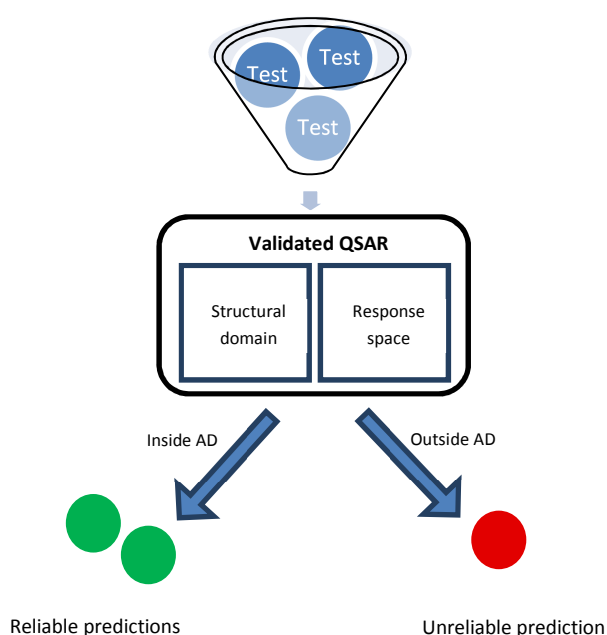


**Figure 1.1** *Evaluating the reliability in prediction for new test samples*

It is crucial that a model is used for predicting only those test samples that are structurally similar to the samples used for training purpose [5-9]. It makes sense because structural similarity implies similarity in the descriptor values, which in turn can fit the trend in deriving a modelled endpoint. In other words, test samples must fall within the structural domain described by its descriptor space. Since, a model is usually aimed to identify a reliable trend between the descriptor values and the modelled endpoint, the

prediction of a structurally similar test sample is likely to fall within the response domain of the training samples. Figure 1.1 informs that test samples satisfying the limitations of a model within its structural domain and response space fall within the Applicability Domain (AD) and are thus, associated with a reliable prediction. On the contrary, those excluded from the AD where unreliably predicted.

### *1.3 Validated QSARs for their regulatory acceptance*

As discussed in the earlier section, QSARs can be thought amongst one of the promising non-testing approaches towards regulatory use. However, to ensure that the QSAR predictions are reliable, several conditions are necessary to be met by such predictive models. The regulatory authorities need to make sure that a QSAR model was strictly validated before being applied for regulatory assessment of chemicals. Before a QSAR model can be accepted for regulatory use, its validity has to be demonstrated, the test sample being predicted has to fall within the AD of that model and reliability in the modelling approach has to be well-documented in order to provide the transparency in the underlying algorithm.

No formal adoption procedure is suggested for QSARs within REACH. Thus, information provided to the regulatory authorities towards demonstrating the model's validity and reliability in its predictive ability will be evaluated in deciding upon the adequacy of a model and its predictions for regulatory acceptance [3]. To address validation procedure, REACH referred to the principles for QSAR validation adopted by OECD in 2004. These principles are internationally agreed and each of them highlights several key aspects relevant to the regulatory acceptance of QSAR models [3,5-10].

For its regulatory consideration, a validated QSAR must be associated with these principles listed in the following order [3,10]:



### a) A defined endpoint

As several experimental methods and conditions are feasible towards prediction of a given physicochemical property or a biological effect, the first OECD principle provides information about the endpoint being modelled.

### b) An unambiguous algorithm

As several modelling approaches have been proposed from time to time, the second principle tries to bring transparency in the algorithm used towards model development.

### c) A defined domain of applicability

In theory, the applicability of a QSAR model is limited to the chemical that are structurally similar to those used to train that model. The third principle tries to highlight this feature and informs about the limitations of a proposed model in its structural domain and response space.

### d) Appropriate measures of goodness-of-fit, robustness and predictivity

To better evaluate for the model's performance, it is essential to understand if it's robust, is not overfitted and is able to reliably predict the modelled endpoint for external test samples. To achieve this, the fourth principle for model validation provides with all the necessary information derived performing an internal and external validation using the training and an external test set, respectively.

### e) A mechanistic interpretation, if possible

The mechanistic relevance between the set of descriptors used towards model development and the endpoint being modelled, can further add to the confidence in a model, however, it is also understandable that deriving such mechanistic interpretation is not always possible and thus, the fifth principle recommends a model developer to provide mechanistic basis for the descriptors and its relevance to the modelled endpoint, whenever possible.

### *1.4 Applicability domain for reliable predictions*

As discussed earlier, the third principle of QSAR validation deals with defining model's AD. It is one of the prerequisites to have a well-defined AD before a model can be considered as validated. Several approaches have been discussed from time to time in the existing literature towards defining a model's AD and an entire section of this thesis is dedicated discussing these methodologies [5].

In theory, all these approaches attempted to characterize the interpolation space for reliable predictions using different algorithms [6,11-13]. The efficiency of a strategy can be estimated based on its ability to maximize the retention of reliable test predictions. Depending on the nature of endpoint being modelled, QSAR models can be divided into two major categories, regression and classification models. Regression models are implemented for quantitative endpoints, such as LC50 in aquatic toxicity, Bioconcentration factor and so on. On the other hand, classification models deal with endpoints of qualitative nature, for instance if a test molecule is ready biodegradable or not ready biodegradable, is a carcinogen or non-carcinogen. In a case of regression model, the reliability measure is quantitative where a lowest prediction error is desirable, while in the case of classification models, the underlying algorithm tries to achieve reliability by maximizing the allocation of test molecules to their correct classes.

If a test molecule is associated with a very high prediction error or is allocated to a wrong class, the reliability in its prediction decreases. There can be several reasons behind deriving an unreliable prediction for instance, the new test molecule contains some specific functional groups that are unknown to the training space, the test molecule reacts with a specific mode of action which cannot be described well with the set of descriptors used for training that model or there are no structurally similar training molecules identified for a given test molecule. There may be several other explanations behind deriving an unreliable prediction; however, most of them converge to a single conclusion that is the test molecule could be beyond the scope of that model.

One of the major concerns about QSARs from a regulatory perspective is the reliability in their predictions. A QSAR model with a defined a domain of applicability makes predictions with a defined level of reliability. When this model is applied to a new set of test molecules, the resulting predictions that fall within its AD can be associated with that given level of reliability. In other words, there exists a trade-off between the applicability of a model and the reliability in its predictions. Thus, from a regulatory perspective, a prediction falling outside the model's AD is associated with a lower level of reliability. A well-defined AD can allow the regulatory authorities to better evaluate the structural domain in which a model can predict reliably and prevents from extrapolating beyond the scope of that model [2-3].

There are several ways in which a model's AD could be addressed. For instance, in a model's descriptor space, the defined AD can be thought to be restricted to the test molecules with relevant descriptor values; in a mechanistic domain the defined AD can be limited to the test molecules acting based on the same mode of action represented by the training set molecules; in a metabolic domain, the AD can be defined based on the possibilities of the molecules to undergo transformation or get metabolized [2-3]. With growing awareness about the QSAR validation for its regulatory acceptance, the development and implementation of different AD strategies has become one of the promising areas of research in the field of QSAR in the current years.

From time to time, more efficient approaches have been proposed overcoming several of the prevailing issues, however until now, no strategy towards defining a model's AD has been officially accepted or recognized [14]. Nevertheless, emerging awareness towards non-testing approaches is likely to keep the QSARs in focus. A joint effort between regulators, industry and researchers can shape a better future of such alternative methods

*PART II*



*THEORY*

### *Classical ways of characterizing the interpolation space*

This chapter discusses several classical approaches towards defining the Applicability Domain of a QSAR model in its descriptor space. The major focus is given on the methodology used to characterize the interpolation space where the model is expected to make reliable predictions. Most of the discussed approaches were associated with their own advantages and limitations. Their implementation on a two-dimensional simulated dataset and the resulting contour plots allowed a better understanding of their defined domain of applicability.

#### *2.1 An introduction to the AD methodologies*

Characterization of the interpolation space is very significant to define the AD for a given QSAR model. This characterised space can be associated with reliable predictions derived from the model and helps the user to evaluate the reliability in prediction for a given query molecule. Depending upon how efficiently the interpolation space is defined, the clarity and transparency in distinguishing quality predictions from extrapolations also improves. Several AD approaches have been already proposed and primarily they all differ in the way how they characterize the interpolation space defined by the descriptors used. They can be classified into following four major categories based on the methodology used for interpolation space characterization in the model's descriptor space: range-based methods, geometric methods, distance-based methods and Probability Density Distribution based methods [5-6,11-13].

This chapter discusses all the above-mentioned classical approaches which were then implemented on the two-dimensional simulated datasets shown in Figures 2.1 and 2.2.

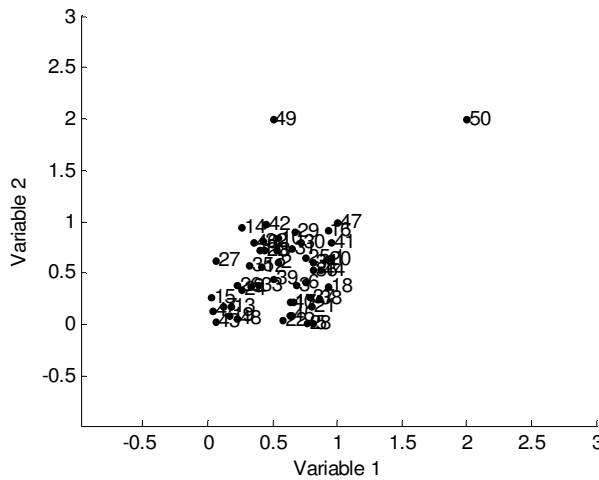


**Figure 2.1** Scatter plot for the first simulated dataset

As shown in Figure 2.1, the first simulated dataset consists of a cluster with 48 training samples and 2 isolated samples (49 and 50) which were localized distant from each other as well as the cluster.

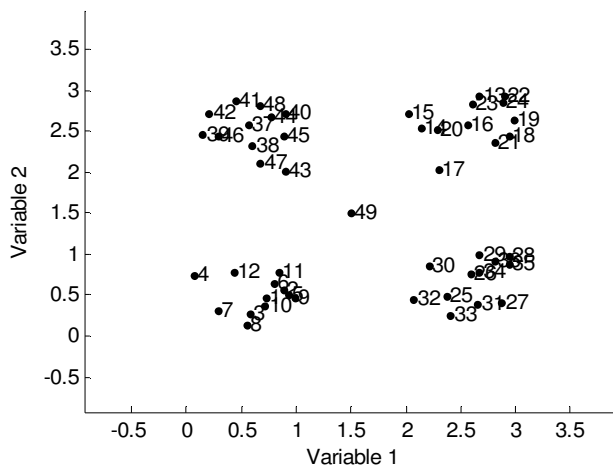


**Figure 2.2** Scatter plot for the second simulated dataset

As shown in Figure 2.2, the second simulated dataset comprised of four clusters of samples and an isolated sample (49) between them.

The AD defined implementing each of these approaches was visualized using contour plots for the simulated datasets derived projecting several data points enough to fill its training space. These plots allowed a better understanding of the features relevant to the interpolation space characterized with these existing approaches and wherever possible, also reflected the prevailing drawbacks in their methodologies.

### *2.2 Range-based and Geometric Methods*

These are considered as the simplest methods to characterize a model's interpolation space.

#### *2.2.1 Bounding Box*

This approach considers the range of individual descriptors used to build the model. Assuming a uniform distribution, resulting domain of applicability can be imagined as a Bounding Box which is a  $p$ -dimensional hyper-rectangle defined on the basis of maximum and minimum values of each descriptor used to build the model. The sides of this hyper-rectangle are parallel with respect to the coordinate axes. However, there are several drawbacks associated with this approach: since only descriptor ranges are taken into consideration, empty regions in the interpolation space cannot be identified and also the correlation between descriptors cannot be taken into account [11,12].

Figure 2.3 provides with the contour plot implementing Bounding Box on the simulated datasets introduced earlier. As shown in the Figure 2.3a, the characterized interpolation space accounts for a considerable empty space between the cluster and two isolated samples.

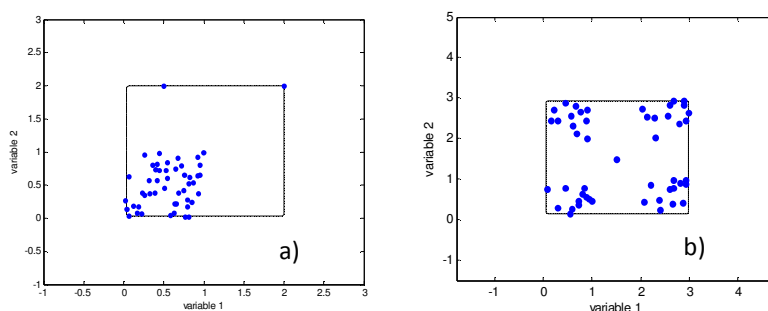


**Figure 2.3** Contour plots for the simulated datasets derived implementing Bounding Box. First simulated dataset (2.3a) and second simulated dataset (2.3b)

This implies that the presence of one or more outliers in the training extremities can have a huge impact on the defined AD, which is not desirable. Figure 2.3b provides with the contour plot for the second simulated dataset using Bounding Box. As expected, empty regions between the clusters were considered within the AD as a result of which the isolated sample (49) was rendered as reliable.

### 2.2.2 PCA Bounding Box

Principal Component Analysis (PCA) transforms the original data into a new coordinate system by the rotation of axes, such that the new axes are orthogonal to each other and aligned in the direction having maximum variance within the data. These new axes are called Principal Components (PCs) representing the maximum variance within the dataset [15]. A M-dimensional hyper-rectangle (where M is the number of significant components) is obtained similar to the previous approach by considering the projection of the molecules in the principal component space, however taking into account the maximum and minimum values for the PCs. The implementation of Bounding Box with PCA can overcome the problem of correlation between descriptors but empty regions within the interpolation space still remains an issue [11-13]. Moreover, selection of appropriate number of components is significant to implement this approach. For all the case studies discussed in this thesis, only those PCs having eigenvalues greater than the average eigenvalue (which corresponds to 1 when data are autoscaled) were considered. This criterion was chosen in order not to



include the influence of noise that is taken into account by the remaining PCs with lower eigenvalues. However, in the case of two dimensional datasets (like the simulated dataset being discussed here), by default both the resulting PCs were considered.

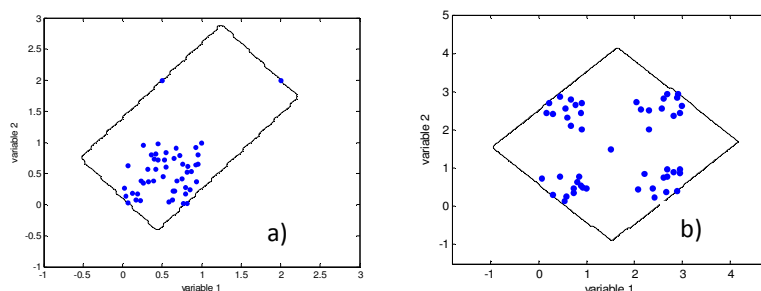


**Figure 2.4** Contour plot for the simulated datasets derived implementing PCA Bounding Box. First simulated dataset (2.4a), second simulated dataset (2.4b).

The contour plot in Figure 2.4a was derived implementing the PCA Bounding Box approach on the first simulated dataset. As clear from the figure, the issue of accounting for undesirable empty regions in the defined interpolation space still prevails. As shown in the Figure 2.4b, like the earlier approach, PCA bounding box included unnecessary empty regions between the clusters within the defined AD for the second simulated dataset.

### 2.2.3 Convex Hull

With this geometric approach, interpolation space is defined by the smallest convex area containing the entire training set. Implementing a Convex Hull could be challenging with increasing data complexity [16]. For two or three dimensional data, several algorithms are proposed; however, increase in dimensions contributes to the order of complexity. This could be a major drawback for this approach since in practice, not all the QSARs are limited to a small number of molecular descriptors. Several descriptors at times are needed to efficiently identify the trends in the modelled endpoint. Thus in theory, the implementation of this approach is limited to QSAR models with very limited number of descriptors. Apart from this issue, set boundaries are analysed without considering the actual data distribution. Similar to the

range-based approaches, Convex Hull cannot identify the potential internal empty regions within the interpolation space [11-12].

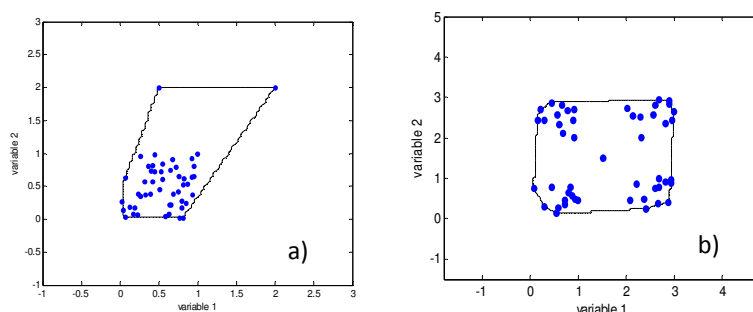


**Figure 2.5** *Contour plots derived for the simulated datasets implementing Convex Hull. First simulated dataset (2.5a), second simulated dataset (2.5b).*

Figure 2.5a shows the convex hull defined for the first simulated dataset. The defined hull reflects the interpolation space for reliable predictions. Like the range-based approaches, this strategy cannot overcome the existing limitation towards accounting for the empty regions. The AD defined for the second simulated dataset is shown in the contour plot of Figure 2.5b. The derived convex hull enclosed all the four clusters within a common interpolation space thus including the empty regions between the clusters within the defined AD.

The implementation of this approach in this case was quite simple as the simulated datasets were two-dimensional. In practice, QSAR models can have much higher level of complexity with multiple descriptors which could render this approach quite time consuming.

### 2.3 Distance-Based Methods

These approaches calculate the distance of test molecules from a defined point, (usually the data centroid) within the descriptor space of the training data. The general idea is to compare the distances measured between this defined point and the test molecules with a pre-defined threshold. The threshold is a user-defined parameter and is set to maximize the separation of

dense regions within the original data. However, the cut-off value does not entirely reflect the actual data density [5-6,11-13]. No strict rules were evident from the literature about defining thresholds for distance-based approaches and thus it is up to the user how to define them.

### 2.3.1 Centroid-based distance approach

In this approach, the distances of the training molecules from their centroid are calculated and based on a user-defined criterion, a cut-off distance value is considered as the threshold. For all the case studies dealt in this thesis, the distance value of the training molecules from their centroid corresponding to the 95<sup>th</sup> percentile was considered as the threshold. Later, the distances of the test samples from the centroid of the training set were derived and compared with the threshold value. If they were lesser or equal to the threshold, those test molecules were included within the model's AD, else discarded.

In theory, this approach can be implemented using a wide range of distance measures available in the literature however, for all the case studies dealt in this thesis work, following three distance measures will be considered: Euclidean, Manhattan and Mahalanobis distances.

**Table 2.1** Formulas for different distance measures

Distance measure	Formula
<i>Euclidean</i>	$d_{st} = \sqrt{\sum_{j=1}^p (x_{sj} - x_{tj})^2}$
<i>Manhattan</i>	$d_{st} = \sum_{j=1}^p  x_{sj} - x_{tj} $
<i>Mahalanobis</i>	$d_{st} = \sqrt{(\mathbf{x}_s - \mathbf{x}_t)^T \mathbf{S}^{-1} (\mathbf{x}_s - \mathbf{x}_t)}$ where $\mathbf{S}$ is the covariance matrix

Given a multidimensional matrix  $\mathbf{X}$  whose rows represent molecules and columns their corresponding descriptor values, Table 2.1 provides with the formulas to derive three different distances between two objects  $s$  and  $t$  described by  $p$  variables.  $x_{sj}$  and  $x_{tj}$  represent the  $j$ th variable describing the objects  $s$  and  $t$ , respectively.  $\mathbf{X}_s$  and  $\mathbf{X}_t$  represent the  $p$ -dimensional vectors for the objects  $s$  and  $t$ , respectively [17].

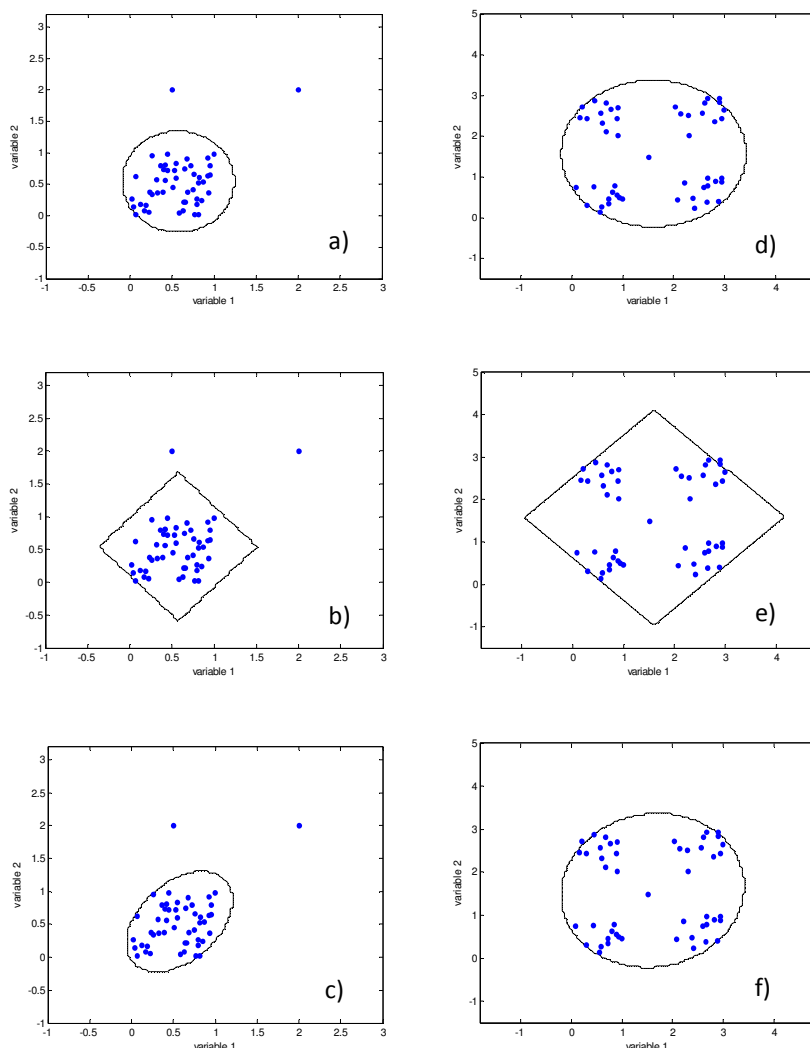


**Figure 2.6** Contour plots derived for the simulated datasets implementing centroid-based distance approach. First simulated dataset: Euclidean (2.6a), Manhattan (2.6b), Mahalanobis (2.6c). Second simulated dataset: Euclidean (2.6d), Manhattan (2.6e), Mahalanobis (2.6f).

Iso-distance contours constitute the regions having constant distance measures and generally their shapes differ with approaches according to the distance measure considered, for example, ellipsoids for Mahalanobis or spherical for Euclidean distances [12].

Figure 2.6 shows the contour plots derived on the both simulated datasets using three different distance measures. As the threshold was set to 95<sup>th</sup> percentile, the two isolated training samples were not included in the defined AD with all the three distance measures. The interpolation space mainly represented the regions around the cluster; the only difference was in the shape of the iso-distance contours depending on the distance measure used.

Approaches based on calculating leverages are also quite recommended for defining the AD of a QSAR model [18]. Leverage of a query chemical is proportional to its Mahalanobis distance measure from the centroid of the training set. For a given descriptor matrix **X** with rows as molecules and columns representing the descriptor values, its leverage matrix (**H**) is obtained with the following equation :

$$\mathbf{H} = \mathbf{X}(\mathbf{X}^T\mathbf{X})^{-1}\mathbf{X}^T \quad (2.1)$$

where **X** is the model matrix while **X<sup>T</sup>** is its transpose matrix.

Diagonal values in the **H** matrix represent the leverage values for different molecules in a given dataset. The molecules that are far from the centroid will be associated with higher leverages and are considered to be influential in model building. Leverage is proportional to Hotellings  $T^2$  statistic and Mahalanobis distance measure but can be applied only on the regression models. The approach can be associated with a threshold, generally 2.5 times the average of the leverage that corresponds to  $p+1/n$  where  $p$  is the number of model descriptors while  $n$  is the number of training molecules. A query chemical with leverage higher than the warning leverage can be associated with unreliable predictions. Such chemicals are outside the descriptor space and thus be considered outside the AD [11-13].

Figure 2.7 shows the contour plots derived on both the simulated datasets using leverage approach. Based on the above-discussed threshold, the defined AD for the first dataset (Figure 2.7a) was in the form of an ellipsoid oriented in the direction showing maximum variance in the data.

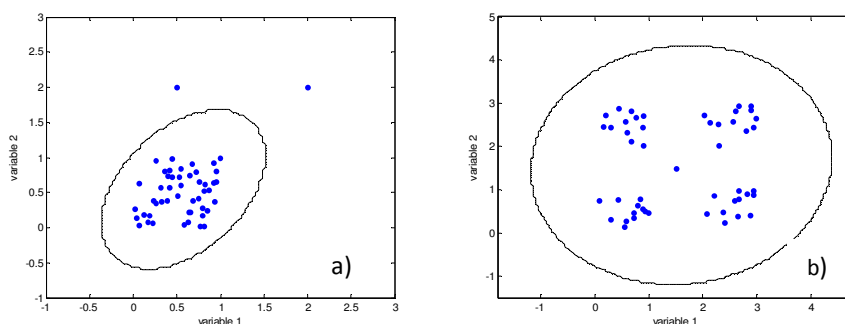


**Figure 2.7** Contour plots derived for the simulated datasets implementing Leverage approach. First simulated dataset (2.7a), second simulated dataset (2.7b)

The defined AD didn't include the two isolated training samples and the prevailing issue of accounting for empty regions within the training space seems partially resolved here. At a first glance, both the isolated samples are clearly potential outliers in the training space. As a result, it would be reasonable to expect a minimum possible influence of such isolated samples on the resulting AD. The use of above-discussed statistically significant threshold excludes these two outliers and their surrounding descriptor space from the resulting AD, indicating that these isolated samples have no role to play in defining the interpolation space. Thus, the resulting AD was mainly surrounded around the extremities of the huge cluster. On the hand, the defined AD for the second simulated dataset (Figure 2.7b) resembled the AD defined with Euclidean and Mahalanobis distances using the centroid based approach.

### 2.3.2 *K-Nearest Neighbours based approaches*

This set of approaches is based on providing similarity measure for a new test molecule with respect to the molecules within the training space. The similarity is accessed by finding the distance of a test molecule from nearest

training molecule or its average distances from  $k$  nearest neighbours in the training set. If these distance values are within the user defined threshold, the test molecule with higher similarity is indicated to have higher number of training neighbours and therefore, is considered to be reliably predicted. Thus, similarity to the training set molecules is significant for this approach in order to associate a test molecule with a reliable prediction [9]. Two variants of the kNN-based approach were implemented.

The first variant of the kNN-based AD approach [9, 19] was implemented by calculating average distances of all the training samples from their  $k$  nearest neighbours since the choice of thresholds didn't follow any strict rules in the existing literature, the value corresponding to 95<sup>th</sup> percentile in this vector of average distances was considered as general threshold. If the average distance of a test sample from its  $k$  nearest training neighbours was lesser than or equal to the threshold value, the test sample was retained within the AD.

Usually for classification purposes where kNN-based approaches are quite commonly applied, a smaller number of nearest neighbours is preferred to avoid any sort of bias. In theory, this makes sense because a higher number of  $k$  neighbours could take into account training neighbours which may not be significant towards structural similarity. In the literature, a small number of neighbours like  $k = 3$  or  $5$  are quite commonly used to implement different kNN-based approaches.

Figure 2.8 provides with the contour plots derived for both the simulated datasets implementing three different distance measures. To derive the plots, the approach was implemented taking 5 nearest neighbours ( $k = 5$ ) into account. The differences between the defined AD using different distance measures were clearer for the second dataset. The AD was more adapted to the shape of the clusters for Mahalanobis distances (Figure 2.8f) while some empty regions were included in the defined AD with the Manhattan distance (Figure 2.8e).

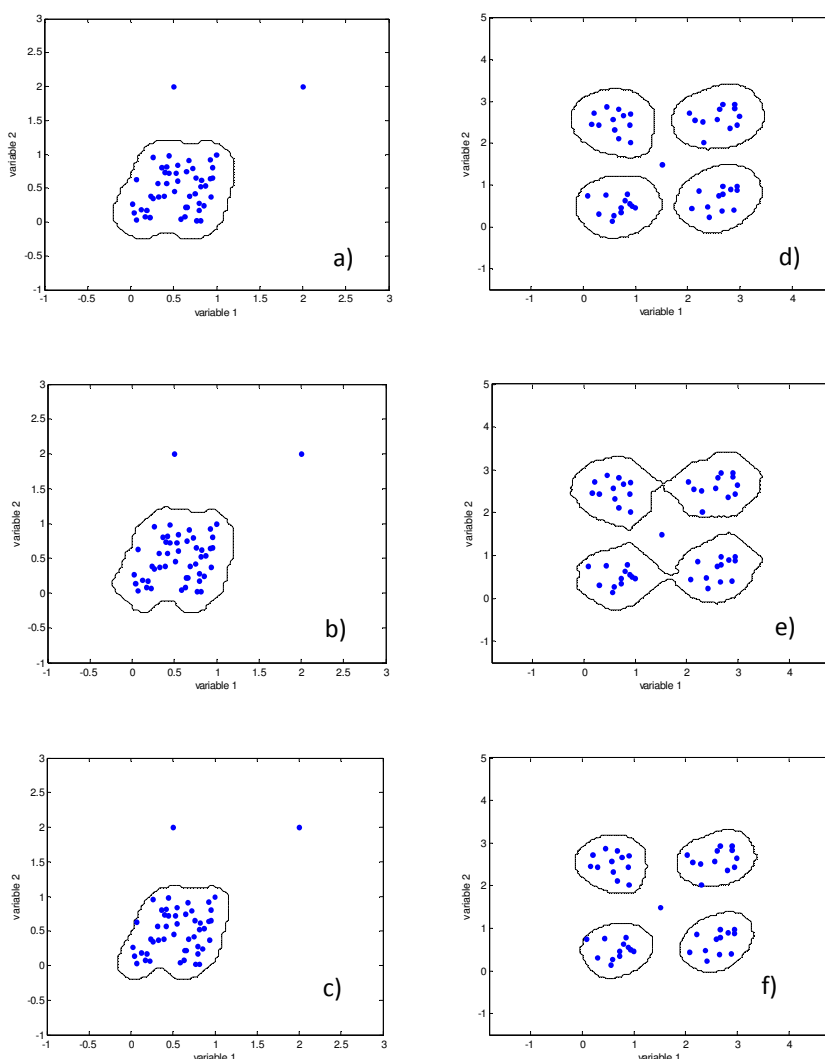


**Figure 2.8** Contour plots derived for the first simulated dataset implementing  $k$ -Nearest Neighbours based approach. First simulated dataset: Euclidean (2.8a), Manhattan (2.8b), Mahalanobis (2.8c). Second simulated dataset: Euclidean (2.8d), Manhattan (2.8e), Mahalanobis (2.8f).

The second variant of the kNN-based AD approach is a nearest neighbour method for probability density function estimation [20]. In this approach, the choice of  $k$  is crucial and is usually approximately equal to  $n^{1/2}$ .

In a  $p$ -dimensional space, let  $d_k(\mathbf{x})$  be the Euclidean distance from a test molecule  $\mathbf{x}$  to its  $k$ -th nearest training molecule. The dimensional volume of



the  $p$ -dimensional sphere having radius  $d_k(\mathbf{x}t)$  is given by  $V_k(\mathbf{x}t)$ , then the nearest neighbour density estimator at the data point  $\mathbf{x}t$  is given by:

$$f(\mathbf{x}t) = \frac{k/n}{V_k(\mathbf{x}t)} = \frac{k/n}{c_p [d_k(\mathbf{x}t)]^p} \quad (2.2)$$

Here,  $c_p$  is the volume of the unit sphere in  $p$  dimensions. In simple terms, here the probability density function estimate is defined with a window width  $d_k(\mathbf{x}t)$ .

Being prone to the local noise, the overall estimates with this approach do not seem quite convincing. The approach suffers from the irregularities resulting due to the dependence of the resulting estimator on the  $d_k(\mathbf{x}t)$  function [20].

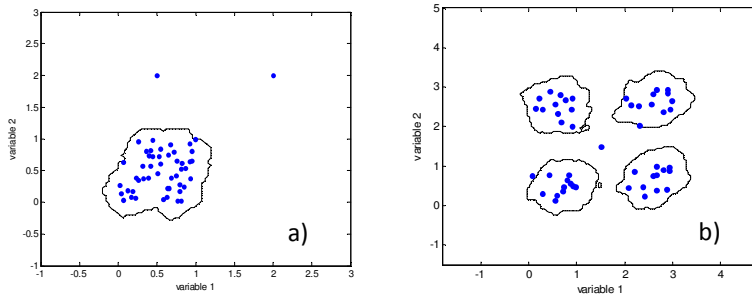


**Figure 2.9** Contour plots derived for the simulated datasets using Nearest Neighbour density estimator.

Figure 2.9 provides with the contour plots for the simulated datasets implementing this density estimator using  $k = 5$ . The defined AD seems to be well localized around the data clusters excluding the isolated data samples in both the datasets.

## 2.4 Probability Density Function Methods

Considered as one of the most advanced approaches for defining AD, these methods are based on estimating the Probability Density Function (PDF) for the given data. This is feasible by both, parametric methods where the density function has the shape of a standard distribution (Gaussian or

Poisson distribution, for instance) and non-parametric methods which do not have any such assumptions concerning the data distribution. A main feature of these approaches is their ability to identify the internal empty regions. Moreover, if needed, the actual data distribution can be reflected by generating concave regions around the interpolation space borders [11-12]. However, there are also several drawbacks associated with this set of approaches, discussed later in this chapter.

Generally these approaches are implemented by estimating probability density of the dataset followed by identifying Highest Density Region that consists of a known fraction (given as user input) from the total probability mass [11].

Let  $X$  be some random quantity with PDF  $f$ . Based on this function which actually describes the distribution of  $X$ , the probabilities associated with  $X$  can be obtained using the relation,  $P(a < X < b) = \int_a^b f(x) dx$  for all  $a < b$ .

Consider that some observed data points, assumed to be samples from an unknown probability density function are provided, then the estimate of the density function from these observed data can be constructed using density estimators [20].

For the random variable  $X$  with density  $f$ , we can have

$$f(x) = \lim_{h \rightarrow 0} \frac{1}{2h} P(x-h < X < x+h) \quad (2.3)$$

Thus for a given  $h$ , based on the sample proportion falling within the interval,  $P(x-h < X < x+h)$  can be easily estimated. Given a weight function  $w$ , the naive estimator can be written as:

$$\hat{f}(x) = \frac{1}{nh} \cdot \sum_{i=1}^n w\left(\frac{x - X_i}{h}\right) \quad (2.4)$$

The above equation indicates that the density estimator was derived by placing a box of width  $2h$  and height  $(2nh)^{-1}$  on each observation and later

the summation on all the observations was performed to obtain the final estimate [20].

Replacing the weight function  $w$  with a kernel function  $K$  such that,

$\int_{-\infty}^{\infty} K(x) dx = 1$ , the kernel estimator can be derived as:

$$\hat{f}(x) = \frac{1}{nh} \cdot \sum_{i=1}^n K\left(\frac{x - X_i}{h}\right) \quad (2.5)$$

where  $h$  is the window width, also referred to as smoothing parameter or bandwidth.

Taking the analogy of a naive estimator being the construction of density by sum of boxes centred at different data points, a kernel estimator can be considered as sum of ‘bumps’ on different data points. Shape of such bumps is identified by the kernel function  $K$  while their width is decided by the window width  $h$  [20].

The idea of defining the kernel estimator as the summation of bumps placed on different data points can be extended to the multivariate datasets. For a multivariate data set  $\mathbf{x}_1, \dots, \mathbf{x}_n$ , the resulting multivariate kernel density estimator with kernel  $K$  and window width  $h$  can be defined using the following equation:

$$\hat{f}(\mathbf{x}) = \frac{1}{n} \cdot \sum_{i=1}^n K\left\{\frac{\mathbf{x} - \mathbf{x}_i}{h}\right\} \quad (2.6)$$

where  $K(\mathbf{x}, \mathbf{x})$  is the kernel function for  $p$ -dimensional  $\mathbf{x}$ .  $K$  usually is a radially symmetric unimodal PDF, for instance a standard multivariate normal density function, defined as follows:

$$K(\mathbf{x}, \mathbf{x}_i) = \frac{1}{h^p \cdot (2\pi)^{p/2}} \cdot \exp\left(-\frac{1}{2}(\mathbf{x} - \mathbf{x}_i)^T (\mathbf{x} - \mathbf{x}_i)\right) \quad (2.7)$$

As can be seen in equation 2.6, a single smoothing parameter was used indicating that the kernel placed on all the data points will be equally scaled

in all the directions. Like for several other statistical procedures, in multivariate analysis pre-scaling the data could result quite useful as it will avoid getting extreme differences of spread in different coordinate directions. For the data scaling carried out, the standard kernel estimator in equation could be used without using different complicated variants usually involving more than one smoothing parameters [20].

Once the density estimation was carried out for all the training samples, the probability density value of the training sample corresponding to a cut-off percentile was considered as the threshold for AD definition. The test samples  $\mathbf{x}_t$  that were associated with a probability density lesser than this threshold were considered outside the model's AD [5].

#### *2.4.1 Gaussian kernels*

Among the multivariate kernel density methods which use the standard multivariate normal density function as the kernel function, the following three variants of Gaussian kernel estimators were implemented:

##### *a) Fixed Gaussian kernel*

'Fixed' indicates that with this kernel, the smoothing parameter/bandwidth  $h$  is constant over all training objects.

For this kernel, the optimal bandwidth was calculated as follows [20]:

$$h_{\text{opt}} = A(K) n^{-1/(p+4)} \quad (2.8)$$

where the constant  $A(K)$  in  $p$  dimensions was defined as:

$$A(K) = \{4 / (2p + 1)\}^{1/(p+4)} \quad (2.9)$$

Finally, the kernel estimate of PDF was then derived using the equation 2.7.

There are some drawbacks associated with this kernel method. Since the smoothing is constant, there are several chances of taking spurious noise into account in the estimates. Even in case the estimates were efficiently

smoothed, this could be compromised with the essential details in the distribution getting masked [20].

### *b) Optimized Gaussian kernel*

Instead of using a constant smoothing parameter  $h$ , this is optimized by leave-one-out cross-validation taking into account the differences in standard deviation of the variables [21].

The kernel estimate is derived as:

$$K(\mathbf{x}_t, \mathbf{x}_i) = \prod_{j=1}^p \frac{1}{h_{opt} \cdot s_j \cdot \sqrt{2\pi}} \exp\left(-\frac{1}{2} \cdot \frac{(x_{tj} - x_{ij})^2}{h_{opt}^2 \cdot s_j^2}\right) \quad (2.10)$$

where  $s_j$  is the standard deviation of the  $j$ th variable.

The optimization procedure requires the estimate of the parameter  $h$  so that:

$$\max \left[ \prod_{i=1}^n \hat{f}(\mathbf{x}_i) \right] \quad (2.11)$$

where  $\hat{f}(\mathbf{x}_i)$  is the probability density of  $i$ th sample in cross-validation.

### *c) Variable Gaussian kernel*

With this kernel, smoothing is adapted to the local density of the data. The strategy towards the construction of estimate is quite similar to that with classical kernel estimate, however, allowing the scale parameter for bumps to vary from one point to the other. Moreover, flatter kernels will be allocated to the sparse regions within the data. For all the case studies discussed in this thesis, this kernel was implemented with a bandwidth calculated as the inverse function of the Euclidean distance to  $k$ -th neighbour [21].

Given kernel function  $K$ , bandwidth  $h$ , a positive integer  $k$  and  $d_k(\mathbf{x}_t)$  being the Euclidean distance between the test point  $\mathbf{x}_t$  from its  $k^{th}$  nearest training neighbour, the variable Gaussian kernel estimate was derived as follows:

$$K(\mathbf{x}t, \mathbf{x}_i) = \prod_{j=1}^p \frac{1}{h_{opt} \cdot d_k(\mathbf{x}t) \cdot s_j \cdot \sqrt{2\pi}} \cdot \exp\left(-\frac{1}{2} \cdot \frac{(xt_j - x_{ij})^2}{h_{opt}^2 \cdot [d_k(\mathbf{x}t)]^2 \cdot s_j^2}\right) \quad (2.12)$$

In this case, the window width on  $\mathbf{x}t$  is proportional to the distance between  $\mathbf{x}t$  and its  $k^{th}$  nearest neighbour; the flatter kernels will be associated with sparse data regions. The bandwidth decides the overall smoothing while its response to the very local detail will be depending upon the value of  $k$ . With this kernel, the estimate will inherit the local smoothing properties, like in the case of ordinary kernel estimator [20].

Figure 2.10 provides with the contour plots derived for the both the simulated datasets implementing the three variants of Gaussian Kernel. For the first dataset, the AD defined in all the three cases were very much adapted to the shape of the cluster and like the distance-based approaches, the percentile approach to define thresholds left both the isolated samples excluded from the AD. The results derived with Fixed and Variable kernels converged to a great extent showing no clearly visible differences. The AD defined with Optimized kernel was slightly more adapted to the shape of the clusters.

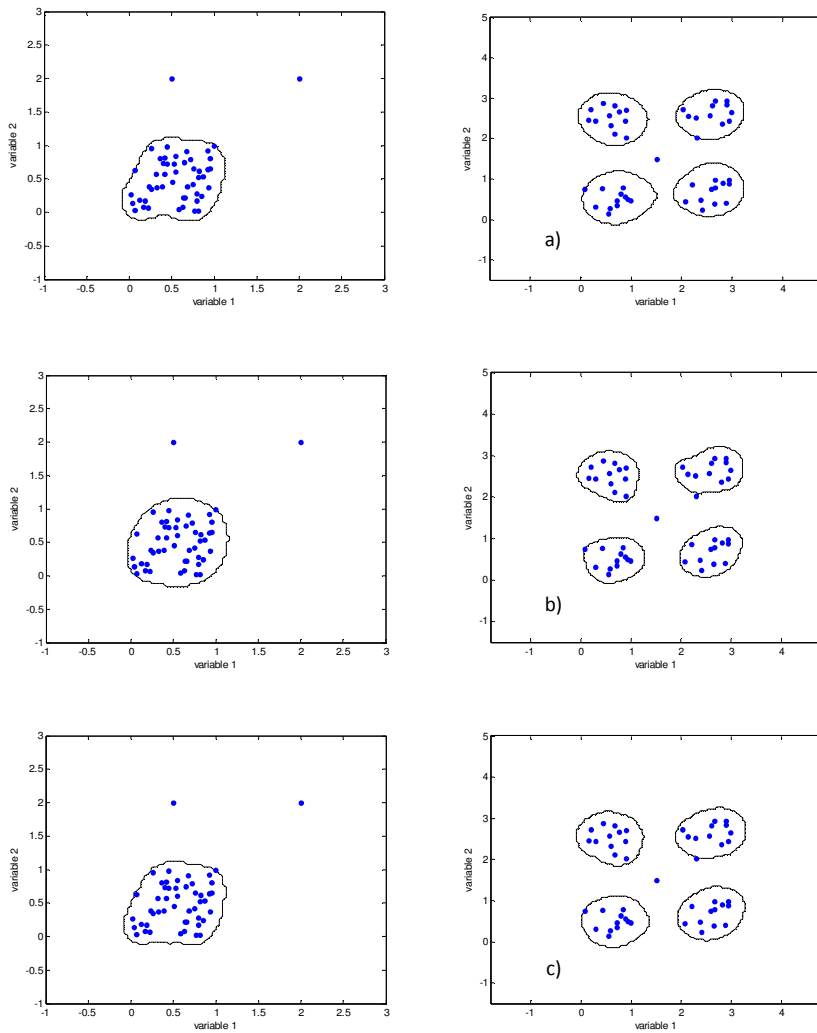


**Figure 2.10 :** Contour plots derived for both the simulated datasets implementing three variants of the Gaussian kernel. First simulated dataset: Fixed Gaussian kernel (2.10a), Optimized Gaussian kernel (2.10b) and Variable Gaussian kernel (2.10c), Second simulated dataset: Fixed Gaussian kernel (2.10d), Optimized Gaussian kernel (2.10e) and Variable Gaussian kernel (2.10f).

### 2.4.2 Adaptive kernel methods

Combining the features of kernel and Nearest Neighbours approach, this strategy constructs the kernel estimate at observed data points allowing the window width of kernels to vary from one point to another. There is a two stage procedure involved in determining if a given observation is associated within a lower density region [20]:

In the first stage, a pilot estimate is constructed making use of other density estimation methods. This estimate provides a rough understanding of the density and in turn provides with a pattern of bandwidths that are used to construct the adaptive estimator in the second stage.

Step 1: Pilot estimate  $\tilde{f}(\mathbf{x}_i)$  is found for all the  $i^{th}$  observation such that,  $\tilde{f}(\mathbf{x}_i) > 0$ .

Step 2: Local bandwidth factors  $\lambda_i$  are defined as follows:

$$\lambda_i = \left\{ \tilde{f}(\mathbf{x}_i) / g \right\}^{-\alpha} \quad (2.13)$$

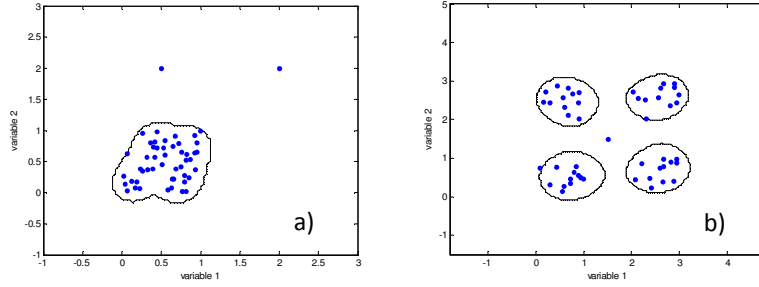
where  $\alpha$  is called sensitivity parameter, such that  $0 \leq \alpha \leq 1$  and  $g$  is the geometric mean of the  $\tilde{f}(\mathbf{x}_i)$ .

Step 3: Adaptive kernel estimate with kernel function  $K$  and bandwidth  $h$  can be defined as:

$$\hat{f}(\mathbf{xt}) = \frac{1}{n} \cdot \sum_{i=1}^n \frac{1}{\lambda_i^p} \cdot K \left\{ \frac{\mathbf{xt} - \mathbf{x}_i}{h \cdot \lambda_i} \right\} \quad (2.14)$$

Dependence of the bandwidth factors on the power of pilot density provides flexibility to the overall approach. When a higher power  $\alpha$  is used, the method will be quite sensitive to the variations in the pilot density, whereas approach will be implemented as fixed width kernel approach when  $\alpha$  is reduced to 0 [20]. For all the case studies discussed in this thesis, an adaptive kernel method was implemented with fixed Gaussian kernel as the pilot estimate and sensitivity parameter  $\alpha$  equal to 1/2 [14,20].





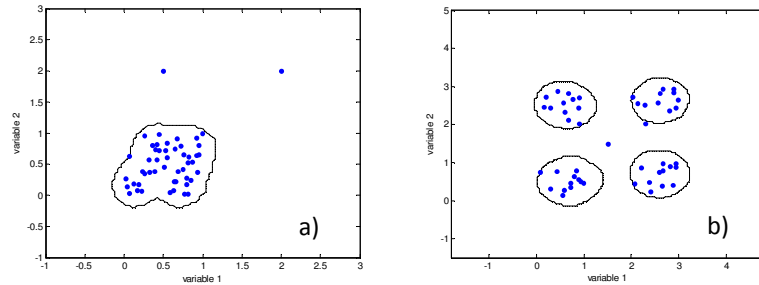
**Figure 2.11** Contour plots derived for simulated datasets implementing the Adaptive kernel. First simulated dataset (2.11a), Second simulated dataset (2.11b)

Figure 2.11 provides with the contour plot derived for the simulated datasets implementing the Adaptive kernel. The resulting interpolation space resembled to those derived with different variants of the Gaussian kernels.

#### 2.4.3 Triangular kernel

For an observation  $\mathbf{x}_t$  in multidimensional space, this kernel can be determined as follows:

$$K(\mathbf{x}_t, \mathbf{x}_i) = \begin{cases} 1 - \left| (\mathbf{x}_i - \mathbf{x}_t)^T (\mathbf{x}_i - \mathbf{x}_t) \right| & \text{if } \left| (\mathbf{x}_i - \mathbf{x}_t)^T (\mathbf{x}_i - \mathbf{x}_t) \right| < 1 \\ 0 & \text{otherwise} \end{cases} \quad (2.15)$$



**Figure 2.12** Contour plots derived for simulated datasets implementing the Triangular kernel. First simulated dataset (2.12a), Second simulated dataset (2.12b)

Figure 2.12 provides with the resulting contour plot for the simulate datasets implementing this kernel. Again the resulting AD for both the simulated datasets were quite similar to those defined using different variants of Gaussian kernels as well as Adaptive kernel.

#### 2.4.4 Epanechnikov kernel

This is an optimal kernel to minimize the integrated mean errors. The multivariate Epanechnikov kernel is defined as [20]:

$$K(\mathbf{x}_t, \mathbf{x}_i) = \begin{cases} \frac{1}{2} c_p^{-1} (p+2) \left( 1 - \frac{1}{h} \cdot (\mathbf{x}_i - \mathbf{x}_t)^T (\mathbf{x}_i - \mathbf{x}_t) \right) & \text{if } \left| \frac{1}{h} \cdot (\mathbf{x}_i - \mathbf{x}_t)^T (\mathbf{x}_i - \mathbf{x}_t) \right| < 1 \\ 0 & \text{otherwise} \end{cases}$$

where  $c_p$  is the volume of the unit  $p$ -dimensional sphere. (2.16)

The bandwidth  $h$  has been calculated as [20]:

$$h = \left( n^{-1/(p+4)} \right) \cdot \left\{ \frac{8p(p+2)(p+4)(2\sqrt{\pi})^p}{(2p+1)c_p} \right\}^{1/(p+4)} \quad (2.17)$$

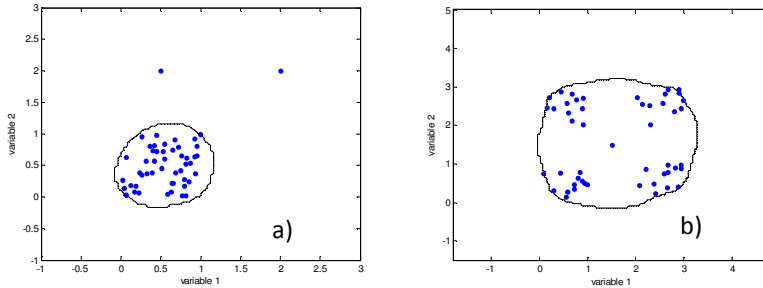


**Figure 2.13** Contour plots derived for simulated datasets implementing the Epanechnikov kernel. First simulated dataset (2.13a), Second simulated dataset (2.13b)

The contour plot for the simulated dataset implementing this kernel is shown in Figure 2.13. For the first dataset, the defined AD remained localized around the cluster while for the second dataset, the AD enclosed the entire

training space taking into account empty regions like with range and geometric based approaches.

Probability density distribution methods are advanced and but their efficiency is also associated with disadvantages of different kernels. For instance, kernel methods are usually associated with under-smoothing the tails while the nearest neighbourhood approach tries to overcome this issue however, by over-smoothing the tails. The adaptive kernel method overcomes such issues, however being adaptive to the local density.

All the classical AD methodologies discussed in this chapter will be further implemented on several QSAR models considered as case studies later in this thesis work. The results derived on these case studies will allow a further understanding of these discussed methodologies, as well as their advantages and disadvantages. It will be also interesting to see if the similarities in the approaches used to characterise the interpolation space is also evident from the common set of test molecules being excluded from the model's AD.

### *A novel $k$ -Nearest Neighbours based Applicability Domain evaluation*

Although existing literature discusses several approaches towards defining the Applicability Domain (AD) of QSAR models, an optimal approach has yet not been recognized. This chapter proposes a novel approach that defines the AD of QSAR models taking data distribution into account and derives a heuristic decision rule exploiting the  $k$ -Nearest Neighbours (kNN) principle. The proposed approach is a three stage procedure as a part of which, training thresholds are allocated, criterion deciding if a given test sample should be retained within the AD is defined and finally, the reliability in the derived results is reflected by taking model statistics and prediction error into account.

#### *3.1 Background and motivation*

As discussed in the previous chapter, several approaches were proposed in the past years to define the AD of QSAR models. All these approaches were associated with their own advantages and limitations [5, 11-14]. From time to time, several approaches were proposed that were aimed to be more efficient or were thought to overcome several limitations of the existing approaches.

Due to its simplicity and easy implementation,  $k$ -Nearest Neighbours had been a preferred choice for several proposed QSAR studies [4,9,19,22-26]. The kNN principle basically reflects upon the structural similarity of a test

sample to the training samples used to build that model. In theory, the distance of a query sample is considered from its  $k$  closest data points in the chemical space. Lower distance values correspond to a higher similarity, while the increasing distances signify higher levels of structural mismatch. The  $k$  value plays a significant role in defining how constraint the approach will be and thus, it can be referred to as the smoothing parameter.

This chapter proposes a new heuristic approach towards defining the AD of QSAR models. The basis of this novel strategy is inspired from the kNN approach and adaptive kernel methods for probability density estimation (Kernel Density Estimators, KDE) [27]. In the classical kNN approach for AD evaluation [9,19], average distances of all the training samples from their  $k$  nearest neighbours are calculated and used to define a unique threshold to decide if a test sample is inside or outside the model's AD (for example, 95<sup>th</sup> percentile). Moreover, in the framework of the probability density function estimation, the nearest neighbour method provides density estimates depending on the Euclidean distance to the  $k$ -th nearest data point [20]. Following the same concept, the proposed method tries to integrate the kNN principle with the salient features of adaptive kernel methods [27], which define local bandwidth factors corresponding to the training data points and use them to build the density estimate at a given point.

The novelty of the kNN based AD approach proposed here lies in the overall strategy that is properly executed in a three-stage procedure to encapsulate and reflect upon several significant aspects towards model validation. Moreover, some features common to most of the AD approaches were dealt differently with this approach; for instance, rather than defining a general threshold as in all the distance-based approaches, each training sample in this approach was associated with its individual threshold; in order to find an optimal smoothing parameter  $k$ , this approach performed a  $k$ -optimization procedure based on Monte Carlo validation; additionally, model's statistical parameters and other relevant aspects were dealt simultaneously to reflect upon the reliability in the derived results.

### 3.2 Methodology

A stepwise execution of the following three stages characterises the workflow of this approach:

- 1) defining thresholds for training samples
- 2) evaluating AD for new/test samples
- 3) optimizing the smoothing parameter  $k$

To allow a better interpretation of the proposed approach, results on both the two-dimensional simulated datasets (introduced in Figures 2.1 and 2.2 of Chapter 2) will be considered throughout the major part of this discussion and wherever applicable.

#### 3.2.1 Defining thresholds for training samples

Thresholds have a great influence in characterising the AD for reliable predictions; a test sample that exceeds the threshold condition is associated with an unreliable prediction.

Like the adaptive kernel methods, instead of defining a general unique threshold as seen with several classical AD approaches, the proposed approach allocates a set of thresholds corresponding to the various training samples.

For a given value of  $k$ , threshold allocation process can be summarised as follows:

- a) The distances of each training molecule from the remaining  $n - 1$  molecules are calculated and ranked in increasing order,  $n$  being the total number of training molecules. This will result in a  $n \times (n - 1)$  neighbour table  $\mathbf{D}$ ; an entry  $D_{ij}$  of the table corresponds to the distance of the  $i$ -th molecule from its  $j$ -th nearest neighbour:

$$D_{i1} \leq D_{i2} \leq \dots \leq D_{i,n-1}$$

- b) The average distance of each  $i$ -th molecule from its  $k$  nearest neighbours is calculated considering the first  $k$  entries in  $i$ -th row of the neighbour table:

$$\bar{d}_i(k) = \frac{\sum_{j=1}^k D_{ij}}{k} \quad \text{where, } 1 \leq k \leq n-1 \quad \text{and} \quad \bar{d}_i(k) \leq \bar{d}_i(k+1) \quad (3.1)$$

A vector  $\bar{\mathbf{d}}(k)$  of average distance values is then derived considering all the molecules in the training set.

- c) Next, a reference value (from now on referred as *Ref Val*),  $\tilde{d}(k)$  is determined as follows:

$$\tilde{d}(k) = Q3(\bar{\mathbf{d}}(k)) + 1.5 \cdot [Q3(\bar{\mathbf{d}}(k)) - Q1(\bar{\mathbf{d}}(k))] \quad (3.2)$$

where,  $Q1(\bar{\mathbf{d}}(k))$  and  $Q3(\bar{\mathbf{d}}(k))$  are the values corresponding to the 25<sup>th</sup> and 75<sup>th</sup> percentiles in the vector  $\bar{\mathbf{d}}(k)$ , respectively [28].

- d) Next, the ordered distances of each  $i$ -th training sample from all other  $n - 1$  training molecules are compared with the *Ref Val*. If the distance value of the  $i$ -th molecule from its given  $j$ -th training neighbour (where  $1 \leq j \leq n - 1$ ) is less than or equal to the *Ref Val*, then that distance value is retained, otherwise is discarded. The number  $K_i$  of neighbours satisfying this condition, minimum zero and maximum being  $n - 1$ , defines the density of the  $i$ -th sample neighbourhood:

$$K_i: \{D_{ij} \leq \tilde{d}(k)\} \quad \forall j: 1, n-1 \quad (3.3)$$

- e) Finally, each  $i$ -th training molecule is associated with a threshold  $t_i$  which defines the width of its neighbourhood as:

$$t_i = \frac{\sum_{j=1}^{K_i} D_{ij}}{K_i} \quad (3.4)$$

If no distance value was retained for a given  $i$ -th training molecule ( $K_i = 0$ ), then its threshold  $t_i$  would be theoretically settled to 0, but a pragmatic solution is to set it equal to the smallest threshold of the training set.

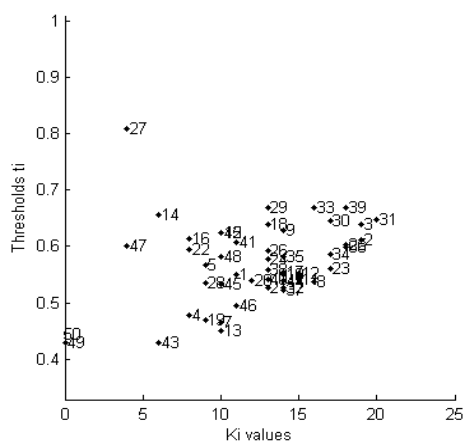


**Figure 3.1** First simulated data set. Thresholds  $t_i$  vs. number of training neighbours  $K_i$  plot ( $k = 12$ ).

The plot in Figure 3.1 provides with an overview of the thresholds for all the 50 samples in the simulated dataset. As expected, most of the training samples within the cluster (for instance, samples 2, 33 and 39) were associated with higher  $K_i$  values. On the other hand, obvious potential outliers (samples 49 and 50) had their thresholds equal to 0 since they couldn't satisfy the threshold criterion even for a single training neighbour (i.e.  $K_i = 0$ ), thus no distance values contributed to their threshold calculation. Nevertheless, they were associated with the minimum threshold equal to 0.42, i.e. the threshold of sample 43.

### 3.2.2 Evaluating AD for new/test samples

Until this point, each training molecule was associated with its individual threshold. The next step will be to characterise the AD which usually relies upon a set of conditions that will decide if a given test molecule can be associated with a reliable prediction or not.

The criterion used by this approach to associate a given test sample to be within the domain of applicability can be summarised below.



Given a test molecule, its distance from all the  $n$  training molecules is calculated and simultaneously, compared to be less than or equal to the thresholds associated with each training molecule. If this condition holds true with at least one training molecule, the test molecule will be considered inside the domain of applicability for that model. Otherwise, the prediction for that test sample will be rendered unreliable.

More formally, given the training set  $TR$ , for each test molecule  $j$ , the AD decision rule is:

$$j \in AD \quad \text{iff} \quad \exists i \in TR: D_{ij} \leq t_i \quad (3.5)$$

where  $D_{ij}$  is the distance between the  $j$ -th test molecule and the  $i$ -th training molecule and  $t_i$  is the individual threshold of the latter. In addition, each test/new molecule will be associated with the number  $K_j$  of nearest training neighbours for which the previous condition holds true. This number can be assumed as a measure of potential prediction reliability; indeed, high values of  $K_j$  indicate that the new molecule falls within a dense training region of the model's space, while low values of  $K_j$  denote that the new molecule still belongs to the model's space, but located in sparse training regions.  $K_j$  equal to zero rejects the molecule as it being outside the model's AD since no training neighbours are identified.

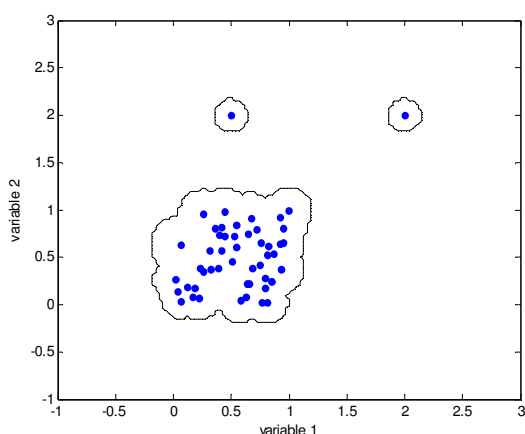


**Figure 3.2 :** Contour plot to demonstrate how the AD was characterised for the first simulated dataset. Metric used: Euclidean distance;  $k = 12$ .

Figure 3.2 provides with the contour plot for the simulated dataset derived projecting several data points enough to fill the training space. Thresholds were calculated using 12 nearest neighbours and Euclidean distance. This choice of  $k = 12$  nearest neighbours was based on the results derived performing an internal  $k$ -optimization, discussed later in this article. The space enclosed around the cluster represented as black line indicates that all the data points within this enclosed region are inside the AD. Thus, this region reflects in a way how the AD was characterised for this two-dimensional dataset. Area of this enclosed region tends to expand or shrink depending upon the number of nearest neighbours used for threshold calculation.

As explained earlier, the extreme outliers in the training space will be associated with the number  $K_i$  of neighbours equal to zero and the lowest possible threshold in the training set. Consider the sample 49 from the simulated dataset which is an extreme outlier with its threshold equal to 0.42. If there is a test sample that seems to be quite in the vicinity of this potential outlier within the descriptor space, the test sample will be associated with an unreliable prediction since its distance from sample 49 will likely exceed the small threshold. Now, consider a case, where the descriptor values for another test sample exactly overlap or are very similar to those for this potential outlier. In this situation, the distance of that sample from the outlier will be less than the threshold and thus it will be considered within the domain of applicability. In theory, this is not wrong because the potential outlier is still a part of the training space. Practically, the approach retains all the training samples to characterize the AD but minimizing the role of potential outliers in doing so. That's the reason why the first test sample was excluded from being reliably predicted while the second sample was not.

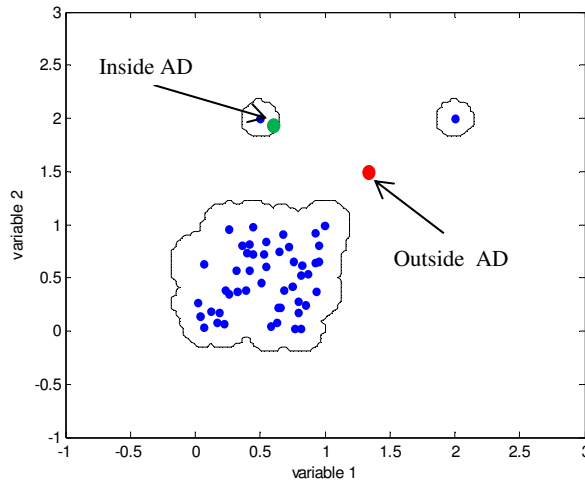


**Figure 3.3** An illustration of two test samples towards AD criterion of the proposed approach for the simulated dataset.

However, for the latter the number  $K_j$  of nearest training neighbours will likely be equal to one indicating that its prediction has some degree of uncertainty. In conclusion, there exists a relation between the defined AD and the impact of training samples in characterising it based on their threshold values.

### 3.2.3 Optimizing the smoothing parameter $k$

Another important aspect is concerning the choice of an appropriate smoothing parameter  $k$ , whose theoretical range is between 1 and  $n-1$ . It can be seen from the AD defined for the simulated dataset using different  $k$  values in Figure 3.4, very low  $k$  values will restrict the domain of applicability in a very strict manner as compared to the AD derived opting for larger  $k$  values. This is because, an opted  $k$  value will have a direct impact on the threshold calculations which in turn can make it more rigid or easier for test samples to satisfy the threshold criterion. The strategy implemented in this thesis to select an appropriate  $k$  value was performed by Monte Carlo validation in ' $n$ ' iterations, maximizing the percentage of the test samples considered within the AD, i.e. satisfying AD criterion (Equation 3.5).

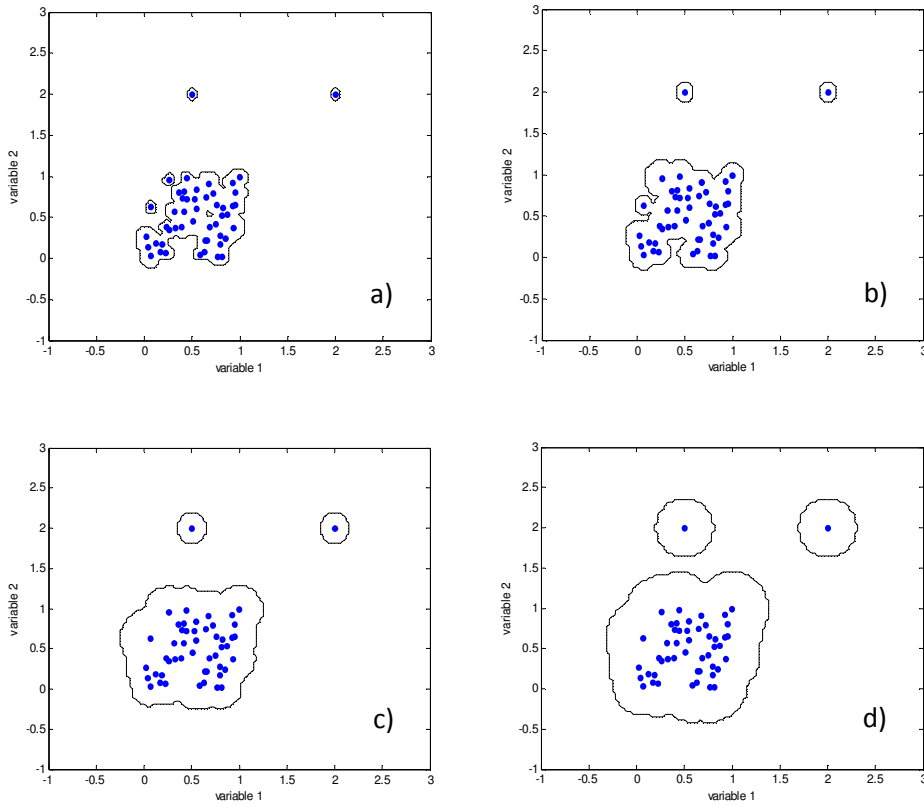


**Figure 3.4** *Impact of different  $k$  values on the defined AD for simulated dataset. a)  $k=1$ , b)  $k=5$ , c)  $k=15$  and d)  $k=25$ .*

To perform this validation, in each iteration, 20 percent of the training samples were randomly chosen as the test set and the above discussed AD procedure was executed using a range of  $k$  values, defined by the user. Percentage of test samples retained inside the model's AD for each  $k$  value in every iteration was recorded. Box-and-whisker plots (box plots) were produced to get an overview of all these derived results. For instance, consider the plot in Figure 3.3 derived for the simulated dataset showing percentage of test samples retained within the AD with different  $k$  values (optimization carried out with 20% of samples in the test set and 1000 iterations).

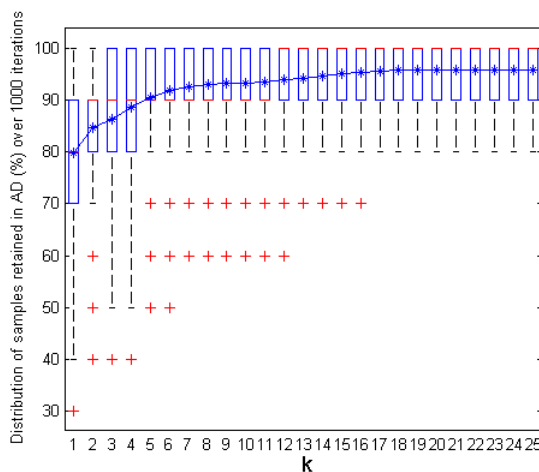


**Figure 3.5** First simulated data set. Box-and-whisker plot of test samples (%) retained within the AD for different  $k$  values during  $k$ -optimization.

Figure 3.5 shows that the spread of the box plots for initial  $k$  values is quite large. This may have resulted due to the impact of restricted training thresholds that excluded several test samples from the AD. With an increase in  $k$  values, the spread narrowed, however the outliers were still present until  $k = 17$ . After this point, the box plots remained unchanged throughout the plot with no outliers. Similar observations were derived from the mean line plot which showed a significant rise initially followed by a stable curve until the first half of the  $k$  values. The plot didn't show any major changes for the second half of the  $k$  values. In order to avoid very high  $k$  values good enough to unnecessarily expand the defined AD, a  $k$  value of 12 was opted as appropriate  $k$  for this dataset. The plots dealt earlier (Figures 3.1 and 3.2) for this dataset were thus derived using this opted  $k$  value.

Median quartile in the middle of the box (marked in red) can be referred for all the  $k$  values to get a hint about how many test samples were retained on average during the optimization process for a given  $k$  value. About their usefulness in the proposed AD approach, box plots showing limited spread and allowing majority of test samples to be retained within the AD can be favoured and their corresponding range of  $k$  values can be considered to finally opt for the most appropriate  $k$ . Additionally, a line plot is integrated in

the same figure indicating the mean percentage of test samples that were considered within the AD for each  $k$  value. A simultaneous interpretation of both these plots can make it easier for a user to decide upon an appropriate  $k$  value.

It was concluded that optimization of  $k$  can be a time-demanding procedure especially in the case of a huge number of samples, but it was also observed that this approach is quite insensitive to the smoothing parameter  $k$ , except for very small  $k$  values which led to the results influenced by local noise. Therefore, for many applications the optimization of the smoothing parameter can be avoided and reasonable results can instead be obtained by a fixed  $k$  value empirically calculated as  $n^{1/3}$ .

#### 3.2.4 An overview of results on other simulated datasets

The simulated dataset discussed so far was used to facilitate a better understanding of how the proposed approach works. This part of the chapter provides an overview of how using the same approach the resulting AD was defined on other simulated datasets.

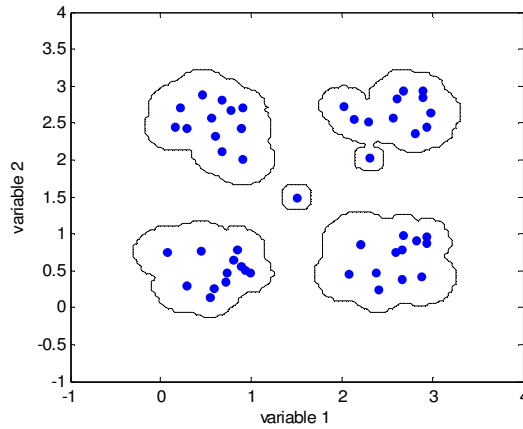


**Figure 3.6** *Second simulated data set. Contour plot to demonstrate how the AD was characterised. Metric used: Euclidean distance;  $k = 4$ .*

The contour plot for the AD defined on second simulated dataset (introduced in Figure 2.2 of Chapter 2) with the new approach is shown in Figure 3.6 which was derived using  $k = 4$ . For range and geometric based approaches,

the isolated sample (49) was considered inside but taking into account unnecessary descriptor space between the clusters, while for the distance and probability density distribution approaches, this sample was considered outside the AD approach due to the percentile-based threshold. With the proposed approach, all the clusters were enclosed in their own interpolation space. Since sample 49 was associated with the minimum training threshold, a small descriptor space around it was considered within the AD indicating that a test sample extremely similar to sample 49 could be considered as reliably predicted.

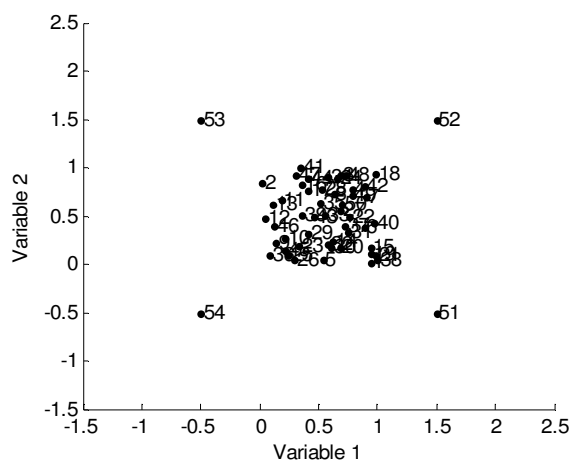


**Figure 3.7** *Scatter plot for the third simulated dataset.*

Figure 3.7 provides with the scatter plot for an additional simulated dataset considered to better evaluate the proposed AD approach. As shown in the figure, this dataset has a cluster of data points in the middle and four isolated samples surrounding it. It could be easily interpreted that with several classical approaches like convex hull or bounding box, a lot of unnecessary interpolation space could be taken into account considering the four isolated samples within the model's AD.

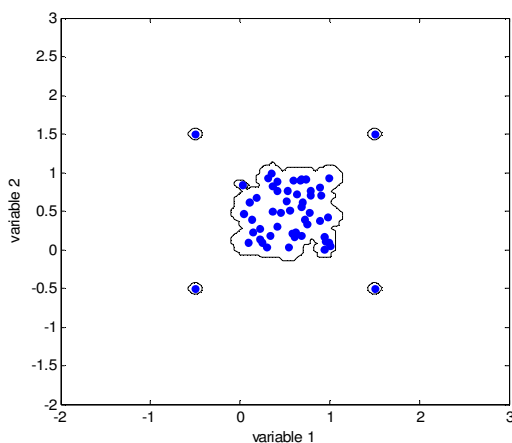


**Figure 3.8** *Third simulated data set. Contour plot to demonstrate how the AD was characterised. Metric used: Euclidean distance;  $k = 4$ .*

Figure 3.8 provides with the contour plot for this simulated dataset. Since the potential outliers with this approach are associated with minimum training threshold, a small descriptor space surrounding these isolated samples was considered inside the model's AD. As expected, all the clustered data points were included within the common AD space. The above contour plot was derived using  $k = 4$ .

The overall strategy for this novel approach in defining the AD will be clearer when the performance of this approach will be further evaluated later in this thesis using several QSARs from the existing literature as the case studies. The results derived with this approach will be also compared with those derived using several other existing AD approaches discussed earlier in Chapter 2.



## *Outlier detection from an Applicability Domain perspective*

Presence of potential outliers in the training space can have a huge impact on characterizing the interpolation space and the resulting Applicability Domain (AD) may not be restrictive enough to exclude unreliable test molecules. On the other hand, the test molecules detected as outliers when projected on the training space can hint for their prediction being unreliable and thus can be excluded from the model's AD. This chapter introduces a novel Mahalanobis distance measure (namely, a pseudo-distance) termed as Locally-centred Mahalanobis distance and discusses its usefulness towards outlier detection. The proposed outlier detection approach hints some useful alerts towards the presence of test molecules that could be rendered as unreliable after AD evaluation. This chapter implements this newly derived distance matrix to propose the second novel approach towards evaluating for a model's AD.

### *4.1 Introduction and the scope of this study*

Outliers represent the observations that fail to follow the general pattern of the majority of data samples [29]. Thus, it is critical to detect and appropriately treat such anomalous observations, contributing to undesired performance degradation, or, alternatively, suggesting unexpected but interesting patterns. In recent years, there had been a growing attention towards dealing with outliers since they can highly impact the variance and

correlation between variables and as a result, several approaches addressing outlier detection have been proposed in the literature [30].

Several supervised and unsupervised-learning methods have been proposed to address outlier mining [31]. Most of the proposed techniques to deal with outliers were either diagnostic or robust approaches [32,33]. Several classical techniques performed well, provided the given set of data contained only a single outlier, however, their inefficiency emerged while dealing with multiple outliers [34]. Increasing dimensionality of data adds to the complexity of detecting such outliers. Lacking visual perception for data with more than two dimensions, restricted the reliable use of such classical approaches only for two-dimensional data [29]. Moreover, masking and swamping considerably restricted the usefulness of such classical approaches towards detection of multiple outliers in calibration. Many times the presence of some outliers can somehow mask the detection of other outliers. As a result, some outliers are wrongly identified as normal samples. This phenomenon is referred to as masking. On the contrary, swamping refers to the cases where the presence of a subset of observations makes normal samples being incorrectly identified as potential outliers [32, 33].

Several new and improved detection approaches emerged from time to time and were attempting to overcome major limitations of classical outlier detection techniques, however, this domain of data exploration perhaps may always leave a room for further improvement towards developing an approach that can tackle the increasing data complexity without comprising upon the quality of detection accuracy.

The outliers detected amongst molecules constituting the training space can be quite interesting from an AD perspective. The training molecules detected as outliers can have a huge impact on the interpolation space defined by different AD approaches. This impact of training outliers further depends upon the AD approach being implemented. For instance, range-based approaches are highly sensitive to such outliers and thus their defined interpolation space may be unnecessarily broadened accounting for several empty regions in the descriptor space. On the contrary, the Probability

density distribution-based approaches as well as the novel kNN based AD approach (discussed earlier in Chapter 3) will try to minimize the impact of such potential outliers in defining the interpolation space. Later, test molecules considered as extreme outliers when projected on the training space could be more likely to be unreliably predicted upon AD evaluation. This implies that the outlier detection approaches can be quite useful in determining the test molecules that are extreme outliers when projected on the training space. This resulting subset of test molecules can be excluded from the model's AD, rendering them unreliably predicted in the model's descriptor space.

In this chapter, a new distance measure, called *locally-centred Mahalanobis distance*, based on the covariance matrix centred on each dataset molecule, is introduced and its salient properties are discussed. Two new parameters, remoteness and isolation degree derived from the resulting pairwise distance matrix are introduced, in order to better explore the isolation of the molecules in their local and global space. The information corresponding to these new parameters when plotted can allow the analyst to better explore several interesting features of the data, particularly, in terms of detecting those molecules that are quite diverse from the major pattern followed by the data [35]. Later, the novel distance measure can be calculated for the test molecules with respect to the training set molecules. The resulting remoteness and isolation degree values for test samples can be projected along with those for the training set molecules. Provided that the thresholds for training remoteness and isolation degree are defined, test molecules associated with values for these parameters exceeding their thresholds can be excluded from the model's AD. The performance of this new outlier detection approach towards AD evaluation is better explained taking into account the results derived on two-dimensional simulated datasets introduced earlier (Figures 2.1 and 2.2) in Chapter 2. Later, the performance of this novel outlier detection approach will be further evaluated considering several case studies later in this thesis.

### 4.2 Definition of the Locally-Centred Mahalanobis distance

Let the data matrix  $\mathbf{X}$  be comprised of  $n$  molecules and  $p$  descriptors, defined as:  $\mathbf{X} = (\mathbf{x}_1^T, \mathbf{x}_2^T, \dots, \mathbf{x}_n^T)^T$ , where  $\mathbf{x}_i$  are column vectors representing the  $n$  observations ( $i = 1, 2, \dots, n$ ).

The data are assumed to be independently sampled from a multivariate normal distribution  $N_p(\boldsymbol{\mu}, \boldsymbol{\Sigma})$ . A general measure of squared distance from an observation  $\mathbf{x}_i$  to the centroid of the  $p$ -dimensional space  $\boldsymbol{\mu}$ , for  $i = 1, \dots, n$ , can thus be written as follows:

$$d_i^2 = (\mathbf{x}_i - \boldsymbol{\mu})^T \cdot \mathbf{M} \cdot (\mathbf{x}_i - \boldsymbol{\mu}) \quad (4.1)$$

where  $\mathbf{M}$  is a  $p \times p$  symmetrical matrix. If  $\mathbf{M} = \boldsymbol{\Sigma}^{-1}$  where  $\boldsymbol{\Sigma}$  is the population covariance matrix, the squared Mahalanobis distance is obtained as:

$$d_i^2 = (\mathbf{x}_i - \boldsymbol{\mu})^T \cdot \boldsymbol{\Sigma}^{-1} \cdot (\mathbf{x}_i - \boldsymbol{\mu}) \quad (4.2)$$

These distances are distributed according to  $\chi_p^2$  and if the parameters  $\boldsymbol{\mu}$  and  $\boldsymbol{\Sigma}$  are estimated by the arithmetic mean  $\bar{\mathbf{x}}$  and the molecule's covariance matrix  $\mathbf{S} = \frac{1}{n-1} \cdot \sum_{i=1}^n (\mathbf{x}_i - \bar{\mathbf{x}})(\mathbf{x}_i - \bar{\mathbf{x}})^T$  respectively, the (estimated) squared Mahalanobis distances are:

$$MD_i^2 = (\mathbf{x}_i - \bar{\mathbf{x}})^T \cdot \mathbf{S}^{-1} \cdot (\mathbf{x}_i - \bar{\mathbf{x}}) \quad (4.3)$$

The distribution is given by  $\frac{(n-1)^2}{n} MD_i^2 \sim \text{Beta}(\frac{p}{2}, \frac{n-p-1}{2})$ , (e.g., see reference [7]). If  $\mathbf{S}$  and  $\mathbf{x}_i$  are independent, then  $\frac{n-p}{(n-1)p} MD_i^2 \sim F_{p, n-p}$ .

Now, if a vector  $\mathbf{v} \in \mathbf{R}^p$  is selected in the  $p$ -dimensional space, the covariance matrix, centred at  $\mathbf{v}$ , denoted by  $\mathbf{S}_{(\mathbf{v})}$ , can be calculated as:

$$\mathbf{S}_{(\mathbf{v})} = \frac{1}{n-1} \cdot \sum_{i=1}^n (\mathbf{x}_i - \mathbf{v})(\mathbf{x}_i - \mathbf{v})^T \quad (4.4)$$

Then, it can be easily verified that,

$$\mathbf{S}_{(\mathbf{v})} = \mathbf{S} + \frac{n}{n-1} \cdot (\bar{\mathbf{x}} - \mathbf{v})(\bar{\mathbf{x}} - \mathbf{v})^T \quad (4.5)$$

Finally, the squared Mahalanobis distances considering  $\mathbf{v}$  as the space centre can be derived as:

$$MD^2(i, \mathbf{v}) = (\mathbf{x}_i - \mathbf{v})^T \cdot \mathbf{S}_{(\mathbf{v})}^{-1} \cdot (\mathbf{x}_i - \mathbf{v}) \quad i = 1, \dots, n \quad (4.6)$$

If the above mentioned vector  $\mathbf{v}$  is now replaced by an observation  $\mathbf{x}_j$ , for  $j = 1, \dots, n$ , the new locally-centred squared Mahalanobis distance between observations  $i$  and  $j$  is defined as:

$$MD_L^2(i, j) = (\mathbf{x}_i - \mathbf{x}_j)^T \cdot \mathbf{S}_{(j)}^{-1} \cdot (\mathbf{x}_i - \mathbf{x}_j) \quad (4.7)$$

where  $\mathbf{S}_{(j)}$  is the covariance matrix centred on the  $j$ -th observation.

It should be noted that the classical covariance matrix  $\mathbf{S}$ , being centred on the arithmetic mean vector, minimizes the data variance, while, the new defined locally-centred covariance matrix encodes different information, data variance depending on the selected centre. Thus, the new distance measure is more informative than the classical Mahalanobis distance, which considers only the arithmetic mean as the data centre.

In order to obtain distances that are independent of the number of descriptors  $p$ , the distance values can be divided by  $p$ , thus obtaining locally-centred average squared Mahalanobis distances:

$$\overline{MD}_L^2(i, j) = \frac{MD_L^2(i, j)}{p} = \frac{1}{p} \cdot [(\mathbf{x}_i - \mathbf{x}_j) \cdot \mathbf{S}_{(j)}^{-1} \cdot (\mathbf{x}_i - \mathbf{x}_j)] \quad i, j = 1, \dots, n \quad (4.8)$$

Hereinafter these average distances will be considered, for the sake of simplicity, they will be often shortly referred to as locally-centred squared Mahalanobis distances, still using the symbol  $MD_L^2$ .

#### 4.2.1 Salient features of the novel distance measure

There are two important key aspects related to this novel distance. Like the distances derived using the classical covariance matrix, the locally-centred

Mahalanobis distances are invariant to any sort of variable scaling. Secondly, unlike the classical Mahalanobis distance, the resulting object-centred distance is asymmetric and consequently is a pseudo-distance; indeed, the distance between two observations  $i$  and  $j$  depends on whether the selected centre is  $i$  or  $j$ :

$$MD_L^2(i, j) \neq MD_L^2(j, i) \quad (4.9)$$

This asymmetry is accounted due to the presence of all other observations and their resulting overall influence in deriving the distances, thus reflecting the significance of information retrieved from the locally-centred covariance matrix.

The asymmetry between  $MD_L^2(i, j)$  and  $MD_L^2(j, i)$  seems to have a significant meaning. In fact, a higher value of  $MD_L^2(i, j)$  in contrast with a corresponding lower value for  $MD_L^2(j, i)$  indicates that the molecule  $i$  belongs to a relatively denser region with respect to the molecule  $j$ , which appears to be more isolated. This consideration can be further supported by the fact that, when  $j$  is isolated being the centred object, it shows a higher variance than the case when  $i$  is the centred molecule, which unlike the earlier, is surrounded by several molecules in its vicinity. As seen from the way these locally-centred Mahalanobis distances are derived, the variance is calculated as the reciprocal in the distance formula and as a result,  $j$  tends to seem closer to  $i$ , while on the contrary, molecule  $i$  with a lower variance tends to seem comparatively further distant from  $j$ . Usually, the molecules with lower variance can be thought of being either located in a cluster or surrounded by several similar molecules in their vicinity.

The variable space based on Mahalanobis distances calculated using the classical covariance matrix is estimated by an ellipsoid (or hyper-ellipsoid), while in the case of locally-centred Mahalanobis distances, the variable space is defined by a family of ellipsoids (or hyper-ellipsoids) due to the multi-centred approach. Thus, a more data-driven shaped descriptor space is determined using this novel distance measure.

### 4.3 Remoteness and Isolation degree plot

It is quite easy to interpret the significance of columns and rows in the pairwise distance matrix  $\mathbf{MD}_L^2$  resulting from the novel average locally-centred squared Mahalanobis distances. In fact, each  $j$ -th column constitutes the data centre and represents how that  $j$ -th molecule "globally perceives" each  $i$ -th molecule, also taking into account the overall influence of all the other molecules, while each  $i$ -th row represents how that  $i$ -th molecule is "globally perceived" by all the other molecules.

Each  $j$ -th column of the  $\mathbf{MD}_L^2$  matrix contains information about the distances of all other  $i$  molecules from the  $j$ -th molecule being the centre. The minimum value of a  $j$ -th column can be taken into account to represent the squared distance of the  $j$ -th molecule from its nearest neighbour; this is termed as *Isolation degree* (*Idg*):

$$Idg_j = \min_i \left( [\mathbf{MD}_L^2]_{ij} \right) \quad i \neq j \quad (4.10)$$

Similarly, each  $i$ -th row of the  $\mathbf{MD}_L^2$  matrix contains information about the squared distances of the  $i$ -th molecule as it is perceived from all the other molecules. Thus, the average squared distance value for each  $i$ -th row is taken into account and termed as *Remoteness* (*Rem*):

$$Rem_i = \frac{\sum_{j=1}^n [\mathbf{MD}_L^2]_{ij}}{n-1} \quad (4.11)$$

The values of remoteness can range from a minimum greater than zero and a maximum equal to  $(n-1)/p$ , while isolation degree for any given molecule remains localized between 0 and 1. It should be also noted that:

$$\frac{\sum_{i=1}^n Rem_i}{n} = \frac{\sum_{i=1}^n \sum_{j=1}^n [\mathbf{MD}_L^2]_{ij}}{n \cdot (n-1)} = 1 \quad (4.12)$$

i.e., the average value of the remoteness vector or, in other words, the average value of the matrix  $\mathbf{MD}_L^2$  elements is equal to one. Then, the

remoteness could be interpreted as the influence that each molecule exerts over the covariance structure of the data, i.e. the values significantly larger than one identify the most influent molecules.

#### 4.3.1. Usefulness towards outlier detection

The remoteness highlights objects which are far from the bulk of the remaining objects, i.e. they can be considered as classical outliers in the selected variable space; the Isolation degree detects a different kind of “anomalous” objects, i.e. those objects that, although located within the variable space, are isolated from the other ones or, in other words, these objects are surrounded by objects not so near. Therefore, a scatter plot of Remoteness vs. Isolation degree, called *RI plot*, for the data set in analysis can be a useful tool for exploratory purposes.

The thresholds to detect remote and isolated samples, for the two distributions of remoteness and isolation degree, are defined as the upper “fences” in the box & whisker plots [28]:

$$threshold = Q_3 + 1.5 \cdot (Q_3 - Q_1) \quad (4.13)$$

where  $Q_1$  and  $Q_3$  are the first and third quartiles for remoteness and isolation degree values, respectively, and their difference is the interquartile range.

To better evaluate the role of remoteness and isolation degree towards potential outlier detection, the results for both the simulated data sets introduced in Chapter 2 were analysed. As mentioned earlier, the first dataset consists of a cluster of 48 data samples and two additional samples (49 and 50) quite distant from each other as well as from the main sample cluster (Figure 2.1) while the second dataset had its data samples roughly divided within four clusters and a single data sample (49) localized more or less between these clusters (Figure 2.2).

The locally-centred squared Mahalanobis distances were calculated for the two simulated and the object-oriented pair-wise distance matrix  $\mathbf{MD}_L^2$  was derived. The average distance values from each row and the minimum distance values from each column were retrieved from this distance matrix to



derive the remoteness and isolation degree vectors, respectively. The values of these two parameters were used as the point coordinates of all the data samples in the RI plot.

Thresholds for both remoteness and isolation degree were calculated according to equation 4.13 and reported in the RI plots by red lines. The data samples associated with very high values for remoteness were classified as outliers of first type being far from the variable space defined by the bulk of the data, i.e. remote samples; the data samples associated with high values of isolation degree were classified as outliers of second type, they being isolated from the other samples in spite of their position within the variable space, i.e. isolated samples.

The RI plot obtained by the locally-centred Mahalanobis distance for first simulated dataset is shown in Figure 4.1. As expected, two data samples 49 and 50 were highly isolated from the cluster and far from the bulk of the data. Both these data samples were associated with high values for remoteness and isolation degree which clearly indicated that they are quite isolated in their local and global spaces. Moreover, data sample 27 was associated with a higher value of isolation as compared to the other samples in that cluster.

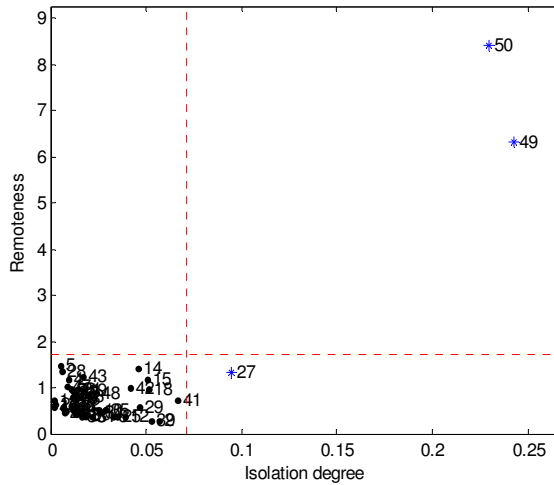


**Figure 4.1** *RI plot for the first simulated data set*

A careful observation of the scatter plot in Figure 2.1 indicates that sample 27 is within the extremities of the cluster as well as no other data samples from the cluster are very closely located in its vicinity. This indicates that the new approach is quite sensitive to the isolation of the samples

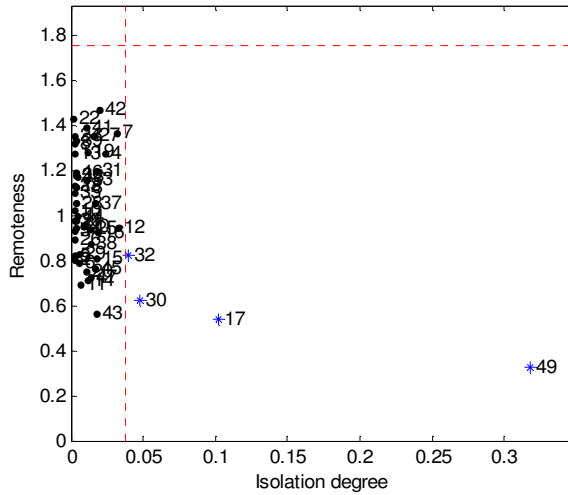


**Figure 4.2** *RI plot for the second simulated data set.*

The second data set used as case study was a two-dimensional simulated data set introduced in chapter 2 with data samples roughly divided within four clusters and a single data sample (49) localized more or less between these clusters. The scatter plot of this data set (Figure 2.2) indicates this isolated sample clearly being a potential outlier; however, it was also interesting to see how the outlier detection techniques were able to analyse this data.

As shown in Figure 4.2, the novel outlier detection approach was able to clearly identify sample 49 as a second type outlier based on its extreme value for isolation degree. Remoteness for the data samples was not extremely high for any specific data sample and then no first type outliers are detected. Samples 17, 30 and 32 that were not very closely located to their nearest of the four clusters were also identified with higher values of isolation degree.

#### 4.4 Implementing the novel approach towards AD evaluation

So far, the usefulness of remoteness and isolation degree was explored towards outlier detection. As pointed earlier, if these new matrix parameters can be calculated also for test samples and simultaneously projected with those for the training samples, the resulting plot could be quite useful to evaluate if the test samples can be reliably predicted or not. The test samples exceeding the defined training thresholds for remoteness or isolation degree or both of them can be excluded from the model's AD.

To implement this strategy for AD evaluation, remoteness and isolation degree of the test samples were determined as follows:

For a given test set  $\mathbf{X}_t$  with  $m$  observations, the remoteness of the test sample  $\mathbf{x}_t$  was derived by calculating its locally-centred Mahalanobis distance from each training observation  $\mathbf{x}_j$  centering at  $\mathbf{x}_j$ , such that  $j = 1, \dots, n$ . and then finding the mean of the resulting distance vector:

$$\overline{MD}_L^2(i, j) = \frac{MD_L^2(i, j)}{p} = \frac{1}{p} \cdot \left[ (\mathbf{x}_t - \mathbf{x}_j)^T \cdot \mathbf{S}_{(j)}^{-1} \cdot (\mathbf{x}_t - \mathbf{x}_j) \right] \quad j=1, \dots, n \quad (4.14)$$

$$\text{where } \mathbf{S}_{(j)} = \frac{1}{n-1} \cdot \sum_{i=1}^n (\mathbf{x}_i - \mathbf{x}_j)(\mathbf{x}_i - \mathbf{x}_j)^T$$

On the other hand, the isolation degree of the test sample  $\mathbf{x}_t$  was derived by calculating its locally-centred Mahalanobis distance from each training observation  $\mathbf{x}_j$  centering at the  $i$ -th test object  $\mathbf{x}_t$  and then finding the minimum value from the resulting distance vector:

$$\overline{MD}_L^2(j, i) = \frac{MD_L^2(j, i)}{p} = \frac{1}{p} \cdot \left[ (\mathbf{x}_j - \mathbf{x}_t)^T \cdot \mathbf{S}_{(i)}^{-1} \cdot (\mathbf{x}_j - \mathbf{x}_t) \right] \quad j=1, \dots, n \quad (4.15)$$

$$\text{where, } \mathbf{S}_{(i)} = \frac{1}{n} \cdot \sum_{j=1}^n (\mathbf{x}_j - \mathbf{x}_t)(\mathbf{x}_j - \mathbf{x}_t)^T$$

The test molecules exceeding the remoteness and isolation degree thresholds in equation 4.13 can be excluded from the model's AD.

Considering these definitions for remoteness and isolation degree for training and test molecules, contours plot was derived by projecting several test samples enough to fill the training space of both the simulated datasets.

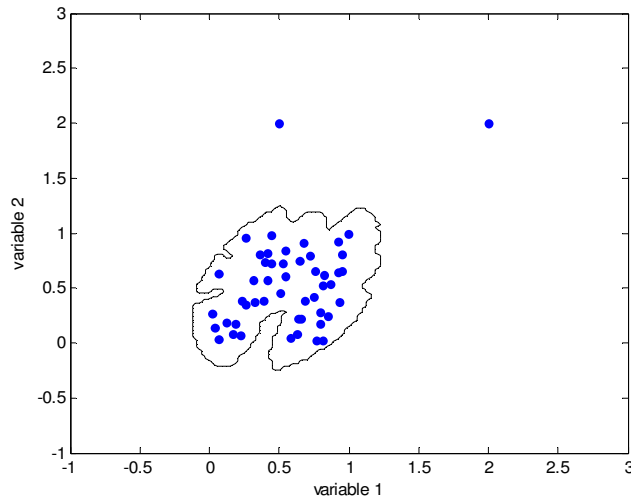


**Figure 4.3** *AD contour plot for the first simulated dataset*

Figure 4.3 provides with the contour plot for the first simulated dataset. The defined interpolation space consisted of all the test samples that had their remoteness and isolation degree values below the defined thresholds. The AD seems quite adapted to the shape of the data cluster which was not so clearly interpretable with other classical approaches. Moreover, the choice of slightly higher thresholds for test samples is quite visible in the plot.

Figure 4.4 provides with the contour plot for the second simulated dataset. The defined interpolation was mainly concentrated around the four clusters. Due to the choice of thresholds, the defined AD seemed slightly extended around the cluster's extremities. Like in the case of first novel AD approach, this approach also considered the descriptor space around the isolated sample (49) within the defined AD.

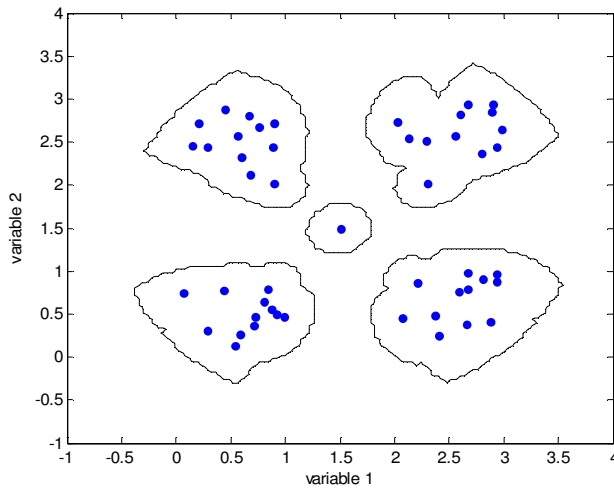


**Figure 4.4** *AD contour plot for the second simulated dataset*

Both the simulated datasets were simpler in dimensions and were mainly chosen to provide with a better understanding of the proposed approach towards AD evaluation. The potential of this novel approach will be further clearer while deriving the AD for several multidimensional case studies later in this thesis.

## *PART III*



## *APPLICATIONS*

## *Case studies*

This section is entirely dedicated towards implementing the already discussed classical and novel AD approaches on several QSAR models from the existing literature. Each case study is initially introduced highlighting the five major OECD principles for model validation, followed by discussing the results derived evaluating for their AD using various approaches. The test samples considered as consensus outliers with different AD approaches hint the possible similarities in the underlying AD algorithms as well as higher chances of rendering those test samples being unreliably predicted. Finally, the impact on model's statistics was evaluated after excluding the test samples that were rendered outside the model's AD using all the listed approaches.

### *5.1 An overview of the case studies*

The earlier chapters discussed several classical approaches from the existing literature towards defining the AD of QSAR models. Moreover, two new AD approaches were also introduced and illustrated using simulated datasets. In this section, several QSAR models from the existing literature will be used as case studies to evaluate their AD implementing different classical and novel approaches discussed earlier. All these models will be introduced based on the five OECD principles for model validation. This will help to better understand the validity of these models. Later, the results derived implementing all the earlier discussed AD approaches on these models will be provided. An overview of all the test samples excluded from the model's

AD with different approaches will be provided including their names, CAS numbers and their error in prediction will be provided.

Most of the case studies discussed in this chapter are of regulatory relevance. CAESAR Bioconcentration factor models [36-38] and QSAR models for ready biodegradability of chemicals [39], for instance were clearly developed to contribute to the REACH implementation. The other two QSAR models to predict soil adsorption coefficient [40-41] and the OH tropospheric degradation of volatile organic compounds [42] were retrieved from the Joint Research Centre (JRC) QSAR Model Reporting Format (QMRF) repository [43].

## 5.2 Assessing reliability in derived results

For all the regression models considered, before the AD evaluation was performed, an overview of the model's statistics (retaining the test set in its entirety) was provided using the following key parameters:

a) Determination coefficient  $R^2$

$$R^2 = 1 - \frac{\sum_{i=1}^{n_{TR}} (\hat{y}_i - y_i)^2}{\sum_{i=1}^{n_{TR}} (y_i - \bar{y}_{TR})^2} \quad (5.1)$$

b) Root-Mean-Square Error  $RMSE$

$$RMSE = \sqrt{\frac{\sum_{i=1}^{n_{TR}} (\hat{y}_i - y_i)^2}{n_{TR}}} \quad (5.2)$$

c) Predictive squared correlation coefficient  $Q^2$  [43,44]

$$Q^2 = 1 - \frac{\left[ \sum_{j=1}^{n_{TS}} (\hat{y}_j - y_j)^2 \right] / n_{TS}}{\left[ \sum_{i=1}^{n_{TR}} (y_i - \bar{y}_{TR})^2 \right] / n_{TR}} \quad (5.3)$$



d) Root-Mean-Square Error in Prediction *RMSEP*

$$RMSEP = \sqrt{\frac{\sum_{j=1}^{n_{TS}} (\hat{y}_j - y_j)^2}{n_{TS}}} \quad (5.4)$$

where,  $y_i$  is the measured response value for the  $i$ -th training sample and  $\hat{y}_i$  its predicted value;  $y_j$  is the measured response value for the  $j$ -th test sample and  $\hat{y}_j$  its predicted value;  $n_{TR}$  and  $n_{TS}$  represent the total number of training and test samples, respectively, and  $\bar{y}_{TR}$  is the mean response of the training set.

Later, when different AD approaches were implemented on these models, in order to reflect upon the model's predictive ability, following key parameters were evaluated:

- a) Number of test samples excluded from the model's AD.
- b)  $Q^2$  calculated from the test samples retained within the AD
- c) List of all the test samples (their sample IDs) considered outside the AD.

Additionally, for the novel  $k$ NN based AD approach discussed in Chapter 3:

- a) For each  $j$ -th test sample, its absolute standardized error calculated as:

$$SE_j = \frac{|y_j - \hat{y}_j|}{s_Y} \quad (5.5)$$

where,  $y_j$  is the measured value for the  $j$ -th test sample and  $\hat{y}_j$  its predicted value;  $s_Y$  the standard error of estimate derived from the training set.

- b) The information about how many times the threshold criterion (Equation 3.5) is satisfied by each test sample, that is, how many training neighbours (i.e.  $K_j$ ) are located at a distance less than or equal to their threshold values, from a given test sample.

In theory, a test sample satisfying the threshold criterion several times (i.e. having high  $K_j$ ) is expected to be predicted with higher accuracy. This can

be desired since less distant training neighbours indicate a higher structural similarity of the test sample. On the contrary, a test sample satisfying the threshold criterion for no training neighbours ( $K_j = 0$ ) indicates that there wasn't any training sample similar enough to reliably predict that test sample.  $K_j$  (number of training neighbours) vs. absolute standardised error plot for all the test samples derived was derived.

For all the classification models on ready biodegradability of chemicals, following key parameters were evaluated to determine their predictive ability [38]:

a) Specificity ( $Sp$ )

$$Sp = \frac{TN}{TN + FP} \quad (5.6)$$

where, TN (True Negatives) is the number of not ready biodegradable samples that were classified as not ready biodegradable. FP (False Positives) is the number of not ready biodegradable samples wrongly classified as ready biodegradable.

b) Sensitivity ( $Sn$ )

$$Sn = \frac{TP}{TP + FN} \quad (5.7)$$

where, TP (True Positives) is the number of ready biodegradable samples correctly predicted as ready biodegradable. FN (False Negatives) is the number of ready biodegradable samples wrongly predicted as not ready biodegradable.

c) Error Rate is calculated as the complement of the average of specificity and sensitivity.

It should be remembered that all the AD approaches discussed in this thesis define a model's AD in its descriptor space. However, an attempt has been made in this chapter to better understand if the observations made evaluating for a model's AD in its descriptors space can be well reflected on its response domain. To achieve this, test samples excluded from the model's

AD were evaluated for their corresponding error in prediction (absolute difference in their experimental and predicted response values). It could be interesting to see if the test samples rendered as unreliable in the model's descriptor space are also associated with higher prediction error or not. In theory, this is a reasonable assumption since structurally similar chemicals can be associated with similar descriptor values which collectively are able to capture the increasing or decreasing trend of the modelled endpoint. Thus, if a query/test chemical is excluded from the model's descriptor space, it cannot be predicted reliably either. However, in practice, exceptions may arise due to several reasons for instance, defects in experimental techniques/experimental variability or even over-fitted models.

### *5.3 CAESAR Bioconcentration factor models*

#### *5.3.1 Model description*

##### *OECD principle 1: A defined endpoint*

CAESAR hybrid model provides prediction for Bioconcentration factor (BCF) in fish. Experimental data on BCF was obtained for two fish species, Cyprinus Carpio and salmonids using the OECD 305 protocol.

From regulatory point of view, BCF is of very high significance for REACH implementation. The BCF value for a given chemical can decide if it can be identified as bioaccumulative (if  $BCF > 2000$  or  $\log BCF > 3.3$ ) or very bioaccumulative (if  $BCF > 5000$  or  $\log BCF > 3.7$ ).

All the experimental BCF values used for developing this model were converted to their log units [38].

##### *OECD principle 2: An unambiguous algorithm*

CAESAR BCF model is a hybrid model derived combining the outputs from two different models (model A and model B). The training set of both these models consists of 378 samples, while the validation was carried out using a test set with 95 samples.

Both these models are Radial Basis Function Neural Network (RBFNN) [46], however, the earlier used an heuristic approach while the latter

implemented Genetic Algorithm for descriptor selection. Table 5.1 reports the descriptors associated with model A and B, respectively. AD evaluation will be carried out for both these models [36-38].

**Table 5.1** *List of descriptors used to develop CAESAR BCF models*

Descriptor	Description	Models
<i>MlogP</i>	Moriguchi octanol-water partition coefficient	Models A and B
<i>CI-089</i>	CI attached to C1(sp <sup>2</sup> )	Model A
<i>GATS5V</i>	Geary autocorrelation – lag 5/weighted by atomic van der Waals volumes	Model A
<i>X0Solv</i>	Solvation connectivity index	Model B
<i>SsCI</i>	Sum of all (–CI) E-State values in molecule	Model B
<i>AEige</i>	Absolute eigenvalue sum from electronegativity weighted distance matrix	Model A
<i>BEHp2</i>	Highest eigenvalue n. 2 of Burden matrix / weighted by atomic polarizabilities.	Models A and B
<i>MATS5V</i>	Moan autocorrelation – lag 5/weighted by atomic van der Waals volumes	Model B

### *OECD principle 3: A defined domain of applicability*

The CAESAR model allows a user to understand its defined domain of applicability in the following three ways:

- a) By evaluating the ranges of descriptor values:* If a given test sample has any of its descriptor values outside the defined ranges, the user will be provided with an alert.
- b) Identifying chemical fragments not included within the training space:* If a test sample contains a chemical fragment that is not included within the chemical diversity of the training set, an error message will be generated.
- c) Identifying the most similar training samples:* For each test sample, six most similar training samples are shown. This allows a better understanding of the structural similarity between the predicted sample and the training space. This can also provide a good basis to interpret the reliability in prediction derived for the test samples [36-38].

### *OECD principle 4: Appropriate measures of goodness-of-fit, robustness and predictivity*

Table 5.2 provides with the default statistical parameters for model A and B, retaining all the test samples within the model's AD.

**Table 5.2** Model statistics for the CAESAR BCF models.

Model	Training set		Test set	
	$R^2$	$RMSE$	$Q^2$	$RMSEP^{(d)}$
1) Model A	0.804	0.591	0.797	0.600
2) Model B	0.810	0.581	0.774	0.634

*OECD principle 5: A mechanistic interpretation, if possible*

The authors provided the following a posteriori interpretation towards the model descriptors in the QSAR Model Reporting Format (QMRF) of this model: The model is significantly relying on the MlogP descriptor. This descriptor seems to work quite well with chemicals containing C, N and O atoms, while it may not be very accurate for samples containing other atoms like Cl and P [38].

*5.3.2 AD evaluation for CAESAR BCF model A*

Table 5.3 provides with an overview of the results derived implementing various classical and novel AD approaches. Implementing PCA Bounding Box rendered two test samples outside the AD providing the most noticeably positive impact on the resulting  $Q^2$ . These samples were retained within the AD with classical Bounding Box. Excluding 29 samples outside the model's AD, Optimized Gaussian kernel approach was associated with the most restricted AD and the highest recorded  $Q^2$  of 0.830 but obviously due to several test samples being outside the AD. The  $Q^2$  slightly improved with the novel kNN-based AD approach, while no positive impact was observed with the LCMD based method with 8.4 % of the test samples discarded from the model's AD.

**Table 5.3** An overview of the results for AD evaluation on CAESAR BCF model A (Test set:95 samples)

AD method	Samples outside AD (%)	$Q^2$	List of samples outside AD
<i>Bounding Box</i>	0	0.797	None
<i>PCA Bounding Box (Using first 2 PCs)</i>	2.1	0.804	33 40
<i>Convex Hull</i>	0	0.797	None
<i>Leverage approach</i>	4.2	0.803	18 33 43 61
<i>Centroid dist. (Euclidean, 95 percentile)</i>	4.2	0.804	33 43 61 91
<i>Centroid dist. (Manhattan, 95 percentile)</i>	4.2	0.804	33 43 61 91
<i>Centroid dist. (Mahalanobis, 95 percentile)</i>	4.2	0.803	18 33 43 61
<i>kNN general thr (Euclidean, k=5)</i>	8.4	0.797	3 33 34 40 61 82 83 94
<i>kNN general thr. (Manhattan, k=5)</i>	7.4	0.799	3 33 34 61 82 83 94
<i>kNN general thr. (Mahalanobis, k=5)</i>	10.5	0.794	3 33 34 40 61 80 82 83 91 94
<i>Gaussian kernel: fixed</i>	10.5	0.794	3 24 33 34 40 61 82 83 91 94
<i>Gaussian kernel: optimized</i>	30.5	0.830	3 9 12 22 24 33 34 38 40 45 47 51 53 54 56 61 68 69 75 76 80 82 83 87 89 91 93 94 95
<i>Gaussian kernel: variable</i>	15.8	0.787	3 9 24 33 34 40 43 61 80 82 83 89 91 94 95
<i>Adaptive kernel</i>	7.4	0.800	3 33 43 61 82 83 91
<i>Epanechnikov kernel</i>	8.4	0.800	3 33 40 43 61 83 91 94
<i>kNN kernel (k=8)</i>	9.5	0.797	3 33 34 40 43 61 83 91 94
<i>Triangular kernel</i>	11.6	0.792	3 24 33 34 40 61 80 82 83 91 94
<i>Novel kNN approach (Euclidean, k=8)</i>	6.3	0.801	3 33 40 61 82 83
<i>Novel kNN approach (Manhattan, k=8)</i>	8.4	0.797	3 33 34 61 80 82 83 94
<i>Novel kNN approach (Mahalanobis, k=8)</i>	8.4	0.797	3 33 34 40 61 82 83 94
<i>Novel LCMD approach</i>	8.4	0.786	3 34 43 61 80 82 83 94

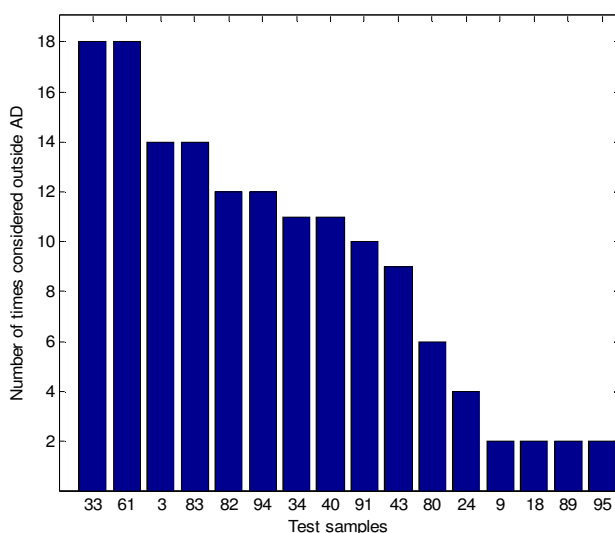


**Figure 5.1** *Consensus test samples excluded from the AD of CAESAR BCF model A*

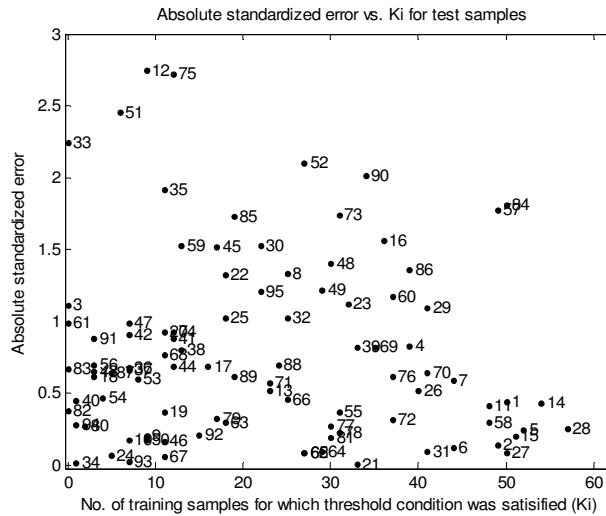
Figure 5.1 provides with the consensus test samples excluded from the model's AD implementing various classical and novel proposed AD approaches. Test samples 33 and 61 were identified as unreliable predictions implementing most of the AD approaches. Such resemblance in the final output from different approaches strengthens the decision to exclude unreliable test samples.

Table 5.4 provides with some useful information about the test samples considered outside the model's AD with different classical and novel approaches. Apart from several unreliably predicted samples, the list in this table also specifies some cases where the prediction error was quite negligible. For instance, sample 34 (tetrabromo-2-chlorotoluene) that was excluded from the model's AD with several approaches but was associated with a prediction error of log 0.01 units.

**Table 5.4** *An overview of all the test samples excluded from the AD of CAESAR model A with different approaches*

Sample ID	Name	CAS	Exp. logBCF	Pred. logBCF	Abs. pred.error
3	Pentachlorophenol	87-86-5	2.50	1.84	0.66
9	3,6-Dichlorodibenzofuran	74918-40-4	3.01	3.13	0.12
12	2,2,4-Trimethyl-1,3-pentanediol	144-19-4	-1.00	0.64	1.64
18	3,4-Dichlorophenol	95-77-2	1.69	1.33	0.36
22	2,6-Dicyclohexylphenol	4821-19-6	2.89	2.10	0.79
24	2-Hydroxy-4-n-octoxybenzophenone	1843-05-6	1.90	1.94	0.04
33	Hexachlorobenzene	118-74-1	4.23	2.90	1.33
34	Tetrabromo-2-chlorotoluene	39569-21-6	3.98	3.97	0.01
38	Monochlorobenzene	108-90-7	1.13	1.61	0.48
40	Pentachlorobenzene	608-93-5	3.49	3.22	0.27
43	Trichlorometane	67-66-3	0.93	0.54	0.39
45	1,10-Dibromodecane	4101-68-2	1.78	2.68	0.90
47	Tetrachloroethylene	127-18-4	1.72	1.13	0.59
51	n-Pentadecane	629-62-9	1.22	2.68	1.46
53	2,2''-Methylenebis(6-t-butyl-4-methylphenol)	119-47-1	1.97	2.33	0.36
54	Benzene-1,2-dicarboxylic acid bis (2-ethylhexyl) ester	117-81-7	1.19	1.47	0.28
56	Triethanolamine	102-71-6	0.59	1.01	0.42
61	2,4,6-Trichloroaniline	634-93-5	2.00	1.41	0.59
68	2,2''-Dichlorohydrazobenzene	782-74-1	3.65	3.19	0.46
69	1-(N-Phenylamino)naphthalene	90-30-2	3.23	2.74	0.49
75	Tris(1,3-dichloro-2-propyl)phosphate	13674-87-8	0.13	1.75	1.62
76	p-Phenylphenol	92-69-3	1.59	1.96	0.37
80	4-Chloro-1-nitro-2(trifluoromethyl) benzene	118-83-2	1.87	2.03	0.16
82	N-Hexamethylolmelamine hexamethylether	3089-11-0	0.28	0.06	0.22
83	Disperse Yellow 163	71767-67-4	1.56	1.16	0.40
87	O,O-Dimethyl-S-(N-methylcarbamoylmethyl) phosphorodithioate	60-51-5	-0.26	0.12	0.38
89	m-nitrobenzene sulfonic acid	98-47-5	0.70	0.33	0.37
91	Tris(p-isopropylphenyl)phosphate	26967-76-0	1.50	2.02	0.52
93	1-Amino-8-naphthol-3,6-disulfonic acid	90-20-0	0.46	0.45	0.01
94	3,3''-Dichloro-5,5''-benzidine disulfonic acid	123251-96-7	0.20	0.04	0.16
95	Disperse Yellow 64	10319-14-9	1.08	1.80	0.72





**Figure 5.2**  $K_j$  vs. Absolute standardized error plot for the test samples of CAESAR BCF model A

Figure 5.2 provides with a plot from the novel kNN based AD approach that tries to compare the observations made in the model's descriptor space and the response domain. The test samples are clearly showing a decreasing pattern from left towards right indicating a lowering prediction error with a corresponding increase in the number of training thresholds satisfied by the test samples. This plot also tries to graphically reflect upon the observations made from the previous table and plot for this model. Samples 33 and 61 for instance, are associated with reasonably higher prediction error and were able to satisfy none of the training thresholds indicating them being unreliably predicted. On the other hand, test sample 14 and 28 were associated with very low prediction error and satisfied maximum training thresholds. Thus, higher structural similarity resulted in better predictions as evident from this plot.

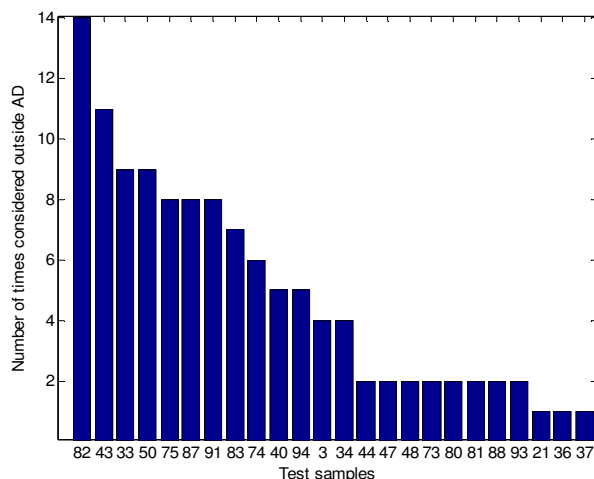
### 5.3.3 AD evaluation for CAESAR BCF model B

Table 5.5 provides with an overview of the results derived implementing various classical and novel AD approaches on CAESAR BCF model B.

**Table 5.5** An overview of the results for AD evaluation on CAESAR BCF model B (Test set: 95 samples)

AD method	Samples outside AD (%)	Q <sup>2</sup>	List of samples outside AD
<i>Bounding Box</i>	0	0.774	None
<i>PCA Bounding Box (First 2 PCs)</i>	0	0.774	None
<i>Convex Hull</i>	0	0.774	None
<i>Leverage approach</i>	3.2	0.767	43 50 91
<i>Centroid dist. (Euclidean, 95 percentile)</i>	3.2	0.767	43 50 91
<i>Centroid dist. (Manhattan, 95 percentile)</i>	5.3	0.764	36 37 43 50 91
<i>Centroid dist. (Mahalanobis, 95 percentile)</i>	3.2	0.767	43 50 91
<i>kNN general thr. (Euclidean, k=5)</i>	1.1	0.772	82
<i>kNN general thr. (Manhattan, k=5)</i>	1.1	0.772	82
<i>kNN general thr. (Mahalanobis, k=5)</i>	4.2	0.783	75 82 87 94
<i>Gaussian kernel: fixed</i>	13.7	0.778	3 33 34 40 43 50 74 75 82 83 87 91 94
<i>Gaussian kernel: optimized</i>	29.5	0.787	3 21 33 34 40 43 44 46 47 48 50 52 54 56 61 73 74 75 80 81 82 83 87 88 91 93 94 95
<i>Gaussian kernel: variable</i>	22.1	0.777	3 33 34 40 43 44 47 48 50 73 74 75 80 81 82 83 87 88 91 93 94
<i>Adaptive kernel</i>	2.1	0.769	43 82
<i>Epanechnikov kernel</i>	3.2	0.769	33 43 82
<i>kNN kernel (k=8)</i>	4.2	0.767	33 40 43 82
<i>Triangular kernel</i>	10.5	0.786	3 33 34 50 74 75 82 83 87 94
<i>Novel kNN approach (Euclidean, k=8)</i>	3.2	0.785	33 75 82
<i>Novel kNN approach (Manhattan, k=8)</i>	7.4	0.779	33 40 74 75 82 83 87
<i>Novel kNN approach (Mahalanobis, k=8)</i>	6.3	0.782	33 74 75 82 83 87
<i>Novel LCMD approach</i>	5.3	0.764	43 50 82 83 91

The range and geometric-based approaches retained all the test samples inside the model's AD. All other set of approaches associated some test samples being unreliably predicted, however, no major impacts were observed on the resulting Q<sup>2</sup>. This includes both the novel proposed AD approaches. This parameter varied slightly even after excluding several other test samples as obvious in the case of Gaussian kernel based approaches.



**Figure 5.3** *Consensus test samples excluded from the AD of CAESAR BCF model B*

Figure 5.3 provides with an overview of the consensus test samples being excluded from the model's AD implementing different approaches. Samples 43 and 82 (Trichlorometane and N-hexamethylolmelamine hexamethylether) were associated with the maximum frequency, thus indicating them being excluded from the AD using several different algorithms independent of each other. Several other test samples that were excluded by only one AD approach were not highlighted in the figure, however, Table 5.6 provides with some useful information about all the test samples excluded by different AD approaches.

**Table 5.6** *An overview of all test samples excluded from the AD of CAESAR model B with different approaches*

Sample ID	Name	CAS	Exp. logBCF	Pred. logBCF	Abs .pred.error
3	Pentachlorophenol	87-86-5	2.50	1.75	0.75
21	Cyclohexane	110-82-7	1.92	1.98	0.06
33	Hexachlorobenzene	118-74-1	4.23	3.57	0.66
34	Tetrabromo-2-chlorotoluene	39569-21-6	3.98	2.77	1.21
36	2,3,4,2'',5''-Pentachlorobiphenyl	38380-02-8	4.02	4.53	0.51
37	2,3'',4,4'',6-Pentachlorobiphenyl	56558-17-9	4.81	4.52	0.29
40	Pentachlorobenzene	608-93-5	3.49	3.48	0.01
43	Trichlorometane	67-66-3	0.93	1.03	0.10
44	1,1,2,2-Tetrachloroethane	79-34-5	0.93	0.91	0.02
46	1,1,2,2-Tetrachloro-1,2-difluoroethane	76-12-0	1.78	1.25	0.53
47	Tetrachloroethylene	127-18-4	1.72	0.66	1.06
48	Dibromoneopentylglycol	3296-90-0	-0.04	0.22	0.26
50	Heptachlor	76-44-8	3.95	4.17	0.22
52	1,3,5-Tri-tert-butylbenzene	1460-02-2	4.37	2.65	1.72
54	Benzene-1,2-dicarboxylic acid bis(2-ethylhexyl) ester	117-81-7	1.19	1.49	0.30
56	Triethanolamine	102-71-6	0.59	0.28	0.31
61	2,4,6-Trichloroaniline	634-93-5	2.00	1.45	0.55
73	2,2''-Dichlorodiethyl ether	111-44-4	-0.08	0.77	0.85
74	Trichloroacetic acid	76-03-9	-0.15	-0.22	0.07
75	Tris(1,3-dichloro-2-propyl)phosphate	13674-87-8	0.13	1.74	1.61
80	4-Chloro-1-nitro-2(trifluoromethyl)benzene	118-83-2	1.87	2.28	0.41
81	3-Nitrophthalic acid	603-11-2	0.72	0.26	0.46
82	N-Hexamethylolmelamine hexamethylether	3089-11-0	0.28	0.46	0.18
83	Disperse Yellow 163	71767-67-4	1.56	1.07	0.49
87	O,O-Dimethyl-S-(N-methylcarbamoylmethyl)phosphorodithioate	60-51-5	-0.26	0.34	0.60
88	2,2-Dichloropropionic acid	N/A	0.85	-0.01	0.86
91	Tris(p-isopropylphenyl)phosphate	26967-76-0	1.50	1.25	0.25
93	1-Amino-8-naphthol-3,6-disulfonic acid	90-20-0	0.46	0.65	0.19
94	3,3''-Dichloro-5,5''-benzidine disulfonic acid	123251-96-7	0.20	0.42	0.22
95	Disperse Yellow 64	10319-14-9	1.08	1.44	0.36

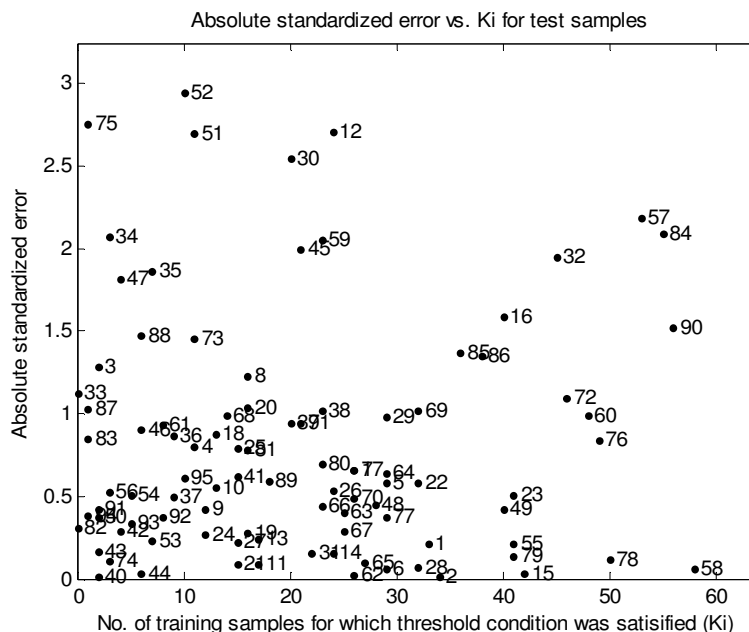


**Figure 5.4 :**  $K_j$  vs. Absolute standardized error plot for the test samples of CAESAR BCF model B

Figure 5.4 provides with the  $K_j$  vs. absolute standardized error plot derived from the novel kNN based AD approach. Several test samples like 30, 32, 57 and 84 were hindering the expected lowering pattern in prediction error with increase  $K_j$  values. Such samples indicate being associated with high predictor error despite of their higher  $K_j$  values which in theory shouldn't be the case. However, this plot tries to reflect the outcome of AD evaluation in the model's descriptor space taking into account the model's response domain and the observations in these two different spaces may not converge necessarily.

#### 5.4 QSAR model for soil adsorption coefficient $K_{oc}$

This model had been retrieved from the Joint Research Centre (JRC) QSAR Model Reporting Format (QMRF) repository. Its QMRF ID in the repository is Q2-10-26-179 [40-41].

#### 5.4.1 Model description

##### *OECD principle 1: A defined endpoint*

The adsorption coefficient serves as a useful indicator for the binding capacity of a given chemical substance to the organic matter of the soil/sludge.

This QSAR model was developed using the adsorption coefficient on soil determined based on the OECD test guideline TG121. The adsorption coefficient (Koc) corresponds to the ratio between the concentration of the substance in the soil or sludge to that in the aqueous phase, when the adsorption equilibrium has been achieved. This endpoint is unitless and for the modelling purpose, all the values were converted to their log unit (logKoc).

##### *OECD principle 2: An unambiguous algorithm*

The model was trained using 108 samples and it was validated on a test set with 54 samples. This QSAR model was developed using Multiple Linear Regression with the set of descriptors given in Table 5.7.

**Table 5.7** List of descriptors used to develop the logKoc model.

Descriptor	Description
<i>Desc1</i>	Polarity parameter (AM1)/distance is the difference of maximum positive and negative partial charges (from AM1 calculations).
<i>Desc2</i>	ALFA polarizability (DIP) (AM1) is the quantum chemically (AM1 method) obtained dipole based polarizability of molecule.
<i>Desc3</i>	Max net atomic charge (AM1) for C atoms is the maximum partial charge on any carbon atom (from AM1 calculation).
<i>Desc4</i>	WNSA 1 Weighted PNSA (PNSA1*TMSA/1000) (Zefirov) is the partially charge weighted partial negatively charged surface aread of molecule.

The resulting MLR equation is as follows:

$$\log K_{oc} = 0.96 - 0.26 * Desc1 + 1.07E-002 * Desc2 - 1.99 * Desc3 + 1.30E-002 * Desc4$$

*OECD principle 3: A defined domain of applicability*

The authors used a range based AD approach considering the range of each descriptor values used for model development. This approach has been already discussed in this thesis as one of the classical AD methodologies. The results for implementing this approach will be provided later in this section where the AD for this model will be evaluated using different approaches.

*OECD principle 4: Appropriate measures of goodness-of-fit, robustness and predictivity*

Table 5.8 provides with the default model statistical parameters, retaining all the test samples within the model's AD.

**Table 5.8** *Model statistics for the logK<sub>oc</sub> model.*

Training set		Test set	
<i>R</i> <sup>2</sup>	<i>RMSE</i>	<i>Q</i> <sup>2</sup>	<i>RMSEP</i>
0.756	0.434	0.737	0.451

*OECD principle 5: A mechanistic interpretation, if possible*

The authors provided the following a posteriori mechanistic interpretation to relate the chosen set of descriptors to the modelled endpoint:

They explained that there exists a close relation between the soil sorption and water solubility as well as hydrophobicity. This indicates that the features useful in determining the latter two properties can be also significant in determining the modelled endpoint for this model. Descriptors Desc2 and Desc4 are sized based descriptors and usually the large chemicals are expected to have higher soil sorption since they are also associated with poor water solubility. On the other hand, descriptors Desc1 and Desc3 are charge based descriptors. The presence of an active functional group next to carbon is indicated by a high charge around it, which in turns indicates higher water solubility. Moreover, higher polarity is also a useful indicator of better

solubility. As a result, the regression coefficients for these descriptors are negative, indicating that their higher values can decrease the soil sorption.

#### 5.4.2 AD Evaluation for the *logK<sub>oc</sub>* model

Table 5.9 provides with an overview of the results derived implementing various classical and novel AD approaches on this model.

Test samples 20 and 21 were associated with the highest frequency and were rendered as unreliable prediction by all the approaches except for those cases where all the test samples were retained inside the model's AD, including both the novel AD approaches. Most of the Gaussian potential function based approaches excluded several other test samples from the model's AD. One of the major reasons for this could be their lower threshold values restricting the defined interpolation space. However, excluding several test samples to such extent didn't have any noticeable positive impact on the model statistics. For instance, Gaussian optimized kernel excluded 33.3% of the test samples; however, the associated  $Q^2$  remained almost the same as for approaches that retained all the test samples within the model's AD.

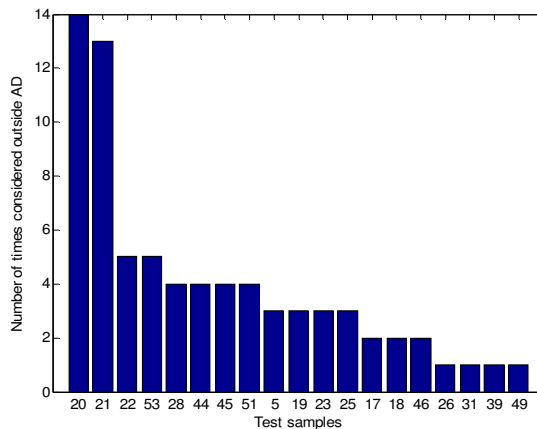


**Figure 5.5** Consensus test samples excluded from the AD of *logK<sub>oc</sub>* model

Figure 5.5 provides with a list of consensus test samples considered outside the AD with different approaches.



**Table 5.9** An overview of the results for AD evaluation on logKoc model (Test set: 54 samples)

AD method	Samples outside AD (%)	Q <sup>2</sup>	List of samples outside AD
<i>Bounding Box</i>	3.7	0.731	20 21
<i>PCA Bounding Box (First 2 PCs)</i>	0	0.737	None
<i>Convex Hull</i>	0	0.737	None
<i>Leverage approach</i>	3.7	0.731	20 21
<i>Centroid dist. (Euclidean, 95 percentile)</i>	3.7	0.731	20 21
<i>Centroid dist. (Manhattan, 95 percentile)</i>	3.7	0.731	20 21
<i>Centroid dist. (Mahalanobis, 95 percentile)</i>	5.6	0.726	18 20 21
<i>kNN general thr. (Euclidean, k=5)</i>	1.9	0.736	20
<i>kNN general thr. (Manhattan, k=5)</i>	0	0.737	None
<i>kNN general thr. (Mahalanobis, k=5)</i>	5.6	0.744	20 21 53
<i>Gaussian kernel: fixed</i>	22.2	0.750	5 19 20 21 22 23 25 28 44 45 51 53
<i>Gaussian kernel: optimized</i>	33.3	0.738	5 17 19 20 21 22 23 25 26 28 31 39 44 45 46 49 51 53
<i>Gaussian kernel: variable</i>	14.8	0.736	20 21 22 28 44 45 51 53
<i>Adaptive kernel</i>	3.7	0.731	20 21
<i>Epanechnikov kernel</i>	5.6	0.731	20 21 22
<i>kNN kernel (k=5)</i>	5.6	0.726	18 20 21
<i>Triangular kernel</i>	25.9	0.740	5 17 19 20 21 22 23 25 28 44 45 46 51 53
<i>Novel kNN approach (Euclidean, k=5)</i>	0	0.737	None
<i>Novel kNN approach (Manhattan, k=5)</i>	0	0.737	None
<i>Novel kNN approach (Mahalanobis, k=5)</i>	0	0.737	None
<i>Novel LCMD approach</i>	0	0.737	None

Table 5.10 provides with an overview of all the test samples excluded from the model's AD with different approaches. Sample 21 (p,p-DDE) is an interesting case since it was associated with a very high frequency of being excluded from the model's AD, however, was very well predicted (with absolute prediction error of 0.01). This indicates that the sample may not be an outlier in the model's response domain despite of it being an extrapolation in the model's descriptor space. Majority of the test samples listed in Table 5.11 were associated with an absolute prediction error lower than 0.5 log units.

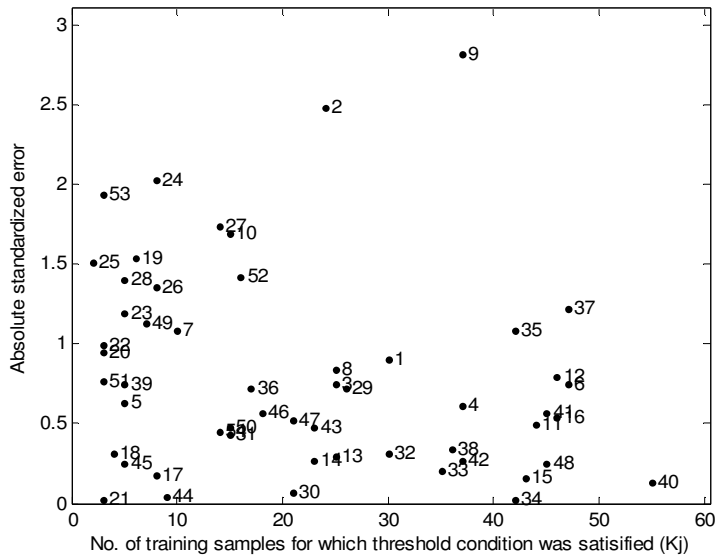


**Figure 5.6 :**  $K_j$  vs. Absolute standardized error plot for test samples of logKoc model

Figure 5.6 provides with the plot derived from the novel kNN based AD approach. As the novel approach didn't exclude any test samples from the model's AD, all the test samples satisfied at least one training threshold. Unlike several other AD approaches, this method did not consider test sample 21 as outside the AD, however, this sample satisfied very few training thresholds which somehow further highlights the fact that it may not be very structurally similar to the training space. On the other hand, test samples 2 and 9 which were not excluded from the model's AD by any of the implemented approaches satisfied a large number of training thresholds but were associated with highest absolute standardized errors.

**Table 5.10** *An overview of all the test samples excluded from the AD of logKoc model with different approaches*

Sample ID	Name	CAS	Exp. logKoc	Pred. logKoc	Abs. pred.error
5	Benomyl	17804-35-2	2.71	2.99	0.28
17	Triallate	2303-17-5	3.35	3.43	0.08
18	Benfluralin	1861-40-1	3.99	3.85	0.14
19	Nitralin	4726-14-1	2.92	3.60	0.68
20	p,p-DDT	50-29-3	5.31	4.89	0.42
21	p,p-DDE	72-55-9	4.82	4.83	0.01
22	Dieldrin	60-57-1	4.55	4.11	0.44
23	Azinphos methyl	86-50-0	2.28	2.81	0.53
25	Diazinon	333-41-5	2.75	2.08	0.67
26	Ethoprophos	13194-48-4	1.80	2.40	0.60
28	Malathion	121-75-5	3.07	2.45	0.62
31	4-Phenoxyphenylurea	78508-44-8	2.56	2.75	0.19
39	Chloroxuron	1982-47-4	3.55	3.22	0.33
44	Imazalil	35554-44-0	3.73	3.71	0.02
45	Oxadiazon	19666-30-9	3.51	3.62	0.11
46	Thiabendazole	148-79-8	3.24	2.99	0.25
49	EPN	2104-64-5	3.12	3.62	0.50
51	Sulprofos	35400-43-2	4.08	3.74	0.34
53	Anilazine	101-05-3	3.00	3.86	0.86

## 5.5 OH tropospheric degradation model

### 5.5.1 Model description

This model had been retrieved from the JRC's QMRF repository (QMRF ID : Q8-10-30-221) [42].

#### *OECD principle 1: A defined endpoint*

This QSAR model predicts the OH tropospheric degradation of volatile organic compounds. Reaction of chemicals with OH radicals highlights a very significant chemical process in the gasphase. Rate constants for OH radical degradation ( $\log K(\text{OH})$ ) were directly measured, converted to their log units and multiplied by -1 in order to obtain positive values [42].

#### *OECD principle 2: An unambiguous algorithm*

The original dataset of 423 samples was split into training and test set. The model was trained using 212 training molecules and it was validated on a test

set with 211 molecules. This QSAR model was developed using Multiple Linear Regression with the set of molecular descriptors shown in Table 5.11.

**Table 5.11** *List of descriptors used to develop the logK(OH) model.*

Descriptor	Description
Desc1	HASA-1/TMSA (AM1) is the relative solvent-accessible surface area of Hbonding acceptor atoms (from AM1 calculation)
Desc2	HOMO energy (AM1) is the energy of highest occupied molecular orbital energy.
Desc3	Relative number of aromatic bonds
Desc4	HACA-2/TMSA (Zefirov) is the sum of solvent-accessible surface area of H-bonding acceptor atoms, selected by threshold charge.

The resulting MLR equation is as follows:

$$\log K(\text{OH}) = 3.61 + 2.15 * \text{Desc1} - 0.698 * \text{Desc2} + 1.67 * \text{Desc3} - 12.7 * \text{Desc4}$$

#### *OECD principle 3: A defined domain of applicability*

The authors used following two ways to address the applicability domain of the model:

*Chemical identity basis:* Different group of chemicals used for training the model including aliphatic and aromatic hydrocarbons, alcohols, amines and halogenated compounds. The test samples are required to be structurally similar to the training samples.

*Descriptor ranges:* The minimum and maximum values for each descriptor were considered. This is a range based AD approach [42].

#### *OECD principle 4: Appropriate measures of goodness-of-fit, robustness and predictivity*

Table 5.12 provides with the default model statistical parameters, retaining all the test samples within the model's AD.

**Table 5.12** Model statistics for the  $\log K(OH)$  model.

Training set		Test set	
$R^2$	RMSE	$Q^2$	RMSEP
0.832	0.422	0.784	0.479

### *OECD principle 5: A mechanistic interpretation, if possible*

The authors provided the following a posteriori mechanistic interpretation to relate the chosen set of descriptors to the modelled endpoint. All the four descriptors used for model development were relevant to the H-abstraction. Descriptors *Desc1* and *Desc4* indicate the H-acceptor bonding as well as the size of the compounds. In theory they provide with different information. *Desc1* counts the solvent accessible surface area for all the H acceptor atoms while *Desc4* accounts for only the charged areas. The nucleophilicity of a molecule is indicated by the descriptor *Desc2* and finally, the aromatic compounds are differentiated from aliphatics by the descriptor *Desc3* [42].

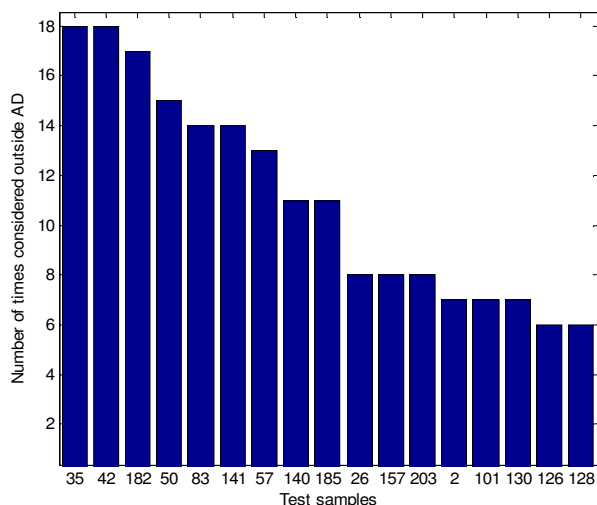
#### *5.5.1 AD evaluation for $\log K(OH)$ model*

Table 5.13 provides with an overview of the results derived implementing various classical and novel AD approaches.

This case study had been quite interesting with respect to the differences visible in the algorithms followed by different AD approaches. For instance, PCA bounding box and Convex hull approaches were the only approaches retaining all the 211 test samples within the model's AD. On the other hand, Gaussian kernels excluded up to one-fourth of the test samples outside the model's AD. No major improvements were observed in terms of  $Q^2$  with most of the approaches, where a reasonable number of test samples were excluded from the model's AD. Highest  $Q^2$  was recorded for Gaussian kernel (optimized) that excluded 28% of the test samples outside the model's AD taking six nearest neighbours into account. With both the novel AD approaches, the  $Q^2$  slightly improved from its default value.

**Table 5.13** An overview of the results for AD evaluation on  $\log K(OH)$  model (Test set: 211 samples)

AD method	Samples outside AD (%)	$Q^2$	List of samples outside AD
<i>Bounding Box</i>	0.9	0.783	26 35
<i>PCA Bounding Box (First 2 PCs)</i>	0	0.784	None
<i>Convex Hull</i>	0	0.784	None
<i>Leverage approach</i>	4.3	0.784	26 35 42 50 58 128 138 140 182
<i>Centroid dist. (Euclidean, 95 percentile)</i>	3.8	0.782	26 35 42 101 128 138 140 162
<i>Centroid dist. (Manhattan, 95 percentile)</i>	4.7	0.782	26 42 57 101 114 128 138 140 162 185
<i>Centroid dist. (Mahalanobis, 95 percentile)</i>	4.7	0.783	26 35 42 50 58 128 138 140 162 182
<i>kNN general thr. (Euclidean, k=5)</i>	3.8	0.786	35 42 50 57 83 141 182 185
<i>kNN general thr. (Manhattan, k=5)</i>	4.7	0.788	35 42 50 57 83 130 141 182 185 203
<i>kNN general thr. (Mahalanobis, k=5)</i>	6.2	0.788	2 35 42 50 57 58 83 130 141 157 182 185 203
<i>Gaussian kernel: fixed</i>	9.5	0.785	2 35 42 50 57 78 83 84 100 116 121 122 130 140 141 157 182 185 200 203
<i>Gaussian kernel: optimized</i>	28.0	0.826	2 9 16 26 29 35 40 42 44 47 50 51 57 58 62 63 65 78 81 83 84 85 86 87 88 91 100 101 102 114 116 118 119 121 122 126 128 129 130 133 139 140 141 142 144 146 157 173 174 178 182 184 185 193 199 200 202 203 204
<i>Gaussian kernel: variable</i>	23.2	0.795	2 9 35 38 39 40 42 44 50 51 57 58 62 63 65 78 83 84 85 88 90 91 100 101 102 116 119 121 122 126 130 133 139 140 141 142 146 157 169 174 178 182 184 185 193 197 200 202 203
<i>Gaussian kernel: adaptive</i>	6.6	0.784	26 35 42 50 57 83 101 128 138 140 141 162 182 185
<i>Epanechnikov kernel</i>	4.3	0.785	35 42 50 57 83 140 141 182 185
<i>kNN kernel (k=5)</i>	5.2	0.784	35 42 50 57 83 116 140 141 157 182 185
<i>Triangular kernel</i>	7.1	0.787	2 35 42 50 57 83 100 121 122 130 141 157 182 185 203
<i>Novel kNN approach (Euclidean, k=6)</i>	4.3	0.787	35 42 50 57 83 84 126 141 182
<i>Novel kNN approach (Manhattan, k=6)</i>	4.3	0.787	35 42 83 126 182 203 126 141 182
<i>Novel kNN approach (Mahalanobis, k=6)</i>	5.2	0.786	2 35 40 42 50 57 83 101 141 157 182
<i>Novel LCMD approach</i>	9.5	0.782	2 26 35 42 50 63 83 88 100 101 121 122 126 130 140 141 157 182 200 203



**Figure 5.7** Consensus test samples excluded from the AD of  $\log K(\text{OH})$  model

Figure 5.7 provides with an overview of the test samples frequently excluded from the model's AD. Since the entire list including the test samples excluded by Gaussian kernel approaches is quite long, the figure was restricted to highlight only those samples with the highest frequency of being excluded. Clearly, samples like 35 and 42 were considered outside the AD with most of the approaches including both the novel AD approaches. On the other hand, a large set of test samples considered exclusively using Gaussian kernel approaches may need attention since excluding them just on the basis of one set of approaches may not be an enough justification. Table 5.15 provides with some useful information about all the test samples listed in Table 5.14.

**Table 5.14** An overview of all the test samples excluded from the AD of  $\log K(\text{OH})$  model with different approaches

Sample ID	Name	CAS	Exp. $-\log K(\text{OH})$	Pred. $-\log K(\text{OH})$	Abs. pred.error
2	Benzene	71-43-2	11.91	11.18	0.73
9	3-methyl-1-butanethiol	541-31-1	10.28	9.98	0.30
16	Chlorofluoromethane	593-70-4	13.38	13.15	0.23
26	1,1-dichloro-2,2,2-trifluoroethane	306-83-2	13.44	14.01	0.57
29	2-chloroethanol	107-07-3	11.85	12.06	0.21
35	1,1,2,2-tetrachloroethene	127-18-4	12.77	12.54	0.23
38	2-butanethiol	513-53-1	10.40	10.02	0.38

## 5. Case studies

Sample ID	Name	CAS	Exp. -logK(OH)	Pred. -logK(OH)	Abs. pred.error
39	1,3-dioxane	505-22-6	11.04	11.42	0.38
40	methyl trifluoroacetate	431-47-0	13.28	13.50	0.22
42	Hexafluorobenzene	392-56-3	12.79	13.42	0.63
44	Fluorobenzene	462-06-6	12.27	11.47	0.80
47	isobutyric acid	79-31-2	11.70	11.87	0.17
50	1,1,2-trichloroethene	79-01-6	11.63	12.33	0.70
51	dimethyl-nitramine	4164-28-7	11.42	11.94	0.52
57	1,1,1-trifluoroethane	420-46-2	14.77	14.05	0.72
58	trans-1,2-dichloroethene	156-60-5	11.75	12.02	0.27
62	Ethanol	64-17-5	11.52	11.29	0.23
63	Aniline	62-53-3	9.93	10.31	0.38
65	Difluoromethane	75-10-5	13.93	13.32	0.61
78	o-nitrotoluene	88-72-2	12.16	11.89	0.27
81	ethyl methyl sulphide	624-89-5	11.07	9.77	1.30
83	hydrogen cyanide	74-90-8	13.52	12.71	0.81
84	dimethyl disulphide	624-92-0	9.70	10.47	0.77
85	trimethyl phosphate	512-56-1	11.13	12.18	1.05
86	1,1-dichloroethene	75-35-4	10.84	12.03	1.19
87	1,1,1-trichloroethane	71-55-6	13.80	13.50	0.31
88	o-dichlorobenzene	95-50-1	12.38	12.03	0.35
90	3-methylfuran	930-27-8	10.03	10.21	0.18
91	Ethanethiol	75-08-1	10.33	10.20	0.13
100	m-dichlorobenzene	541-73-1	12.14	12.16	0.02
101	1,1,1,2-tetrafluoroethane	811-97-2	14.05	14.07	0.01
102	1-bromoethane	74-96-4	12.46	11.89	0.57
114	Naphthalene	91-20-3	10.67	10.66	0.02
116	m-nitrotoluene	99-08-1	12.02	11.94	0.08
118	1,2,3-trichloropropane	96-18-4	12.37	12.57	0.20
119	Monomethylhydrazine	60-34-4	10.19	10.53	0.34
121	p-dichlorobenzene	106-46-7	12.50	12.01	0.49
122	Methanethiol	74-93-1	10.47	10.29	0.18
126	N,N-dimethyl-aniline	121-69-7	9.83	9.89	0.06
128	Trichloromethane	67-66-3	13.00	13.74	0.74
129	Diethylaminoethanol	100-37-8	10.10	10.00	0.10
130	Benzonitrile	100-47-0	12.48	11.65	0.83
133	benzyl alcohol	100-51-6	10.64	10.91	0.26
138	chloro,difluoromethane	75-45-6	14.32	14.02	0.30
139	t-butyl hydroperoxide	75-91-2	11.52	11.53	0.01
140	Glycolaldehyde	141-46-8	11.00	11.28	0.28
141	4-chlorobenzotrifluoride	98-56-6	12.62	12.56	0.06
142	dimethyl sulphide	75-18-3	11.37	9.81	1.56
144	Dichloromethane	75-09-2	12.84	13.11	0.27
146	1,1-dichloroethane	75-34-3	12.59	12.75	0.15
157	Propionitrile	107-12-0	12.71	12.35	0.36
162	1,2-dichloro-1,1-difluoroethane	1649-08-7	13.72	13.77	0.05
169	2-ethoxyethanol	110-80-5	10.92	11.17	0.25
173	Pyridine	110-86-1	12.31	10.63	1.69
174	dimethyl-amine	124-40-3	10.18	10.19	0.01



## 5. Case studies

Sample ID	Name	CAS	Exp. $-\log K(\text{OH})$	Pred. $-\log K(\text{OH})$	Abs. pred.error
178	2-methyl-2-propanethiol	75-66-1	10.47	10.03	0.44
182	1,4-naphthoquinone	130-15-4	11.51	11.88	0.37
184	Methanol	67-56-1	12.03	11.34	0.69
185	2,4-dichlorophenol	120-83-2	11.98	11.73	0.25
193	Tetrahydrothiophene	110-01-0	10.70	9.71	0.99
197	Pyrrole	109-97-7	10.00	9.67	0.33
199	Furan	110-00-9	10.39	10.38	0.01
200	Phenol	108-95-2	10.59	10.73	0.14
202	Methylbenzene	108-88-3	11.21	10.79	0.42
203	Thiophenol	108-98-5	10.95	10.54	0.41
204	3-methyl-1,3-pentadiene	4549-74-0	9.87	10.68	0.81

Figure 5.8 provides with a plot derived from the novel kNN based AD approach. All the test samples are plotted based on their absolute standardized error as well as the number of times they satisfied individual training thresholds. As expected, a decreasing pattern was observed from left to right, indicating lower error in prediction with increasing satisfied threshold conditions ( $K_j$ ).

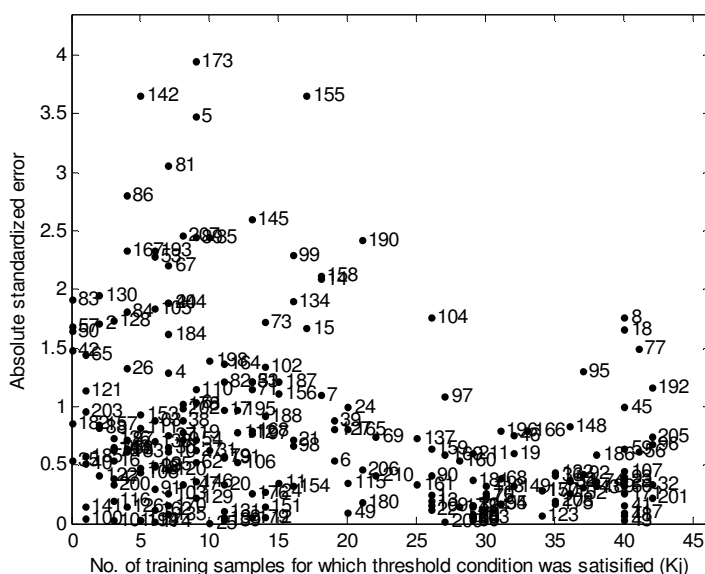


**Figure 5.8**  $K_j$  vs. Absolute standardized error plot for test samples of  $\log K(OH)$  model

Test samples like 35 and 42 (1,1,2,2 tetrachloroethene and hexafluorobenzene) did not satisfy any training thresholds, though were not associated with the highest prediction error. This fact further confirms the fact that extrapolations in the descriptor space may not always reflect the outliers in a model's response domain. It also somehow indicates the model's ability to extrapolate the predictions for test samples that may not be very structurally similar to the training space.

## 5.6 Ready biodegradability of chemicals

### 5.6.1 Model description

#### *OECD principle 1: A defined endpoint*

This set of classification models is aimed at evaluating the persistence of chemical substances in the environment by predicting their ready

biodegradability. Since the accumulation of persistent chemicals could lead to hazardous impacts on a longer time scale, REACH regulation requires the information relevant to the ready biodegradability of chemical substances that are produced or imported in quantities greater than one ton per year. Being classification models, their resulting predictions for query chemicals are either if they are Ready Biodegradable (RB) or not ready biodegradable (NRB) [39].

*OECD principle 2: An unambiguous algorithm*

Three QSAR models were developed using the following different classification modelling techniques to incorporate linear, non-linear and local models:  $k$  Nearest Neighbours (kNN), partial least squares discriminant analysis (PLSDA) and support vector machines (SVM). Since individual models can account for different amounts of noise, two consensus models were developed in order to improve the overall quality in predictions. The first consensus model allocated the most frequent class predicted for a query chemical using the above three classification models. On the other hand, the second consensus model allocated a given query chemical to a class that was predicted the same with all the three individual models; otherwise no class was assigned. Model calibration in all the cases was carried out using a data set of 837 molecules while it was validated on a test set consisting of 218 molecules. Further, the developed models were evaluated on an external validation test set consisting of 670 molecules. Table 5.15 provides with an overview of all the molecular descriptors from the DRAGON 6 package used in developing the three classification models [47]. The descriptor selection for this set of models was performed using Genetic Algorithm (GA).

**Table 5.15** *List of descriptors used to develop the biodegradability models.*

Descriptor	Description	Model
<i>B01[C-Br]</i>	presence/absence of C–Br at topological distance 1	PLSDA
<i>B03[C-Cl]</i>	presence/absence of C–Cl at topological distance 3	PLSDA
<i>B04[C-Br]</i>	presence/absence of C–Br at topological distance 4	PLSDA
<i>C%</i>	percentage of C atoms	kNN–PLSDA
<i>C-026</i>	R–CX–R	SVM
<i>F01[N-N]</i>	frequency of N–N at topological distance 1	kNN
<i>F02[C-N]</i>	frequency of C–N at topological distance 2	SVM
<i>F03[C-N]</i>	frequency of C–N at topological distance 3	kNN
<i>F03[C-O]</i>	frequency of C–O at topological distance 3	PLSDA
<i>F04[C-N]</i>	frequency of C–N at topological distance 4	kNN–PLSDA
<i>HyWi_B(m)</i>	hyper-Wiener-like index (log function) from Burden matrix weighted by mass	PLSDA
<i>J_Dz(e)</i>	Balaban-like index from Barysz matrix weighted by Sanderson electronegativity	kNN
<i>LOC</i>	lopping centric index	PLSDA
<i>Me</i>	mean atomic Sanderson electronegativity (scaled on Carbon atom)	PLSDA
<i>Mi</i>	mean first ionization potential (scaled on carbon atom)	PLSDA
<i>N-073</i>	Ar2NH/Ar3N/Ar2N–Al/R...N...R	PLSDA
<i>nArCOOR</i>	number of esters (aromatic)	SVM
<i>nArNO2</i>	number of nitro groups (aromatic)	PLSDA
<i>nCb-</i>	number of substituted benzene C(sp2)	kNN–SVM
<i>nCIR</i>	number of circuits	PLSDA
<i>nCp</i>	number of terminal primary C(sp3)	kNN
<i>nCrt</i>	number of ring tertiary C(sp3)	SVM
<i>nCRX3</i>	number of CRX3	PLSDA
<i>nHDon</i>	number of donor atoms for H-bonds (N and O)	SVM
<i>nHM</i>	number of heavy atoms	kNN
<i>nN</i>	number of nitrogen atoms	SVM
<i>nN-N</i>	number of N hydrazines	PLSDA–SVM
<i>nO</i>	number of oxygen atoms	kNN–PLSDA
<i>NssssC</i>	number of atoms of type ssssc	kNN–SVM
<i>nX</i>	number of halogen atoms	SVM
<i>Psi_i_1d</i>	intrinsic state pseudoconnectivity index–type 1d	PLSDA
<i>Psi_i_A</i>	intrinsic state pseudoconnectivity index□type S average	SVM
<i>SdO</i>	sum of dO E-states	PLSDA
<i>SdssC</i>	sum of dssC E-states	kNN
<i>SM6_B(m)</i>	spectral moment of order 6 from Burden matrix weighted by mass	SVM
<i>SM6_L</i>	spectral moment of order 6 from Laplace matrix	PLSDA
<i>SpMax_A</i>	leading eigenvalue from adjacency matrix (Lovasz–Pelikan index)	PLSDA
<i>SpMax_B(m)</i>	leading eigenvalue from Burden matrix weighted by mass	SVM
<i>SpMax_L</i>	leading eigenvalue from Laplace matrix	kNN–PLSDA–SVM
<i>SpPosA_B(p)</i>	normalized spectral positive sum from Burden matrix weighted by polarizability	PLSDA
<i>Tl2_L</i>	second Mohar index from Laplace matrix	PLSDA

*OECD principle 3: A defined domain of applicability*

The article from where these models were retrieved does not provide with any direct evaluation of the model's AD. However, an article focussing exclusively on evaluating their AD is currently in preparation.

*OECD principle 4: Appropriate measures of goodness-of-fit, robustness and predictivity*

Table 5.16 provides with the default model statistical parameters, retaining all the test samples within the model's AD. It should be noted that for the second consensus model the not assigned molecules were not considered to evaluate the TP and TN.

*OECD principle 5: A mechanistic interpretation, if possible*

The authors provided following a posteriori mechanistic interpretation to relate the chosen set of descriptors to the modelled endpoint:

The usefulness of the chosen descriptors was interpreted deriving score and loading plots from the PCA study on the training set and projecting test set molecules over the training space. For the PLSDA model, the descriptors were related to biodegradability directly using the latent variables used for model development.

kNN model: Descriptors encoding information about the substituted benzenes and nitrogen (functional group counts based descriptor nCb- and 2D atom pairs based descriptors F01[N-N], F04[C-N], and F03[C-N]) differentiated the NRB from RB molecules based on the presence of cyclic and nitro groups. nHM indicated the presence of heavy atoms which may be more relevant to the NRB molecules. Since RB molecules are less branched than NRB ones, descriptors SdssC, NssssC and nCp were more oriented towards the NRB molecules indicating that increased branching molecules could lower the ready biodegradability.

**Table 5.16** *Model statistics for the biodegradability models.*

Model	Desc	k/LVs/ c	Fitting			test set			validation set		
			ER	Sn	Sp	ER	Sn	Sp	ER	Sn	Sp
kNN	12	6	0.14	0.84	0.89	0.15	0.81	0.9	0.17	0.75	0.91
PLSDA	23	5	0.14	0.88	0.83	0.15	0.83	0.87	0.17	0.80	0.86
SVM	14	5	0.14	0.81	0.92	0.14	0.82	0.91	0.18	0.74	0.91
consensus 1	41		0.11	0.86	0.91	0.13	0.82	0.92	0.17	0.76	0.91
consensus 2	41		0.07 (19% not assigned)	0.91	0.95	0.09 (15% not assigned)	0.88	0.94	0.13 (13% not assigned)	0.81	0.94

Desc: Descriptors used, *k/LVs/c*: indicates the optimal parameters, no. of nearest neighbours (*k*) for kNN, number of latent variables (LVs) for PLSDA and the cost (*c*) for SVM. ER: Error Rate, Sn: Sensitivity indicating correctly predicted non ready biodegradable, Sp: Specificity indicating correctly predicted ready biodegradable

PLSDA model: Matrix based descriptors contained information about the molecular branching and based on the significant latent variables used, they were clearly oriented towards the NRB molecules, which is in agreement with the findings that lower branching favours ready biodegradation.

The descriptors containing information about cycles, nitrogen and halogens were oriented towards NRB molecules like for the kNN model. Descriptors indicating the presence of oxygen further differentiated the RB from NRB molecules, indeed functional groups with oxygen atoms assist biodegradation process.

SVM model: Several descriptors encoding information about the molecular branching, aromatic groups and halogens (including matrix-based descriptors, constitutional indices and atom-centred fragments) differentiated the RB from NRB molecules, being more oriented towards the latter ones.

To better understand the usefulness of matrix-based descriptors towards ready biodegradability, their encoded information was further explored by performing OLS regression between these targeted matrix-based descriptors and DRAGON molecular descriptors. As a result of this analysis, these matrix-based descriptors were associated with properties like molecular branching, cyclicity and molecular size which are significant parameters impacting the biodegradability.

#### *5.6.2 AD evaluation on consensus models*

One of the important aspects of considering this case study is to perform the AD evaluation on consensus models. Since consensus models are mainly relying on the output derived from the set of primary models (in this case, kNN, PLSDA and SVM models), following strategy was adopted to deal with defining the AD of the resulting two consensus models.

The AD of all the three individual models was evaluated like for the other case studies using all the different classical and novel AD approaches discussed earlier (though the results are not discussed for these models). For both the consensus models, a given test sample was considered within its AD with a given approach only if it was retained inside the AD of all the three individual models. The decision rule could be interesting since the final decision to retain or discard a test sample in the AD depends on the output from three different models-local, linear and non-linear. The decision rule adopted towards defining the AD resembles the criterion used by the second model in considering a test sample to be RB or NRB.

Tables 5.17 and 5.18 provide with an overview of the results derived with different classical and novel AD approaches on first and second consensus models, respectively. The test samples listed being outside the AD are the same since the same AD criterion was followed by both the consensus models. The difference however lies in the model statistical parameters since the predicted responses for both these models are different. Moreover, there are some test samples with unassigned class in the case of second consensus

model. In both the cases, no significant impacts were observed on the resulting statistical parameters.

In theory, a test sample can only be considered within the consensus model's AD provided that it was included within the AD of three individual models which were based on very diverse algorithms towards model development. If a test sample falls inside the AD of local, linear and non-linear models, this further adds to the reliability in considering such test samples within the model's AD. However, such strict criterion may also make the defined AD more restrictive to the test samples. For both the consensus models, none of the approaches were able to significantly improve the model statistical parameters retaining reasonable number of test samples within the model's AD.

**Table 5.17** *An overview of the results for AD evaluation on the first consensus model*

AD method	Samples outside AD (%)	ER	Sn	Sp	List of samples outside AD
<i>Bounding Box</i>	4.1	0.14	0.82	0.91	2 73 130 166 181 189 192 215 217
<i>PCA Bounding Box</i>	0.5	0.13	0.82	0.92	217
<i>Convex Hull</i>	-	-	-	-	-
<i>Leverage approach</i>	13.3	0.13	0.84	0.90	2 19 24 27 57 73 74 76 77 78 80 83 91 94 96 130 134 146 159 164 166 186 189 190 192 200 215 216 217
<i>Centroid dist. (Euclidean, 95 percentile)</i>	9.2	0.14	0.82	0.91	57 73 74 76 77 78 94 134 159 164 166 172 186 190 192 200 202 215 216
<i>Centroid dist. (Manhattan, 95 percentile)</i>	8.7	0.14	0.82	0.91	57 73 74 76 77 78 91 94 134 151 152 159 166 192 200 202 215 216 217
<i>Centroid dist. (Mahalanobis, 95 percentile)</i>	10.6	0.13	0.83	0.90	2 27 57 73 74 76 77 78 83 91 94 96 130 134 159 164 166 186 189 192 200 215 217
<i>kNN general thr (Euclidean, k=5)</i>	10.1	0.13	0.83	0.90	27 57 73 76 77 91 94 134 147 151 152 164 166 186 189 190 192 196 200 215 216 217
<i>kNN general thr. (Manhattan, k=5)</i>	8.7	0.14	0.82	0.91	73 76 77 80 91 94 134 147 151 152 166 186 189 190 192 200 215 216 217
<i>kNN general thr. (Mahalanobis, k=5)</i>	16.1	0.13	0.84	0.90	2 24 27 57 73 74 75 76 77 78 80 83 90 91 94 130 134 147 151 152 158 159 164 166 173 186 189 190 192 196 200 212 215 216 217



## 5. Case studies

AD method	Samples outside AD (%)	ER	Sn	Sp	List of samples outside AD
<i>Gaussian kernel: fixed</i>	34.9	0.13	0.85	0.89	2 5 7 19 24 27 30 47 48 51 57 58 62 64 67 69 72 73 75 76 77 78 79 80 82 83 88 89 90 91 92 94 96 105 106 110 111 112 113 115 116 119 121 122 124 126 127 130 133 134 135 137 140 141 142 144 146 147 148 149 151 152 153 154 157 158 159 160 161 164 166 168 172 173 174 178
<i>Gaussian kernel: optimized</i>	88.5	0.00	1.00	1.00	All test samples except 9 14 15 16 17 18 22 41 46 53 74 97 103 108 109 117 128 151 152 153 154 155 156 157 158 167 171 201 202 203 205 206 208 209
<i>Gaussian kernel: variable</i>	14.7	0.13	0.84	0.90	24 27 57 73 74 76 77 78 83 91 94 105 134 135 147 151 152 158 159 161 164 166 186 187 189 190 192 196 200 215 216 217
<i>Adaptive kernel</i>	11.9	0.13	0.83	0.90	27 57 73 74 75 76 77 78 83 94 105 134 147 151 152 164 166 186 189 190 192 196 200 215 216 217
<i>Epanechnikov kernel</i>	20.6	0.14	0.84	0.89	2 24 27 57 73 75 76 77 78 80 83 90 91 94 96 110 112 116 130 133 134 135 144 147 151 152 154 158 159 161 164 166 172 173 185 186 187 189 190 192 196 200 215 216 217
<i>kNN kernel</i>	11.9	0.13	0.84	0.90	24 27 57 73 74 76 77 78 83 91 94 134 147 151 152 164 166 186 189 190 192 196 200 215 216 217
<i>Triangular kernel</i>	77.1	0.05		1.00	All test samples except 9 11 12 13 14 15 16 17 18 22 29 33 34 38 39 41 44 46 53 59 60 66 68 74 84 87 97 99 100 102 103 108 109 114 117 128 162 163 165 167 169 170 171 177 183 201 203 205 206 208 209
<i>Novel kNN approach (Euclidean)</i>	11.0	0.13	0.83	0.90	27 57 73 75 76 77 80 94 134 152 154 158 161 164 166 173 186 189 190 192 200 215 216 217
<i>Novel kNN approach (Manhattan)</i>	11.9	0.14	0.81	0.90	2 57 73 76 77 80 91 94 105 134 135 147 151 152 161 164 166 186 187 189 190 192 200 215 216 217
<i>Novel kNN approach (Mahalanobis)</i>	11.5	0.13	0.83	0.90	2 27 73 76 77 90 91 94 110 134 147 151 152 158 164 166 186 187 189 190 192 200 215 216 217
<i>Novel LCMD approach</i>	11.5	0.14	0.83	0.90	2 27 57 73 74 76 77 78 83 91 94 96 130 134 146 159 164 166 186 189 192 200 215 216 217

## 5. Case studies

**Table 5.18** *An overview of the results for AD evaluation on the second consensus model*

AD method	Samples outside AD (%)	ER	Sn	Sp	List of samples outside AD
<i>Bounding Box</i>	4.1	0.08	0.89	0.94	2 130 166 181 189 192 215 217
<i>PCA Bounding Box</i>	0.5	0.08	0.90	0.94	217
<i>Convex Hull</i>	-	-	-	-	-
<i>Leverage approach</i>	13.3	0.07	0.93	0.93	19 24 27 57 73 74 76 77 78 80 83 91 94 96 130 134 146 159 164 166 186 189 190 192 200 215 216 217
<i>Centroid dist. (Euclidean, 95 percentile)</i>	9.2	0.08	0.90	0.94	57 73 74 76 77 78 94 134 159 164 166 172 186 190 192 200 202 215 216
<i>Centroid dist. (Manhattan, 95 percentile)</i>	8.7	0.08	0.90	0.94	57 73 74 76 77 78 91 94 134 151 152 159 166 192 200 202 215 216 217
<i>Centroid dist. (Mahalanobis, 95 percentile)</i>	10.6	0.08	0.91	0.93	2 27 57 73 74 76 77 78 83 91 94 96 130 134 159 164 166 186 189 192 200 215 217
<i>kNN general thr (Euclidean, k=5)</i>	10.1	0.08	0.91	0.93	27 57 73 76 77 91 94 134 147 151 152 164 166 186 189 190 192 196 200 215 216 217
<i>kNN general thr. (Manhattan, k=5)</i>	8.7	0.08	0.90	0.93	73 76 77 80 91 94 134 147 151 152 166 186 189 190 192 200 215 216 217
<i>kNN general thr. (Mahalanobis, k=5)</i>	16.1	0.07	0.93	0.93	2 24 27 57 73 74 75 76 77 78 80 83 90 91 94 130 134 147 151 152 158 159 164 166 173 186 189 190 192 196 200 212 215 216 217
<i>Gaussian kernel: fixed</i>	34.9	0.07	0.93	0.92	5 7 19 24 27 30 47 48 51 57 58 62 64 67 69 72 73 75 76 77 78 79 80 82 83 88 89 90 91 92 94 96 105 106 110 111 112 113 115 116 119 121 122 124 126 127 130 133 134 135 137 140 141 142 144 146 147 148 149 151 152 153 154 157 158 159 160 161 164 166 168 172 173 174 178
<i>Gaussian kernel: optimized</i>	88.5	0.00	1.00	1.00	All test samples except 9 14 15 16 17 18 22 41 46 53 74 97 103 108 109 117 128 151 152 153 154 155 156 157 158 167 171 201 202 203 205 206 208 209
<i>Gaussian kernel: variable</i>	14.7	0.07	0.93	0.93	24 27 57 73 74 76 77 78 83 91 94 105 134 135 147 151 152 158 159 161 164 166 186 187 189 190 192 196 200 215 216 217

## 5. Case studies

AD method	Test outside AD (%)	ER	Sn	Sp	List of samples outside AD
<i>Adaptive kernel</i>	11.9	0.08	0.91	0.93	27 57 73 74 75 76 77 78 83 94 105 134 147 151 152 164 166 186 189 190 192 196 200 215 216 217
<i>Epanechnikov kernel</i>	20.6	0.08	0.93	0.92	24 27 57 73 75 76 77 78 80 83 90 91 94 96 110 112 116 130 133 134 135 144 147 151 152 154 158 159 161 164 166 172 173 185 186 187 189 190 192 196 200 215 216 217
<i>kNN kernel</i>	11.9	0.07	0.93	0.93	24 27 57 73 74 76 77 78 83 91 94 134 147 151 152 164 166 186 189 190 192 196 200 215 216 217
<i>Triangular kernel</i>	77.1	0.08	0.95	1.00	All test samples except 9 11 12 13 14 15 16 17 18 22 29 33 34 38 39 41 44 46 53 59 60 66 68 74 84 87 97 99 100 102 103 108 109 114 117 128 162 163 165 167 169 170 171 177 183 201 203 205 206 208 209
<i>Novel kNN approach (Euclidean)</i>	11.0	0.07	0.91	0.93	27 57 73 75 76 77 80 94 134 152 154 158 161 164 166 173 186 189 190 192 200 215 216 217
<i>Novel kNN approach (Manhattan)</i>	11.9	0.09	0.89	0.93	57 73 76 77 80 91 94 105 134 135 147 151 152 161 164 166 186 187 189 190 192 200 215 216 217
<i>Novel kNN approach (Mahalanobis)</i>	11.5	0.08	0.91	0.93	27 73 76 77 90 91 94 110 134 147 151 152 158 164 166 186 187 189 190 192 200 215 216 217
<i>Novel LCMD approach</i>	11.5	0.08	0.91	0.93	2 27 57 73 74 76 77 78 83 91 94 96 130 134 146 159 164 166 186 189 192 200 215 216 217

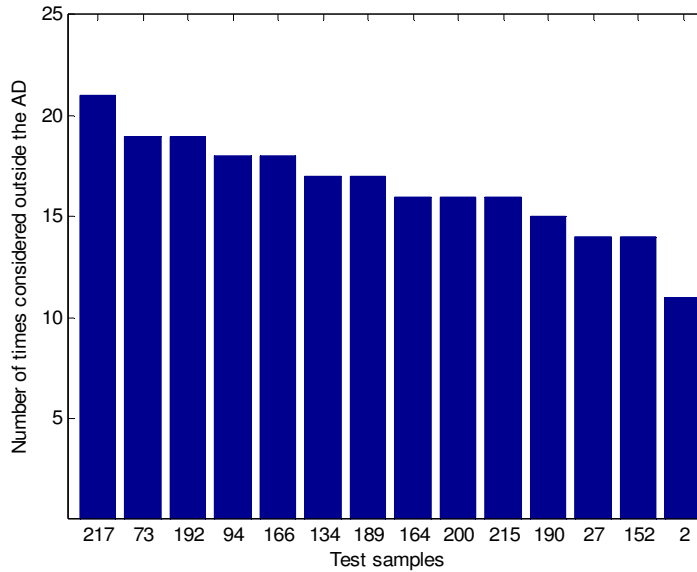


**Figure 5.9** *Consensus test samples excluded from the AD of consensus models*

Figure 5.9 provides with an overview of the most commonly excluded test samples from the AD of the both consensus models.

Table 5.19 provides with an overview of all the test samples considered outside the AD with different approaches. It enlists almost entire test set since with approaches like fixed and optimized gaussian kernel as well as triangular kernel, a huge number of test samples were considered as outside the AD. For each of the test sample listed in this table, its experimental response as well as the predicted class from both the consensus models were provided. Several of the test samples listed in Figure 5.9 were predicted reliably even if they were rendered as unreliable in the model's descriptor space being excluded from the model's AD with several diverse approaches. This resembles the observation made for the regression models dealt as case studies earlier in this thesis work. This implies that the results derived in a model's descriptor space may not necessarily reflect the results derived in the response domain of that model.

**Table 5.19** *An overview of all the test samples excluded from the AD of both consensus models with different approaches*

Sample ID	Name	CAS	Exp.class	consensus 1	consensus 2
1	n-heptane	142-82-5	RB	RB	RB
2	ethylene oxide	75-21-8	RB	RB	RB
3	Toluene	108-88-3	RB	RB	RB
4	di-n-butylamine	111-92-2	RB	RB	RB
5	3,7-dimethyl-1,6-octadien-3-ol	78-70-6	RB	NRB	NRB
6	3,6-dioxadecan-1-ol	112-34-5	RB	RB	RB
7	n-butyraldehyde	123-72-8	RB	RB	RB
8	4-hydroxy-4-methyl-2-pentanone	123-42-2	RB	NRB	not assigned
10	bis(2-ethylhexyl) fumarate	141-02-6	RB	RB	RB
11	12-hydroxyoctadecanoic acid	106-14-9	RB	RB	RB
12	Nonadecaneonitrile	28623-46-3	RB	RB	RB
13	(dichloromethyl)benzene	98-87-3	RB	NRB	NRB
19	bis(2-hydroxyethyl) terephthalate	959-26-2	RB	RB	RB
20	4-hydroxybenzonitrile	767-00-0	RB	NRB	not assigned
21	p-toluenesulfonic acid	104-15-4	RB	RB	not assigned
23	methyl 3-oxo-2-pentylcyclopentylacetate	24851-98-7	RB	RB	not assigned
24	Imidazole	288-32-4	RB	NRB	NRB
25	3-hydroxypyridine	109-00-2	RB	RB	RB
26	1-hexene	592-41-6	RB	RB	RB
27	isopropyl bromide	75-26-3	RB	NRB	NRB
28	n-butylamine	109-73-9	RB	RB	RB
29	hexadecan-1-ol	36653-82-4	RB	RB	RB
30	2-methoxyethanol	109-86-4	RB	RB	RB
31	propyl acetate	109-60-4	RB	RB	RB
32	13-docosenoamide	112-84-5	RB	RB	not assigned
33	adipic acid	124-04-9	RB	RB	RB
34	2-methoxyethyl acrylate	3121-61-7	RB	RB	RB
35	2-hydroxypropyl methacrylate	923-26-2	RB	RB	RB
36	2,4-hexadienic acid (synonym:sorbic acid)	110-44-1	RB	RB	RB
37	2-methylenesuccinic acid	97-65-4	RB	RB	RB
38	butyl acetoacetate	591-60-6	RB	RB	RB
39	Aniline	62-53-3	RB	NRB	not assigned
40	benzyl methacrylate	2495-37-6	RB	RB	RB
42	styrene oxide	96-09-3	RB	NRB	not assigned
43	benzoylaminoacetic acid	495-69-2	RB	RB	RB
44	2-(methylamino)benzoic acid	119-68-6	RB	RB	not assigned
45	alpha-terpineol	98-55-5	RB	NRB	NRB
47	3-acetyl-6-methyl-2,4(3H)-pyrandione (synonym:dehydroacetic acid)	520-45-6	RB	RB	RB
48	Xylitol	87-99-0	RB	RB	RB
49	Benzoin	119-53-9	RB	RB	not assigned
50	beta-alanine	107-95-9	RB	RB	RB

## 5. Case studies

Sample ID	Name	CAS	Exp.class	consensus 1	consensus 2
51	1-chlorooctane	111-85-3	RB	RB	not assigned
52	2-ethoxyethanol	110-80-5	RB	RB	RB
54	methyl dodecanoate	111-82-0	RB	RB	RB
55	succinic acid	110-15-6	RB	RB	RB
56	2-hydroxyethyl acrylate	818-61-1	RB	RB	RB
57	2-hydroxy-1,2,3-propanetricarboxylic acid	77-92-9	RB	RB	not assigned
58	DL-tartaric acid	133-37-9	RB	RB	RB
59	sec-butyl alcohol	78-92-2	RB	RB	RB
60	terephthalic acid	100-21-0	RB	RB	RB
61	Phenylacetone nitrile	140-29-4	RB	RB	RB
62	1-methyl-4-(1-methylvinyl)cyclohexene	138-86-3	RB	NRB	not assigned
63	cyclohexyl methacrylate	101-43-9	RB	RB	RB
64	2-(methylamino)ethanol	109-83-1	RB	RB	RB
65	1,1'-iminodi-2-propanol	110-97-4	RB	RB	RB
66	2-[2-(2-methoxyethoxy)ethoxy]ethanol	112-35-6	RB	RB	RB
67	chloroacetic acid	79-11-8	RB	RB	RB
68	diethyl phthalate(synonym:di-n-octyl phthalate)	117-84-0	RB	RB	RB
69	dicyclohexyl benzene-1,2-dicarboxylate	84-61-7	RB	NRB	not assigned
70	beta-naphthol	135-19-3	RB	NRB	NRB
71	Pyridine	110-86-1	RB	NRB	not assigned
72	sorbitan monolaurate	1338-39-2	RB	RB	RB
73	Perfluoro(1,2-dimethylcyclohexane)	306-98-9	NRB	NRB	NRB
75	1,1,1-trichloro-2,2-bis(4-chlorophenyl)ethane (synonym:DDT)	50-29-3	NRB	NRB	NRB
76	2-(3,5-di-tert-butyl-2-hydroxyphenyl)benzotriazole	3846-71-7	NRB	NRB	NRB
77	2,4-di-tert-butyl-6-(5-chloro-2H-1,2,3-benzotriazol-2-yl)phenol	3864-99-1	NRB	NRB	NRB
78	mixture of 1,2,4,5,6,7,8-octachloro-2,3,3a,4,7,7a-hexahydro-4,7-methano-1H-indene, 1,4,5,6,7,8,8-heptachloro-3a,4,7,7a-tetrahydro-4,7-methano-1H-indene and their analogue compounds	76-44-8	NRB	NRB	NRB
79	1(a),2(a),3(a),4(e),5(e),6(e)-hexachlorocyclohexane (synonym:gamma-BHC)	608-73-1	NRB	NRB	NRB
80	trichloronitromethane (synonym:chloropicrine )	76-06-2	NRB	NRB	NRB
81	N,N,N',N'-Tetramethyl-2,2'-oxybis(ethylamine)	3033-62-3	NRB	NRB	not assigned
82	1,3-dimethylurea	96-31-1	NRB	RB	not assigned
83	2,2-Dibromo-2-cyanoacetamide	10222-01-2	NRB	NRB	NRB
84	2-Chloro-4-nitroaniline	121-87-9	NRB	NRB	NRB
85	4-nitro-o-anisidine	97-52-9	NRB	NRB	NRB
86	2-chloro-1,4-dimethoxybenzene	2100-42-7	NRB	NRB	not assigned
87	3-Methyl-4-(methylsulfanyl)phenol	3120-74-9	NRB	NRB	NRB
88	2-amino-5-nitrobenzonitrile	17420-30-3	NRB	NRB	NRB
89	1,2-difluorobenzene	367-11-3	NRB	NRB	not assigned

## 5. Case studies

Sample ID	Name	CAS	Exp.class	consensus 1	consensus 2
90	N,N,N',N'-Tetrakis(oxiran-2-ylmethyl)-4,4'-methylenedianiline	28768-32-3	NRB	NRB	NRB
91	1,3,5-tris(epoxypropyl)triazinane-2,4,6-trione (synonym: 1,3,5-tris(epoxypropyl)-1,3,5-triazine-2,4,6(1H,3H,5H)-trione)	2451-62-9	NRB	NRB	NRB
92	9-methoxy-7H-furo(3,2-g)chromen-7-one (synonym: 9-methoxy-7H-furo(3,2-g)[1]benzopyran-7-one or methoxalen )	298-81-7	NRB	NRB	not assigned
93	3(or4)-methyl-4-cyclohexen-1,2-dicarboxylic anhydride	5333-84-6	NRB	NRB	not assigned
94	1,1,11-trihydroperfluoroundecanol	307-70-0	NRB	NRB	NRB
95	2-Ethylhexyl hydrogen (2-ethylhexyl)phosphonate	14802-03-0	NRB	NRB	NRB
96	dibutyltin oxide	818-08-6	NRB	NRB	not assigned
98	(2-chloroethyl)benzene	622-24-2	NRB	NRB	NRB
99	o-chlorotoluene	95-49-8	NRB	NRB	NRB
100	p-chlorotoluene	106-43-4	NRB	NRB	NRB
101	1-chloro-4-isopropenylbenzene	1712-70-5	NRB	NRB	NRB
102	N,N-diethylaniline	91-66-7	NRB	NRB	NRB
104	2,4,6-trichloroaniline	634-93-5	NRB	NRB	NRB
105	N-nitrosodiphenylamine	86-30-6	NRB	NRB	NRB
106	Dinonylphenol	1323-65-5	NRB	NRB	NRB
107	2,4-dinitrophenol	51-28-5	NRB	NRB	NRB
110	4-bromo-2,5-dichlorophenol	1940-42-7	NRB	NRB	NRB
111	dibromocresyl glycidyl ether	30171-80-3	NRB	NRB	NRB
112	1,4-bis(benzoyloxyimino)-2,5-cyclohexadiene	120-52-5	NRB	NRB	NRB
113	bis(alpha,alpha-dimethylbenzyl) peroxide	80-43-3	NRB	NRB	NRB
114	4-vinyl-1-cyclohexene	100-40-3	NRB	NRB	NRB
115	Menthol	1490-04-6	NRB	NRB	not assigned
116	tris(dimethylphenyl) phosphate	25155-23-1	NRB	NRB	NRB
118	4-(1-methyl-1-phenylethyl)phenol	599-64-4	NRB	NRB	NRB
119	1-chloronaphthalene	90-13-1	NRB	NRB	NRB
120	1-methoxynaphthalene	2216-69-5	NRB	NRB	not assigned
121	2-tert-butyl-9,10-anthraquinone	84-47-9	NRB	NRB	NRB
122	2-chloroanthraquinone	131-09-9	NRB	NRB	NRB
123	2-naphthalenethiol	91-60-1	NRB	NRB	NRB
124	Carbazole	86-74-8	NRB	NRB	NRB
125	diphenylmethyl 2-chloroethyl ether	32669-06-0	NRB	NRB	NRB
126	5-chloro-2-(2,4-dichlorophenoxy)phenol	3380-34-5	NRB	NRB	NRB
127	bis(1-methyl-2-chloroethyl) ether	108-60-1	NRB	NRB	NRB
129	N,N-diethyl-m-toluamide	134-62-3	NRB	NRB	NRB
130	7H-benzo[d,e]anthracen-7-one (synonym: benzanthrone)	82-05-3	NRB	NRB	NRB
131	12-dodecanolactam	947-04-6	NRB	RB	not assigned
132	Benzothiazole	95-16-9	NRB	NRB	NRB
133	Dichloropropane	78-87-5	NRB	NRB	NRB
134	3,3,4,4,5,5,6,6,7,7,8,8,9,9,10,10,10-heptadecafluorodecan-1-ol	678-39-7	NRB	NRB	NRB
135	1,1-dichloro-N-[(dimethylamino)sulfonyl]-1-fluoro-N-phenylmethanesulfenamide	1085-98-9	NRB	NRB	NRB

## 5. Case studies

Sample ID	Name	CAS	Exp.class	consensus 1	consensus 2
136	Acenaphthylene	208-96-8	NRB	NRB	NRB
137	Chlorotriphenylmethane	76-83-5	NRB	NRB	NRB
138	Triethanolamine	102-71-6	NRB	RB	not assigned
139	ethyl carbamate	51-79-6	NRB	RB	RB
140	O,O-dimethyl S-(N-methylcarbamoylmethyl) dithio phosphate	60-51-5	NRB	NRB	NRB
141	N,N-bis(octylphenyl)amine	26603-23-6	NRB	NRB	NRB
142	p,p'-dioctyldiphenylamine	101-67-7	NRB	NRB	NRB
143	o-toluenesulfonamide	88-19-7	NRB	NRB	NRB
144	tri-p-cumenyl phosphate	26967-76-0	NRB	NRB	NRB
145	Benzenesulfonamide	98-10-2	NRB	NRB	NRB
146	5-methylbicyclo[2.2.1]hept-5-ene-2,3-dicarboxylic anhydride	25134-21-8	NRB	NRB	NRB
147	1-(2,5-dichloro-4-sulfohenyl)-3-methyl-5-pyrazolone	84-57-1	NRB	NRB	NRB
148	2-mercaptoimidazoline	96-45-7	NRB	NRB	NRB
149	pyridine-2,5-dicarboxylic acid	100-26-5	NRB	RB	RB
150	tetrahydro-1,4-oxazine	110-91-8	NRB	RB	RB
151	1,3,5-tris(2-hydroxyethyl)isocyanuric acid	839-90-7	NRB	NRB	NRB
152	4-anilino-3-nitrobenzenesulphonanilide	5124-25-4	NRB	NRB	NRB
153	2-isopropyl-6-methyl-4-pyrimidinol	2814-20-2	NRB	NRB	NRB
154	1,3-dichloropropene	542-75-6	NRB	NRB	not assigned
155	3-methoxypropylamine	5332-73-0	NRB	RB	RB
156	N,N-dimethylacrylamide	07/03/2680	NRB	RB	RB
157	3,3'-iminodipropaneonitrile	111-94-4	NRB	NRB	not assigned
158	tetramethylthiuram disulphide	137-26-8	NRB	NRB	NRB
159	tris(1,3-dichloro-2-propyl) phosphate	13674-87-8	NRB	NRB	NRB
160	1-chloro-2,3-epoxy-2-methylpropane	598-09-4	NRB	NRB	NRB
161	1,1',1'',1'''-(ethylenedinitrilo)tetrakis(propan-2-ol)	102-60-3	NRB	NRB	NRB
162	N-methylaniline	100-61-8	NRB	NRB	NRB
163	N-methylacetanilide	579-10-2	NRB	NRB	NRB
164	N,N'-diphenyl-p-phenylenediamine	74-31-7	NRB	NRB	NRB
165	N,N-dimethylbenzylamine	103-83-3	NRB	NRB	not assigned
166	1-tert-butyl-3,5-dimethyl-2,4,6-trinitrobenzene	81-15-2	NRB	NRB	NRB
168	2,4-dichlorophenyl 4'nitrophenyl ether	1836-75-5	NRB	NRB	NRB
170	2-nitro-4-methoxyaniline	96-96-8	NRB	NRB	NRB
172	bis[1-(tert-butylperoxy)-1-methylethyl]benzene	25155-25-3	NRB	NRB	NRB
173	2,6,6-trimethylbicyclo[3.1.1]heptyl-2-hydroperoxide	5405-84-5	NRB	NRB	NRB
174	3,3,5-trimethylcyclohexanone	873-94-9	NRB	NRB	NRB
175	Terphenyl	26140-60-3	NRB	NRB	NRB
176	1-methylnaphthalene	90-12-0	NRB	NRB	NRB
177	4,4'-methylenediphenol	620-92-8	NRB	NRB	NRB
178	2-[4-(diethylamino)-2-hydroxybenzoyl]benzoic acid	5809-23-4	NRB	NRB	not assigned
179	isobutyl 2-naphthyl ether	2173-57-1	NRB	NRB	NRB
180	2-Aminonaphthalene-1,5-disulfonic acid	117-62-4	NRB	NRB	NRB
181	decahydronaphthalene(mixture of cis-form and trans-form)	91-17-8	NRB	NRB	NRB



## 5. Case studies

Sample ID	Name	CAS	Exp.class	consensus 1	consensus 2
182	(Tricyclo[5.2.1.0(2,6)]decane-4,8-diyl)dimethanol	26896-48-0	NRB	NRB	NRB
183	Anthracene	120-12-7	NRB	NRB	NRB
184	2-aminoanthraquinone	117-79-3	NRB	NRB	NRB
185	1,4-Bis(isopropylamino)-9,10-anthraquinone	14233-37-5	NRB	NRB	NRB
186	1H-1,2,3-benzotriazole	95-14-7	NRB	NRB	NRB
187	5,5-diphenylimidazolidine-2,4-dione (synonym:5,5-diphenyl-2,4-Imidazolidinedione )	57-41-0	NRB	NRB	NRB
188	Thioacetamide	62-55-5	NRB	NRB	not assigned
189	1,1,2,2-tetrabromoethane	79-27-6	NRB	NRB	NRB
190	2,2-dichloro-1,1,1-trifluoroethane	306-83-2	NRB	NRB	NRB
191	3,4-dichloro-1-butene	760-23-6	NRB	NRB	NRB
192	perfluoro(tributylamine)	311-89-7	NRB	NRB	NRB
193	2,2'-dichlorodiethyl ether	111-44-4	NRB	NRB	not assigned
194	2-(isopropoxy)ethanol	109-59-1	NRB	RB	RB
195	3,5,5-trimethylhexanal	5435-64-3	NRB	NRB	NRB
196	Trichloroacetaldehyde	75-87-6	NRB	NRB	NRB
197	Docosanamide	3061-75-4	NRB	RB	not assigned
198	dimethyl phosphonate	868-85-9	NRB	RB	RB
199	tri-n-pentyl phosphate	2528-38-3	NRB	NRB	NRB
200	Perfluorooctanoic acid	335-67-1	NRB	NRB	NRB
202	Pentabromotoluene	87-83-2	NRB	NRB	NRB
204	4'-aminoacetanilide	122-80-5	NRB	NRB	NRB
207	6-tert-butyl-2,4-xlenol	1879-09-0	NRB	NRB	NRB
209	4-(methylthio)phenol	1073-72-9	NRB	NRB	not assigned
210	2-methyl-3-(4-tert-butylphenyl)propionaldehyde	80-54-6	NRB	NRB	NRB
211	4,6-dinitro-o-cresol	534-52-1	NRB	NRB	NRB
212	O,O-diethyl-o-(alpha-cyanobenzylideneamino)thio phosphate	14816-18-3	NRB	NRB	NRB
213	dimethyl 2,6-naphthalenedicarboxylate	840-65-3	NRB	RB	not assigned
214	2,2,6,6-Tetramethylpiperidin-4-on	826-36-8	NRB	NRB	NRB
215	2,2',2''-(2,4,6-trioxo-1,3,5-triazinane-1,3,5-triyl)triethyl triacrylate	40220-08-4	NRB	NRB	NRB
216	2-{N-(2-cyanoethyl)-N-[4-(4-nitrophenylazo)phenyl]amino}ethyl benzoate	40690-89-9	NRB	NRB	NRB
217	chlorophthalocyaninatocopper(II)(synonym:pygmentblue-15)	12239-87-1	NRB	NRB	NRB
218	polychlorobiphenyl(number of chlorine is 2-10)	25512-42-9	NRB	NRB	NRB

## *General conclusions and future prospects*

It is crucial to know the limitations of QSAR models for reliable predictions before they can be applied on a diverse set of test molecules. The predictive ability of QSARs is restricted in their structural and response domain which indicates that only those test samples that are structurally similar to the training set can be given as input to such trained models. With growing awareness about the use of QSARs, more sophisticated algorithms have been proposed from time to time. Availability of such state-of-the-art approaches has allowed QSAR modellers to overcome several prevailing issues in efficient and faster ways. In theory, a QSAR model can be developed based on one of the several available model development algorithms, however its applicability is always restricted since a limited pool of structural diversity is taken into account while developing such predictive models. Thus, addressing the AD of such powerful yet restrictive models can be a useful way to guide the users and keeping them from making predictions which could be unreliable due to extrapolation.

Several classical ways of addressing the AD of QSAR models were introduced and an attempt to better explore their features was made considering simulated models as well as published models from the literature. All of these classical approaches were able to partially overcome some of the prevailing issues in defining the model's AD but simultaneously, were associated with several other drawbacks. Whether it comes to inefficiency with data complexity or issues in defining an interpolation space sufficiently restricting it to reliable predictions, all the approaches had their own salient features accompanied by some disappointing drawbacks most of the times.

The range-based approaches may be the simplest, however PCA bounding box was associated with the most positive impact on model statistics in case of CAESAR model A by excluding just two test molecules outside the model's AD. On the other hand, advanced kernel approaches like optimized

gaussian kernel considered a giant portion of the test set to be excluded from the model's AD, in some cases without any noticeable impact on the model statistics. Thus, being simple or advanced may not restrict the application of such approaches.

Two novel approaches were introduced and their underlying algorithms were discussed. One of them defined the interpolation space relying heavily on an opted  $k$  value while the other applied the salient features of Locally-centred Mahalanobis distances to identify test samples beyond the scope of a model. Both the approaches were quite diverse but their results converged in several cases with each other as well as with those derived for other classical approaches, indicating the presence of several consensus test samples to be excluded from the model's AD. Both the discussed approaches were quite efficient even in higher dimensions, the defined interpolation space was reasonably restricted and the excluded test samples in several cases were associated with higher absolute standardized errors indicating that the results derived in the model's descriptor space can converge to the observations made in the model's response domain.

There is still a lot to explore within and beyond the scope of this thesis work. Development of efficient AD strategies to deal with consensus models could be one of them. Such models are interesting since they don't exist on their own and their predictions are completely reliable on the output of several other models. In the case of biodegradability models, the resulting error rate reduced reasonably implementing consensus models. Usually, with classical and new AD approaches dealt in this thesis, the final output simply indicated if the test sample is inside or outside the model's AD. There can be several test samples that may be structurally similar but not to a sufficient extent. The predictions derived for such test samples may not be completely meaningless. So to deal with such issues, in future some approaches could be developed quantifying the reliability in predictions rather than simply deciding to include or exclude a prediction. It could be also interesting to see if combining the AD output from several approaches could help overcoming their prevailing drawbacks and allow a better reliability in AD assessment.

## List of Figures

**Figure 1.1** Evaluating the reliability in prediction for new test samples

**Figure 2.1** Scatter plot for the first simulated dataset

**Figure 2.2** Scatter plot for the second simulated dataset

**Figure 2.3** Contour plots for the simulated datasets derived implementing Bounding Box. First simulated dataset (2.3a) and second simulated dataset (2.3b)

**Figure 2.4** Contour plot for the simulated datasets derived implementing PCA Bounding Box. First simulated dataset (2.4a), second simulated dataset (2.4b).

**Figure 2.5** Contour plots derived for the simulated datasets implementing Convex Hull. First simulated dataset (2.5a), second simulated dataset (2.5b).

**Figure 2.6** Contour plots derived for the simulated datasets implementing centroid-based distance approach. First simulated dataset: Euclidean (2.6a), Manhattan (2.6b), Mahalanobis (2.6c). Second simulated dataset: Euclidean (2.6d), Manhattan (2.6e), Mahalanobis (2.6f).

**Figure 2.7** Contour plots derived for the simulated datasets implementing Leverage approach. First simulated dataset (2.7a), second simulated dataset (2.7b)

**Figure 2.8** Contour plots derived for the first simulated dataset implementing k-Nearest Neighbours based approach. First simulated dataset: Euclidean (2.8a), Manhattan (2.8b), Mahalanobis (2.8c). Second simulated dataset: Euclidean (2.8d), Manhattan (2.8e), Mahalanobis (2.8f).

**Figure 2.9** Contour plots derived for the simulated datasets using Nearest Neighbour density estimator.

**Figure 2.10** Contour plots derived for both the simulated datasets implementing three variants of the Gaussian kernel. First simulated dataset: Fixed Gaussian kernel (2.10a), Optimized Gaussian kernel (2.10b) and Variable Gaussian kernel (2.10c), Second simulated dataset: Fixed Gaussian kernel (2.10d), Optimized Gaussian kernel (2.10e) and Variable Gaussian kernel (2.10f).

**Figure 2.11** Contour plots derived for simulated datasets implementing the Adaptive kernel. First simulated dataset (2.11a), Second simulated dataset (2.11b)

**Figure 2.12** Contour plots derived for simulated datasets implementing the Triangular kernel. First simulated dataset (2.12a), Second simulated dataset (2.12b).

**Figure 2.13** Contour plots derived for simulated datasets implementing the Epanechnikov kernel. First simulated dataset (2.13a), Second simulated dataset (2.13b).

**Figure 3.1** First simulated data set. Thresholds  $t_i$  vs. number of training neighbours  $K_i$  plot ( $k = 12$ ).

**Figure 3.2** Contour plot to demonstrate how the AD was characterised for the first simulated dataset. Metric used: Euclidean distance;  $k = 12$ .

**Figure 3.3** An illustration of two test samples towards AD criterion of the proposed approach for the simulated dataset.

**Figure 3.4** Impact of different  $k$  values on the defined AD for simulated dataset. a)  $k = 1$ , b)  $k = 5$ , c)  $k = 15$  and d)  $k = 25$ .

**Figure 3.5** Simulated data set. Box-and-whisker plot of test samples (%) retained within the AD for different  $k$  values during  $k$ -optimization.

**Figure 3.6** Second simulated data set. Contour plot to demonstrate how the AD was characterised. Metric used: Euclidean distance;  $k = 4$ .

**Figure 3.7** Scatter plot for the third simulated dataset.

**Figure 3.8** Third simulated data set. Contour plot to demonstrate how the AD was characterised. Metric used: Euclidean distance;  $k = 4$ .

**Figure 4.1** RI plot for the first simulated data set

**Figure 4.2** RI plot for the second simulated data set.

**Figure 4.3** AD contour plot for the first simulated dataset

**Figure 4.4** AD contour plot for the second simulated dataset

**Figure 5.1** Consensus test samples excluded from the AD of CAESAR BCF model A

**Figure 5.2**  $K_j$  vs. Absolute standardized error plot for the test samples of CAESAR BCF model A

**Figure 5.3** Consensus test samples excluded from the AD of CAESAR BCF model B

**Figure 5.4**  $K_j$  vs. Absolute standardized error plot for the test samples of CAESAR BCF model B

**Figure 5.5** Consensus test samples excluded from the AD of logKoc model

**Figure 5.6** Absolute standardized error vs.  $K_j$  plot for test samples of logKoc model

**Figure 5.7** Consensus test samples excluded from the AD of logK(OH) model

**Figure 5.8**  $K_j$  vs. Absolute standardized error plot for test samples of logK(OH) model

**Figure 5.9** Consensus test samples excluded from the AD of both the consensus models

## List of Tables

**Table 2.1** Formulas for different distance measures

**Table 5.1** List of descriptors used to develop CAESAR BCF models

**Table 5.2** Model statistics for the CAESAR BCF models.

**Table 5.3** An overview of the results for AD evaluation on CAESAR BCF model A (Test set: 95 samples)

**Table 5.4** An overview of all the test samples excluded from the AD of CAESAR model A with different approaches

**Table 5.5** An overview of the results for AD evaluation on CAESAR BCF model B (Test set: 95 samples)

**Table 5.6** An overview of all the test samples excluded from the AD of CAESAR model B with different approaches

**Table 5.7** List of descriptors used to develop the logK<sub>oc</sub> model.

**Table 5.8** Model statistics for the logK<sub>oc</sub> model.

**Table 5.9** An overview of the results for AD evaluation on logK<sub>oc</sub> model (Test set: 54 samples)

**Table 5.10** An overview of all the test samples excluded from the AD of logK<sub>oc</sub> model with different approaches

**Table 5.11** List of descriptors used to develop the logK(OH) model.

**Table 5.12** Model statistics for the logK(OH) model.

**Table 5.13** An overview of the results for AD evaluation on logK(OH) model (Test set: 211 samples)

**Table 5.14** An overview of all the test samples excluded from the AD of logK(OH) model with different approaches

**Table 5.15** List of descriptors used to develop the biodegradability models.

**Table 5.16** Model statistics for the biodegradability models.

**Table 5.17** An overview of the results for AD evaluation on the first consensus model

**Table 5.18** An overview of the results for AD evaluation on the second consensus model

**Table 5.19** An overview of all the test samples excluded from the AD of both consensus models with different approaches



## Bibliography

1. REACH. European Community Regulation on chemicals and their safe use. Available online: [http://ec.europa.eu/environment/chemicals/reach/reach\\_intro.htm](http://ec.europa.eu/environment/chemicals/reach/reach_intro.htm)
2. REACH in brief-European Commission-Europa. Available online: [http://ec.europa.eu/environment/chemicals/reach/pdf/2007\\_02\\_reach\\_in\\_brief.pdf](http://ec.europa.eu/environment/chemicals/reach/pdf/2007_02_reach_in_brief.pdf)
3. Chapter R.6: QSARs and grouping of chemicals –ECHA. Available online: [http://echa.europa.eu/documents/10162/13632/information\\_requirements\\_r6\\_en.pdf](http://echa.europa.eu/documents/10162/13632/information_requirements_r6_en.pdf)
4. Tropsha A. Best Practices for QSAR Model Development, Validation, and Exploitation. *Molecular Informatics*, **2010**, 29, 476-488.
5. Sahigara, F.; Mansouri, K.; Ballabio, D.; Mauri, A.; Consonni, V.; Todeschini, R. Comparison of Different Approaches to Define the Applicability Domain of QSAR Models. *Molecules* **2012**, 17, 4791-4810.
6. Dimitrov, S.; Dimitrova, G.; Pavlov, T.; Dimitrova, N.; Patlewicz, G.; Niemela, J.; Mekenyan, O.A. Stepwise approach for defining the applicability domain of SAR and QSAR models. *J. Chem. Inf. Model.* **2005**, 45, 839–849.
7. Worth, A.P.; van Leeuwen, C.J.; Hartung, T. The prospects for using (Q)SARs in a changing political environment: high expectations and a key role for the European Commission's Joint Research Centre. *SAR QSAR Environ. Res.* **2004**, 15, 331–343.
8. Nikolova-Jeliazkova, N.; Jaworska, J. An approach to determining applicability domains for QSAR group contribution models: an analysis of SRC KOWWIN. *Altern. Lab. Anim.* **2005**, 33, 461–470.
9. Sheridan, R.; Feuston, R.P.; Maiorov, V.N.; Kearsley, S. Similarity to molecules in the training set is a good discriminator for prediction accuracy in QSAR. *J. Chem. Inf. Comp. Sci.* **2004**, 44, 1912–1928.

10. OECD. Quantitative Structure-Activity Relationships Project [(Q)SARs]. Available online: [http://www.oecd.org/document/23/0,3746,en\\_2649\\_34377\\_33957015\\_1\\_1\\_1\\_1,00.html](http://www.oecd.org/document/23/0,3746,en_2649_34377_33957015_1_1_1_1,00.html)
11. Netzeva, T.I.; Worth, A.; Aldenberg, T.; Benigni, R.; Cronin, M.T.D.; Gramatica, P.; Jaworska, J.S.; Kahn, S.; Klopman, G.; Marchant, C.A.; *et al.* Current status of methods for defining the applicability domain of (quantitative) structure-activity relationships. The report and recommendations of ECVAM Workshop 52. *Altern. Lab. Anim.* **2005**, *33*, 155–173.
12. Jaworska, J.; Nikolova-Jeliazkova, N.; Aldenberg, T. QSAR Applicability domain estimation by projection of the training set descriptor space: A review. *Altern. Lab. Anim.* **2005**, *33*, 445–459.
13. Worth, A.P.; Bassan, A.; Gallegos, A.; Netzeva, T.I.; Patlewicz, G.; Pavan, M.; Tsakovska, I.; Vracko, M. The Characterisation of (Quantitative) Structure-Activity Relationships: Preliminary Guidance. ECB Report EUR 21866 EN, European Commission, Joint Research Centre; Ispra, Italy, **2005**; p. 95.
14. Sahigara, F.; Ballabio, D.; Todeschini, R.; Consonni, V. Defining a novel k-nearest neighbours approach to assess the applicability domain of a QSAR model for reliable predictions. *Journal of Cheminformatics* **2013**, *5*:27. doi:10.1186/1758-2946-5-27.
15. Wold, S.; Esbensen, K.; Geladi, P. Principal component analysis. *Chemometr. Intell. Lab.* **1987**, *2*, 37–52.
16. Preparata, F.P.; Shamos, M.I. Convex hulls: Basic Algorithms. In *Computational Geometry: An Introduction*; Preparata, F.P., Shamos, M.I., Eds.; Springer-Verlag: New York, NY, USA, **1991**; pp. 95–148.
17. Todeschini, R.; Consonni, V. Molecular Descriptors for Chemoinformatics. Wiley–VCH, Weinheim, **2009**.
18. Tropsha, A.; Gramatica, P.; Gombar, V. The importance of being earnest: validation is the absolute essential for successful application and interpretation of QSPR Models. *QSAR & Comb. Sci.* **2003**, *22*, 69–77.
19. Tetko, I.V.; Sushko, I.; Pandey, A.K.; Zhu, H.; Tropsha, A.; Papa, E.; Oberg, T.; Todeschini, R.; Fourches, D.; Varnek, A. Critical assessment of QSAR models of environmental toxicity against *Tetrahymena pyriformis*: Focusing on applicability domain and overfitting by variable selection. *J. Chem. Inf. Model.* **2008**, *48*, 1733–1746.

20. Silverman, B.W. Density Estimation for Statistics and Data Analysis. London, UK:Chapman and Hall; **1986**.
21. Forina, M; Lanteri, S; Armanino, C; Cerrato, Oliveros C; Casolino, C. V-PARVUS software, User manual. **2004**. <http://parvus.unigr.it>.
22. Asikainen, A.H.; Ruuskanen, J.; Tuppurainen, K.A. Consensus kNN QSAR: a versatile method for predicting the estrogenic activity of organic compounds in silico. A comparative study with five estrogen receptors and a large, diverse set of ligands. *Environ Sci Technol*, **2004**, 38, 6724-6729.
23. Cedeño, W.; Agrafiotis, D.K. Using particle swarms for the development of QSAR models based on K-nearest neighbor and kernel regression. *J Comput Aided Mol Des*, **2003**, 17, 255-263.
24. Golbraikh, A.; Shen, M.; Xiao, Z.; Xiao, Y.D.; Lee, K.H.; Tropsha, A. Rational selection of training and test sets for the development of validated QSAR models. *J Comput Aided Mol Des*, **2003**, 17, 241-253.
25. Itskowitz, P.; Tropsha, A. k Nearest Neighbors QSAR Modeling as a Variational Problem: Theory and Applications. *J Chem Inf Model*, **2005**, 45, 777-785.
26. Nigsch, F.; Bender, A.; Van Buuren B.; Tissen, J.; Nigsch, E.; Mitchell, J.B. Melting point prediction employing k-nearest neighbor algorithms and genetic parameter optimization. *J Chem Inf Model*, **2006**, 46, 2412-2422.
27. Breiman, L.; Meisel, W.; Purcell, E. Variable kernel estimates of multivariate densities. *Technometrics*, **1977**, 19, 135-144.
28. Box plot – MATLAB. Available online: <http://www.mathworks.it/it/help/stats/boxplot.html>
29. Rousseeuw, P.J.; Van Zomeren, B.C. Unmasking Multivariate Outliers and Leverage Points. *J. Amer. Statist. Assoc.* **1990**, 85, 633-639.
30. Campbell, N.A. The Influence Function as an Aid in Outlier Detection in Discriminant Analysis. *Appl. Statist.* **1978**, 27, 251-258.
31. Angiulli, F.; Pizzuti, C. Fast Outlier Detection in High Dimensional Spaces. Principles of Data Mining and Knowledge Discovery. Springer Berlin/Heidelberg, **2002**. 43-78.

32. Pell, R.J. Multiple outlier detection for multivariate calibration using robust statistical techniques. *Chemom. Intell. Lab. Syst.* **2000**, *52*, 87–104.
33. Walczak, B.; Massart, D.L. Multiple outlier detection revisited. *Chemom. Intell. Lab. Syst.* **1998**, *41*, 1–15.
34. Peña, D.; Prieto, F.J. Multivariate Outlier Detection and Robust Covariance Matrix Estimation. *Technometrics*. 2001, *43*, 286–310.
35. Todeschini, R; Ballabio, D; Consonni, V; Sahigara, F; Filzmoser, P. Locally-centred Mahalanobis distance: a new distance measure with salient features towards outlier detection. *Anal Chim Acta* **2013**. doi:10.1016/j.aca.2013.04.034.
36. Zhao, C.; Boriani, E.; Chana, A.; Roncaglioni, A.; Benfenati, E. A new hybrid QSAR model for predicting bioconcentration factor (BCF). *Chemosphere* **2008**, *73*, 1701–1707.
37. Lombardo, A.; Roncaglioni, A.; Boriani, E.; Milan, C.; Benfenati, E. Assessment and validation of the CAESAR predictive model for bioconcentration factor (BCF) in fish. *Chem. Cent. J.* **2010**, *4* (Suppl 1), doi:10.1186/1752-153X-4-S1-S1.
38. BCF-CAESAR. Available online: <http://www.caesar-project.eu/index.php?page=results&section=endpoint&ne=1>
39. Mansouri, K; Ringsted, T; Ballabio, D; Todeschini, R; Consonni, V. Quantitative Structure–Activity Relationship Models for Ready Biodegradability of Chemicals. *J. Chem. Inf. Model.* **2013**, *53*, 867–878.
40. Karelson, M; Dobchev, D; Tamm, T; Tulp, I; Jänes, J; Tämm, K; Lomaka, A; Savchenko, D; Karelson, G. Correlation of blood-brain penetration and human serum albumin binding with theoretical descriptors, *ARKIVOC* **2008**, *16*, 38–60.
41. Karelson, M; Karelson, G; Tamm, T; Tulp, I; Jänes, J; Tämm, K; Lomaka, A; Savchenko, D; Dobchev, D. QSAR study of pharmacological permeabilities, *ARKIVOC* **2009**, *2*, 218 - 238.
42. Molcode QSAR for abiotic degradation in air (OH tropospheric degradation of volatile organic compounds. Available online: <http://qsardb.jrc.it/qmrf/>
43. JRC QSAR Model Reporting Format Inventory. Available online: [http://ihcp.jrc.ec.europa.eu/our\\_databases/jrc-qsar-inventory](http://ihcp.jrc.ec.europa.eu/our_databases/jrc-qsar-inventory)

44. Consonni, V.; Ballabio, D.; Todeschini, R. Comments on the definition of the Q2 parameter for QSAR validation. *J. Chem. Inf. Model.* **2009**, *49*, 1669–1678.
45. Consonni, V.; Ballabio, D.; Todeschini, R. Evaluation of model predictive ability by external validation techniques. *J. Chemometr.* **2010**, *24*, 104–201.
46. Wan, C.; Harrington, P.B. Self-configuring radial basis function neural networks for chemical pattern recognition. *J. Chem. Inf. Comput. Sci.* **1999**, *39*, 1049–1056.
47. DRAGON (Software for Molecular Descriptor Calculations), ver. 6. Talete srl, Milano, Italy. Available online: <http://www.talete.mi.it>

## *List of papers published during the PhD Student period*

Period: 07/2010 – 06/2013

- 
1. Sahigara, F.; Mansouri, K.; Ballabio, D.; Mauri, A.; Consonni, V.; Todeschini, R. Comparison of Different Approaches to Define the Applicability Domain of QSAR Models. *Molecules* **2012**, *17*, 4791-4810.
  2. Todeschini, R; Ballabio, D; Consonni, V; Sahigara, F; Filzmoser, P. Locally-centred Mahalanobis distance: a new distance measure with salient features towards outlier detection. *Analytica Chimica Acta* **2013**. doi:10.1016/j.aca.2013.04.034.
  3. Sahigara, F.; Ballabio, D; Todeschini, R.; Consonni, V. Defining a novel k-nearest neighbours approach to assess the applicability domain of a QSAR model for reliable predictions. *Journal of Cheminformatics* **2013**, *5*:27. doi:10.1186/1758-2946-5-27.
-

The research leading to these results has received funding from the European Community's Seventh Framework Programme [FP7/2007–2013] under Grant Agreement n. 238701 of Marie Curie ITN Environmental Chemoinformatics (ECO) projec

## *APPENDIX*





Article

## Comparison of Different Approaches to Define the Applicability Domain of QSAR Models

Faizan Sahigara, Kamel Mansouri, Davide Ballabio, Andrea Mauri, Viviana Consonni and Roberto Todeschini \*

Milano Chemometrics and QSAR Research Group, Department of Environmental Sciences, University of Milano-Bicocca, P.za della Scienza 1-20126 Milano, Italy;  
E-Mails: faizan.sahigara@unimib.it (F.S.); kamel.mansouri@unimib.it (K.M.);  
davide.ballabio@unimib.it (D.B.); andrea.mauri@unimib.it (A.M.); viviana.consonni@unimib.it (V.C.)

\* Author to whom correspondence should be addressed; E-Mail: roberto.todeschini@unimib.it;  
Tel.: +39-02-6448-2820; Fax: +39-02-6448-2839.

Received: 14 March 2012; in revised form: 13 April 2012 / Accepted: 16 April 2012 /

Published: 25 April 2012

---

**Abstract:** One of the OECD principles for model validation requires defining the Applicability Domain (AD) for the QSAR models. This is important since the reliable predictions are generally limited to query chemicals structurally similar to the training compounds used to build the model. Therefore, characterization of interpolation space is significant in defining the AD and in this study some existing descriptor-based approaches performing this task are discussed and compared by implementing them on existing validated datasets from the literature. Algorithms adopted by different approaches allow defining the interpolation space in several ways, while defined thresholds contribute significantly to the extrapolations. For each dataset and approach implemented for this study, the comparison analysis was carried out by considering the model statistics and relative position of test set with respect to the training space.

**Keywords:** QSAR; model validation; Applicability Domain; interpolation space

---

### 1. Introduction

The quantitative relationship between chemical structures and their properties can be established mathematically by means of QSARs and thus, given that the structural information is available, QSAR

models can be used theoretically to predict the properties for those chemicals [1]. Due to increasing application of such QSAR models, there had been rising concerns with respect to their predictions [2]. Derivation of QSAR models is based primarily on training sets which are structurally limited and thus their applicability to the query chemicals is limited. In other words, the model can provide more reliable prediction for the external compounds that fall within these structural limitations [3].

A new European legislation on chemicals—REACH (Registration, Evaluation, Authorization and restriction of Chemicals) came into force in 2007, which deals with risk assessment of chemicals for their safe use, thus contributing to the human health and environment [4]. This law allows and encourages the use of QSAR model predictions when the experimental data are not sufficiently available or as supplementary information, provided validity of the model is justified [5]. Five OECD principles for QSAR validation adopted in November 2004 are the requisites of any given model proposed for regulatory use and can be significant to demonstrate the validity of QSAR models, which is crucial for REACH implementation.

According to these OECD principles, the QSAR model should have: (1) a defined end point; (2) an unambiguous algorithm; (3) a defined domain of applicability; (4) appropriate measures for goodness-of-fit, robustness and predictivity and (5) a mechanistic interpretation, if possible [6]. The principles, in general, provide user with all the essential information regarding end-point being predicted, model algorithm used, scope of the model and associated limitations, model performance and understanding of how the model descriptors are associated with predicted endpoint [5]. This paper primarily focuses on the third OECD principle that deals with defining the Applicability Domain (AD) of a QSAR model.

The principle of Applicability Domain requires users to define the model limitations with respect to its structural domain and response space. As discussed above, the reliable QSAR predictions are limited generally to the chemicals that are structurally similar to ones used to build that model [7–9]. The query chemicals that satisfy the scope of the model are considered as within the AD and classified as interpolated whereas the rest are extrapolations and thus, outside the AD. Reliability in a given model is higher for predictions falling within the AD and it is most likely to be unreliable for the extrapolations. This implies that the fourth OECD principle dealing with model accuracy is highly dependable on the model's AD since here the chemical space associated with reliable predictions is identified. Molecular descriptors used to build the model also play a significant role in defining the AD. Thus, if a query chemical differs in terms of the structural limitations defined by the training set, it can be considered as an outlier for that chemical space.

Defining a model's AD is essential in order to determine the subspace of chemical structures that could be predicted reliably. In other words, the degree of generalization of a predictive model depends on how broad the domain of applicability is. If the domain is too restricted, this implies the model is capable of giving reliable predictions only for limited chemical structures. Also, for regulatory purposes, like in REACH, it is essential for the user to provide all possible documentation about the model's AD. This is beneficial for the user to see if the endpoint for the chemical structures under evaluation can be reliably predicted. Also, for the cases where several QSAR models are available for chemicals of interest, the knowledge of AD can be applied to compare how reliable the predictions could be for different models [1].

Characterization of the interpolation space is very significant to define the AD for a given QSAR model. Several AD approaches have been already proposed and primarily they all differ in the way how they characterize the interpolation space defined by the descriptors used. They can be classified into following four major categories based on the methodology used for interpolation space characterization in the model descriptor space: Range-based methods, Geometric methods, Distance-based methods and Probability Density Distribution based methods [1–5].

In this study, the above mentioned AD approaches are discussed and compared, focusing on the methodology used and criteria followed to consider a query structure to be within (or outside) the Applicability Domain. The major goal of this paper is to provide a detailed comparison of the results obtained, using these different AD approaches on some selected datasets. Two models from the CAESAR project, which predict the bioconcentration factor (BCF), were chosen as the case study [10,11]. Apart from their own test sets, an alternative test set from EPI Suite package BCFBAF v3.00 was chosen to facilitate further evaluation of AD approaches [12,13]. The number of test compounds considered outside AD for different approaches was calculated and the reliability of these results was further interpreted by analyzing both, the prediction statistics and the relative position of test compounds with respect to the training space. For all distance measures in this study, the pattern of test compounds considered outside the AD was understood by implementing the distance-based approaches with several threshold defining strategies that considered both, the distances of training compounds from their mean as well as the average distances of training compounds from their first 5 nearest neighbors. Finally, comparing the results derived with this analysis, most preferred thresholds for distance-based approaches were chosen for their overall comparison with other AD approaches.

## 2. Applicability Domain Methods

The basis for interpolation is to predict the function value at a given point when the values at neighboring points are known. There are several descriptor based approaches by which the interpolation regions in multivariate space can be estimated for QSAR models. In a given  $p$ -dimensional descriptor space, estimations for new query chemicals are then obtained using the training data [1]. All the approaches used for this study were implemented using MATLAB [14] and are discussed briefly in this section informing their main features to define the interpolation space as well as the thresholds criterion used.

### 2.1. Range-Based and Geometric Methods

These are considered as the simplest methods to characterize a model's interpolation space.

#### 2.1.1. Bounding Box

This approach considers the range of individual descriptors used to build the model. Assuming a uniform distribution, resulting domain of applicability can be imagined as a Bounding Box which is a  $p$ -dimensional hyper-rectangle defined on the basis of maximum and minimum values of each descriptor used to build the model. The sides of this hyper-rectangle are parallel with respect to the coordinate axes. However, there are several drawbacks associated with this approach: since only

descriptor ranges are taken into consideration, empty regions in the interpolation space cannot be identified and also the correlation between descriptors cannot be taken into account [1,2].

### 2.1.2. PCA Bounding Box

PCA transforms the original data into a new coordinate system by the rotation of axes, such that the new axes are orthogonal to each other and aligned in the direction having maximum variance within the data. These new axes are called Principal Components (PCs) representing the maximum variance within the dataset [15]. A  $M$ -dimensional hyper-rectangle (where  $M$  is the number of significant components) is obtained similar to the previous approach by considering the projection of the molecules in the principal component space, however taking into account the maximum and minimum values for the PCs. The implementation of Bounding Box with PCA can overcome the problem of correlation between descriptors but empty regions within the interpolation space still remains an issue [1,2,5]. Moreover, selection of appropriate number of components is significant to implement this approach.

### 2.1.3. Convex Hull

With this approach, interpolation space is defined by the smallest convex area containing the entire training set. Implementing a Convex Hull can be challenging with increasing data complexity [16]. For two or three dimensional data, several algorithms are proposed; however, increase in dimensions contribute to order of complexity. In addition, set boundaries are analyzed without considering the actual data distribution. Similar to the Range-based approaches, Convex Hull cannot identify the potential internal empty regions within the interpolation space [1,2].

## 2.2. Distance-Based Methods

These approaches calculate the distance of query compounds from a defined point within the descriptor space of the training data. The general idea is to compare distances measured between defined point and the dataset with a pre-defined threshold. The threshold is a user defined parameter and is set to maximize the separation of dense regions within the original data. However, the cut-off value does not entirely reflect the actual data density [1–5]. No strict rules were evident from the literature about defining thresholds for distance-based approaches and thus it is up to the user how to define them. In this study, for all the distance measures, several possible threshold defining strategies were considered, the derived results were compared and finally the appropriate thresholds were chosen to overall compare their results with the ones derived from Range-based, Geometric and Probability Density Distribution based approaches. Some commonly used and most useful distance measures in QSAR studies include Mahalanobis, Euclidean and City Block distances [2,5].

The unique feature associated with Mahalanobis measure is the co-variance matrix which can handle the correlated descriptors. The other two distance measures lack this characteristic and thus require an additional treatment; for example, PC rotation to correct for the correlated axes. Iso-distance contours constitute the regions having constant distance measures and generally their shape differs

with approaches according to the distance measure considered, for example, ellipsoids for Mahalanobis and spherical in case of Euclidean distances [2].

Apart from them, similar approaches based on leverage are quite recommended for defining AD of a QSAR model [17]. Leverage of a query chemical is proportional to its Mahalanobis distance measure from the centroid of the training set. The leverages are calculated for a given dataset  $\mathbf{X}$  by obtaining the leverage matrix ( $\mathbf{H}$ ) with the equation below:

$$\mathbf{H} = \mathbf{X}(\mathbf{X}^T\mathbf{X})^{-1}\mathbf{X}^T \quad (1)$$

where  $\mathbf{X}$  is the model matrix while  $\mathbf{X}^T$  is its transpose matrix.

Diagonal values in the  $\mathbf{H}$  matrix represent the leverage values for different points in a given dataset. Compounds far from the centroid will be associated with higher leverage and are considered to be influential in model building. Leverage is proportional to Hotellings  $T^2$  statistic and Mahalanobis distance measure but can be applied only on the regression models. The approach can be associated with a warning leverage, generally three times the average of the leverage that corresponds to  $p/n$  where  $p$  is the number of model parameters while  $n$  is the number of training compounds. A query chemical with leverage higher than the warning leverage can be associated with unreliable predictions. Such chemicals are outside the descriptor space and thus be considered outside the AD [1,2,5]. In this study, the corresponding Mahalanobis measures were used.

### K nearest Neighbors Approach

This approach is based on providing similarity measure for a new chemical with respect to the compounds within the training space. The similarity is accessed by finding the distance of a query chemical from nearest training compound or its distances from  $k$  nearest neighbors in the training set. If these distance values are within the user defined threshold, the query chemical with higher similarity is indicated to have higher number of training neighbors and therefore, is considered to be reliably predicted. Thus, similarity to the training set molecules is significant for this approach in order to associate a query chemical with reliable prediction [9].

### 2.3. Probability Density Distribution-Based Method

Considered as one of the most advanced approaches for defining AD, these methods are based on estimating the Probability Density Function for the given data. This is feasible by both, parametric methods that assume standard distribution and non parametric methods which do not have any such assumptions concerning the data distribution. A main feature of these approaches is their ability to identify the internal empty regions. Moreover, if needed, the actual data distribution can be reflected by generating concave regions around the interpolation space borders [1,2].

Generally these approaches are implemented by estimating probability density of the dataset followed by identifying Highest Density Region that consists of a known fraction (given as user input) from the total probability mass [1].

Potential is created for each molecule in the training set such that it is highest for that molecule and decreases with distance. Once the potential is calculated for all the compounds, global potential is obtained by adding the individual potentials thus indicating the probability density [18,19].

There are several types of potential functions; however, for this study Gaussian function was considered. Given two molecules  $x_i$  and  $x_j$ , it can be determined as below:

$$\Phi(x_i, x_j) = \frac{1}{\sqrt{(2\pi)s}} \cdot \exp\left[\frac{-1}{(2s^2)(x_i - x_j)^2}\right] \quad (2)$$

where  $\Phi(x_i, x_j)$  is the potential induced on  $x_j$  by  $x_i$  and width of the curve is defined by smoothing parameter  $s$ . The cut off value associated with Gaussian potential functions, namely  $f_p$ , can be calculated by methods based on sample percentile [18]:

$$f_p = f_i + (q - j)(f_{j+1} - f_j) \quad (3)$$

with  $q = p \times \frac{n}{100}$ , where  $p$  is the percentile value of probability density,  $n$  is the number of compounds in the training set and  $j$  is the nearest integer value of  $q$ . Test compounds with potential function values lower than this threshold are considered outside the AD.

#### 2.4. Other AD Approaches

Apart from the AD strategies discussed above, several other approaches were published in literature to define the AD of QSAR models, some of which are briefly discussed below. These approaches were not considered for this comparative study since the analysis was limited to the classical AD methodologies used for interpolation space characterization in the model descriptor space.

##### 2.4.1. Decision Trees and Decision Forests Approach

Based on the consensus prediction of Decision Trees (DT), this approach specifies the AD in terms of prediction confidence and domain extrapolation. The main idea here is to minimize the overfitting which can be achieved by combining the DTs and keeping the differences within different DTs to maximum possible. Predictions from all the combined DTs are averaged in order to determine the prediction confidence for a given compound while domain extrapolation provides the prediction accuracy for that compound outside the training space [1,20,21].

##### 2.4.2. Stepwise Approach to Determine Model's AD

This approach is divided into four stages applied in a sequential manner. In the first stage, a query chemical is checked to fall within the range of variation of the physicochemical properties of training set compounds. During the second stage, structural similarity is found within the chemicals that are correctly predicted by the model. The third deals with mechanistic check while the reliability of simulated metabolism is taken into account in the final stage. To be considered within the AD, a query compound is required to satisfy all the conditions specified within these four stages. As a part of this rigorous approach, a chemical is evaluated for similarity, metabolic and mechanistic check, thus addressing the reliability of predictions and allowing a better assessment of model's AD [3,5].

## 2.5. Models and Test Sets

This section deals with models and datasets selected for the comparison of the different AD approaches.

### 2.5.1. CAESAR Models

Bioconcentration factor, which is one of the most important endpoints for environmental fate of chemicals, was chosen for comparing the results derived from the different AD approaches considered in this study. As the procedure requires deep knowledge of the model and also information about its datasets and building methods, two already existing models to predict BCF were considered [10,11].

The QSAR models (Model 2 and Model 5) used in this study were the selected best two BCF models developed under the EU project CAESAR taking into account the REACH requirements [10]. These two models based on Radial Basis Function Neural Network (RBFNN) [22] were rebuilt, each with five descriptors that were calculated using Dragon 5.5 [23]. The obtained statistics are summarized in Table 1.

**Table 1.** An overview of selected CAESAR models.

Model	Training set		Test set	
	$R^2$ <sup>(a)</sup>	$RMSE$ <sup>(b)</sup>	$Q^2$ <sup>(c)</sup>	$RMSEP$ <sup>(d)</sup>
1) Model 2	0.804	0.591	0.797	0.600
2) Model 5	0.810	0.581	0.774	0.634

<sup>(a)</sup> Determination coefficient  $R^2$ ; <sup>(b)</sup> Root-mean-square error  $RMSE$ ; <sup>(c)</sup> Predictive squared correlation coefficient  $Q^2$ ; <sup>(d)</sup> Root-mean-square error of prediction  $RMSEP$ .

### 2.5.2. CAESAR and EPI Suite Test Sets

The CAESAR dataset consisted of 473 compounds, randomly divided into a training set of 378 compounds and a test set of 95 compounds, as explained in the original study [10]. The  $Q^2$  and  $RMSEP$  values for the test sets of CAESAR Model 2 and Model 5 are reported in Table 1.

For a better evaluation of AD approaches, in addition to the CAESAR test set, the validation set of the BCF model from EPI Suite package BCFBAF was selected as an additional test set [12,13]. This test set was comprised of 158 compounds, from which one compound was discarded due to structure inadequacy while other 49 compounds were not considered due to overlapping with the CAESAR training set compounds.

## 3. Results and Discussion

For the AD approaches discussed earlier, general rules to define thresholds are discussed in the literature except for distance-based approaches. Thresholds can be defined in several ways for the distance-based approaches, thus resulting in an ambiguity over selection of appropriate thresholds for this study. As a result, before an overall comparison of results with different AD approaches could be performed, thresholds for distance-based approaches had to be finalized.



To decide upon appropriate thresholds for distance-based approaches, several threshold defining strategies were implemented for the different distance measures considered in this study. All these strategies discussed below required calculating distances of training compounds from their centroid. To evaluate further possibilities, the study was extended implementing these strategies however considering average distance of each training compound from their first 5 nearest neighbors. Model statistics were recorded each time and the most appropriate distance based thresholds were then selected from above mentioned results for all distance measures considered in this study. Until this point, all the four categories of AD approaches were associated with appropriate thresholds and finally subjected to overall comparison of results.

The results were tabulated informing the model's statistics for each AD approach on the compounds considered inside the applicability domain using the following parameters:

- i) Number of test compounds considered outside the domain of applicability;
- ii) Predictive squared correlation coefficient  $Q^2$  [24,25]:

$$Q^2 = 1 - \frac{\left[ \sum_{i=1}^{n_{EXT}} (\hat{y}_i - y_i)^2 \right] / n_{EXT}}{\left[ \sum_{i=1}^{n_{TR}} (y_i - \bar{y}_{TR})^2 \right] / n_{TR}} \quad (4)$$

where  $\hat{y}_i$  is the predicted value for the  $i$ -th compound and  $y_i$  its experimental value;  $n_{TR}$  is the number of compounds in the training set and  $n_{EXT}$  the number in the test set;  $\bar{y}_{TR}$  is the mean response of the training set. Moreover, in order to somehow quantify the role of the compounds considered inside and outside AD,  $\Delta RMSEP$  was defined by the following equation:

$$\Delta RMSEP = RMSEP_{OUT} - RMSEP_{IN} \quad (5)$$

where  $RMSEP_{OUT}$  is the root mean square error in prediction for the test compounds outside AD, while  $RMSEP_{IN}$  is the root mean square error in prediction for the test compounds inside AD. Negative values indicate that the compounds detected outside AD are predicted better than the compounds inside AD, thus highlighting some possible drawbacks in the definition of interpolation space. On the contrary, positive values of  $\Delta RMSEP$  indicate a reliable partition for the compounds detected as inside and outside AD.

Multi Dimensional Scaling (MDS) was used to visualize the relative position of test compounds with respect to the training space. MDS enables the representation of  $p$ -dimensional data by means of a 2D plot. The implementation allowed a better understanding of how the interpolation space was characterized and if the compounds outside the AD were more concentrated around the training set extremities or not.

### 3.1. Defining Thresholds for Distance-Based AD Approaches

Initially, the distances of training compounds from their centroid were calculated and from this resulting vector, the maximum and average distance value (*maxdist* and *d*) were derived. The first threshold strategy defined the AD considering *maxdist* as threshold [2]. The second and third strategies considered twice and thrice the values of *d* as their thresholds, respectively. The fourth strategy



performed percentile approach on the above derived vector of distances sorted in ascending order and the distance value corresponding to 95 percentile ( $p95$ ) was chosen as the threshold. Finally, the fifth strategy ( $dsz$ ) considered average distance  $d$  as well as the standard deviation from the distance vector ( $std$ ) and the threshold was then defined as  $d + std \times z$ , where  $z$  is the arbitrary parameter and is set to 0.5 as default value [26].

For all the cases, distance of a test compound from the training set centroid is compared with the defined threshold. If the distance of this test compound from the training set centroid is less than or equal to the threshold value, it is considered inside the AD. Thus, these approaches differ the way in which thresholds are derived, however the principle behind considering a given test compound to be inside or outside AD remains the same. Results derived with all the four threshold strategies are shown in Table 2 for CAESAR Model 2 considering different distance measures.

**Table 2.** Statistics for CAESAR Model 2 implementing distance-based approaches with different thresholds. For the acronyms *maxdist*, *d*, *p95*, *dsz*, and *ARMSEP*, refer to text.

Approach	Thresholds	Compounds outside the AD		$Q^2$		ARMSEP	
		CAESAR out of 95 (%)	EPI Suite out of 108 (%)	CAESAR	EPI Suite	CAESAR	EPI Suite
Euclidean ( <i>maxdist</i> )	0.942	0 (0.0)	4 (3.7)	0.797	0.703	-	1.436
Euclidean ( $3*d$ )	1.018	0 (0.0)	1 (0.9)	0.797	0.676	-	0
Euclidean ( $2*d$ )	0.679	7 (7.4)	12 (11.1)	0.802	0.718	0.146	0.753
Euclidean ( <i>p95</i> )	0.663	7 (7.4)	12 (11.1)	0.802	0.718	0.146	0.753
Euclidean ( <i>dsz</i> )	0.423	15 (15.8)	36 (33.3)	0.791	0.741	-0.064	0.381
CityBlock ( <i>maxdist</i> )	1.472	0 (0.0)	1 (0.9)	0.797	0.676	-	2.713
CityBlock ( $3*d$ )	1.863	0 (0.0)	0 (0.0)	0.797	0.616	-	-
CityBlock ( $2*d$ )	1.242	3 (3.1)	6 (5.5)	0.804	0.699	0.267	-1.049
CityBlock ( <i>p95</i> )	1.084	8 (8.4)	11 (10.1)	0.801	0.705	0.068	0.717
CityBlock ( <i>dsz</i> )	0.748	18 (18.9)	38 (35.1)	0.786	0.739	-0.093	0.361
Mahalanobis ( <i>maxdist</i> )	6.614	0 (0.0)	0 (0.0)	0.797	0.616	-	-
Mahalanobis ( $3*d$ )	6.027	0 (0.0)	0 (0.0)	0.797	0.616	-	-
Mahalanobis ( $2*d$ )	4.018	6 (6.3)	5 (4.6)	0.791	0.624	-0.174	0.162
Mahalanobis ( <i>p95</i> )	4.034	6 (6.3)	5 (4.6)	0.791	0.624	-0.174	0.162
Mahalanobis ( <i>dsz</i> )	2.497	21 (22.1)	27 (25.0)	0.778	0.706	-0.138	0.354

No test compounds emerged outside the AD with first two strategies considering CAESAR test set, due to the higher threshold values; however, comparing the model statistics with the other approaches, this probably implies some possible drawbacks of these strategies in defining the interpolation space. Comparable results were derived considering the third and fourth strategies which imply the thresholds corresponding to twice the value of  $d$  and that corresponding to 95 percentile converged significantly for both the test sets. Model statistics improved in most of the cases, thus reflecting a reasonable choice of compounds outside AD. The final strategy taking into account also the standard deviation provided the maximum number of test compounds outside the AD, however with no (or significant) improvement to the model statistics for both the test sets. A similar pattern was observed for

compounds considered outside the AD with both the test sets, however, with respect to the number of compounds considered outside the AD with different threshold strategies, the values were comparatively higher with EPI Suite test set. This reflected how diverse both the test sets were in terms of their compounds and indicating that the CAESAR test set comprised of compounds more similar to the training data as compared to the other test set. None of the strategies performed well with Mahalanobis distance measure for CAESAR test set resulting in a negative  $\Delta RMSEP$ . Similar pattern for compounds outside AD was observed for CAESAR model 5 and the corresponding results can be found in Table 3.

**Table 3.** Statistics for CAESAR Model 5 implementing distance-based approaches with different thresholds. *Maxdist*: Maximum distance between training compounds and centroid of the training set; *d*: Average distance of training compounds from their mean;  $\Delta RMSEP$ : Difference between *RMSEP* for compounds outside and inside the AD.

Approach	Thresholds	Compounds outside the AD		$Q^2$		$\Delta RMSEP$	
		CAESAR out of 95 (%)	EPI Suite out of 108 (%)	CAESAR	EPI Suite	CAESAR	EPI Suite
Euclidean ( <i>maxdist</i> )	0.942	0 (0.0)	2 (1.8)	0.774	0.647	-	0.598
Euclidean ( $3*d$ )	0.958	0 (0.0)	2 (1.8)	0.774	0.647	-	0.598
Euclidean ( $2*d$ )	0.639	3 (3.1)	9 (8.3)	0.783	0.665	0.329	0.354
Euclidean ( <i>p95</i> )	0.614	4 (4.2)	11 (10.1)	0.783	0.673	0.266	0.367
Euclidean ( <i>dsz</i> )	0.393	23 (24.2)	32 (29.6)	0.753	0.646	-0.128	0.044
CityBlock ( <i>maxdist</i> )	1.472	0 (0.0)	2 (1.8)	0.774	0.647	-	0.598
CityBlock ( $3*d$ )	1.791	0 (0.0)	1 (0.9)	0.774	0.634	-	0.037
CityBlock ( $2*d$ )	1.194	1 (1.0)	5 (4.6)	0.772	0.657	-0.417	0.457
CityBlock ( <i>p95</i> )	1.085	4 (4.2)	11 (10.1)	0.767	0.665	0.309	0.308
CityBlock ( <i>dsz</i> )	0.723	21 (22.1)	32 (29.6)	0.751	0.639	-0.156	0.022
Mahalanobis ( <i>maxdist</i> )	6.957	0 (0.0)	0 (0.0)	0.774	0.633	-	-
Mahalanobis ( $3*d$ )	6.121	0 (0.0)	0 (0.0)	0.774	0.633	-	-
Mahalanobis ( $2*d$ )	4.081	3 (3.1)	6 (5.5)	0.767	0.621	-0.445	-0.275
Mahalanobis ( <i>p95</i> )	3.859	5 (5.2)	6 (5.5)	0.764	0.621	-0.327	-0.275
Mahalanobis ( <i>dsz</i> )	2.495	23 (24.2)	18 (16.6)	0.760	0.637	-0.081	0.035

The study was further extended by implementing the above mentioned threshold strategies for each distance measure, but considering average distance of each training compound from its first 5 nearest neighbors. Given a  $n$  by  $n$  distance matrix where  $n$  is total number of training compounds, in all the cases, average distance of each training sample from its first five nearest training neighbors is found. Later, the gross average is derived from these average distance values which will be denoted henceforth as  $D$ . In the first and second case, twice and thrice the value of  $D$  is considered as threshold, respectively. For the third case, percentile approach discussed earlier in potential density distribution methods, is applied on the sorted average distances of all training compounds (used to calculate  $D$ ) and the value corresponding to 95 percentile (*p95*) is considered as threshold [27]. For the last strategy (*DSZ*), besides calculating the gross average distance  $D$  from the first five nearest neighbors, also the

standard deviation (*Std*) is calculated on the average distances. Finally, the threshold is defined as  $D + Std \times z$ , where  $z$  is the arbitrary parameter and is set to 0.5 as default value [26]. For all the cases, average distance of a test compound from its first five nearest neighbors in the training set is compared with the defined threshold. If the average distance for this test compound is less than or equal to the threshold value, it is considered inside the AD.

Results derived with all the four threshold strategies are shown in Tables 4 and 5 for CAESAR Model 2 and Model 5, respectively, considering different distance measures.

**Table 4.** Statistics for CAESAR Model 2 implementing different 5NN based threshold strategies. For the acronyms *D*, *p95*, *DSZ*, and *ARMSEP*, refer to text.

Approach	Thresholds	Compounds outside the AD		$Q^2$		<i>ARMSEP</i>	
		CAESAR out of 95(%)	EPI Suite out of 108(%)	CAESAR	EPI Suite	CAESAR	EPI Suite
Euclidean (3*D)	1.522	2 (2.1)	1 (0.9)	0.804	0.676	0.394	2.713
Euclidean (2* D)	1.015	9 (9.5)	16 (14.8)	0.795	0.750	−0.037	0.765
Euclidean ( <i>p95</i> )	1.164	8 (8.4)	13 (12.0)	0.797	0.745	0.859	1.342
Euclidean ( <i>DSZ</i> )	0.693	14 (14.7)	31 (28.7)	0.787	0.767	−0.113	0.517
CityBlock (3*D)	2.371	4 (4.2)	5 (4.6)	0.803	0.679	0.187	0.968
CityBlock (2*D)	1.581	10 (10.5)	18 (16.7)	0.794	0.742	−0.042	0.664
CityBlock ( <i>p95</i> )	1.918	7 (7.4)	11 (10.2)	0.799	0.741	0.034	0.944
CityBlock ( <i>DSZ</i> )	1.083	16 (16.8)	27 (25.0)	0.801	0.731	0.037	0.446
Mahalanobis (3*D)	1.718	3 (3.2)	4 (3.7)	0.803	0.628	0.221	0.295
Mahalanobis (2*D)	1.145	9 (9.5)	18 (16.7)	0.794	0.748	−0.045	0.691
Mahalanobis ( <i>p95</i> )	1.388	6 (6.3)	11 (10.2)	0.801	0.735	0.908	1.183
Mahalanobis ( <i>DSZ</i> )	0.786	19 (20.0)	29 (26.9)	0.795	0.745	−0.019	0.470

**Table 5.** Statistics for CAESAR Model 5 implementing different 5NN based threshold strategies. *D*: The gross average distance of training set compounds from their 5NN; *ARMSEP*: Difference between *RMSEP* for compounds outside and inside the AD.

Approach	Thresholds	Compounds outside the AD		$Q^2$		<i>ARMSEP</i>	
		CAESAR out of 95 (%)	EPI Suite out of 108 (%)	CAESAR	EPI Suite	CAESAR	EPI Suite
Euclidean (3*D)	1.681	0 (0.0)	2 (2.8)	0.774	0.644	-	0.364
Euclidean (2* D)	1.121	7 (7.4)	13 (12.0)	0.781	0.690	0.130	0.437
Euclidean ( <i>p95</i> )	1.331	1 (1.0)	7 (6.5)	0.772	0.656	−0.331	0.126
Euclidean ( <i>DSZ</i> )	0.782	18 (18.9)	22 (20.4)	0.784	0.743	0.072	0.512
CityBlock (3*D)	2.684	1 (1.1)	5 (4.6)	0.772	0.648	−0.456	0.307
CityBlock (2*D)	1.789	9 (9.5)	12 (11.1)	0.788	0.690	0.190	0.462
CityBlock ( <i>p95</i> )	2.302	2 (2.1)	8 (7.4)	0.785	0.657	0.529	0.310
CityBlock ( <i>DSZ</i> )	1.232	19 (20.0)	30 (27.8)	0.782	0.753	0.055	0.433
Mahalanobis (3*D)	2.006	0 (0.0)	4 (3.7)	0.774	0.624	−0.326	−0.149
Mahalanobis (2*D)	1.337	6 (6.3)	10 (9.3)	0.779	0.683	0.115	0.482
Mahalanobis ( <i>p95</i> )	1.668	2 (2.1)	6 (5.6)	0.771	0.631	−0.193	−0.043
Mahalanobis ( <i>DSZ</i> )	0.933	21 (22.1)	24 (22.2)	0.792	0.713	0.110	0.356

As obvious from Table 4, lowest number of test compounds were considered outside AD with the strategy considering  $3*D$  as threshold. When the thresholds were lowered to  $2*D$ , several other test compounds were considered outside the AD, however, the model performed worse with CAESAR test set. Same pattern was observed considering EPI Suite test set however, without lowering the model statistics and the number of test compounds outside the AD were comparatively higher in this case. Strategy taking into account also the standard deviation, was associated with the lowest threshold value thus, restricting the AD. Large number of compounds were considered outside the AD without improving the model statistics. The percentile approach considered reasonable number of test compounds outside AD without any major impact on the model statistics and the results were comparatively better with EPI Suite test set. Similar results and considerations were derived with CAESAR model 5.

The next and the final step was to finalize upon one threshold strategy for distance-based approaches. All the four above mentioned strategies behaved differently depending on the distance measure considered. A strategy that improved the model statistics for one distance measure couldn't have similar impact for another distance measure. This observation couldn't allow an easy interpretation towards finalizing upon one strategy. However, considering improved model statistics with reasonable number of test compounds considered outside the AD, the percentile approach was a preferred choice. Moreover, when the methodologies for different AD methods were described earlier, Probability Density Distribution method reflected the statistical significance of defining percentiles. These considerations concluded finalizing upon the percentile approach for overall comparison of the results. This approach was implemented initially considering the distance of training compounds from their centroid ( $p95$ ) and in the later case, based on average distance of training compounds from their 5 nearest neighbors ( $p95$ ). Both the considerations were different in defining the interpolation space and thus, resulted in different number of compounds outside the AD with the same distance measure. Information derived in both the cases was significant and thus was retained for the overall comparison of the results.

### 3.2. Overall Comparisons

The distance-based approaches were then compared with other previously discussed AD approaches, considering the both CAESAR (95 compounds) and EPI suite (108 compounds) test sets. The results are summarized in Tables 6 and 7 for CAESAR Model 2 and Model 5, respectively.

As shown in Table 6, by performing PCA analysis along with Bounding Box approach on Model 2, two test compounds were considered outside the AD. Convex Hull and Probability Density approach led to maximum number of test compounds outside the AD, thus decreasing the generalization ability of the models.  $p95$  approach lowered the model statistics for Mahalanobis distance measure.  $Q^2$  slightly lowered for Convex Hull that considered several test compounds outside the AD. On the other hand, model statistics improved for Probability Density Distribution approach which was associated with the maximum number of test compounds outside the AD (42.6%). As a general remark, the model statistics improved for several approaches with increase in number of test compounds considered outside the AD. Since the CAESAR test set comprised compounds more similar to the training set, not many test compounds emerged outside the AD; however, the EPI suite test set is comparatively

different from the training data and thus considerably more compounds were outside the AD by different approaches.  $\Delta RMSEP$  remained positive considering most of the AD approaches. Similar pattern for compounds outside the AD was derived for CAESAR model 5 and the corresponding results are reported in Table 7.

**Table 6.** Statistics for CAESAR Model 2 applied to CAESAR and EPI Suite test sets for different AD approaches.

Approach	Compounds outside the AD		$Q^2$		$\Delta RMSEP$	
	CAESAR out of 95 (%)	EPI Suite out of 108 (%)	CAESAR	EPI Suite	CAESAR	EPI Suite
Euclidean Dist. ( $p95$ )	7 (7.4)	12 (11.1)	0.802	0.718	0.146	0.753
City Block Dist. ( $p95$ )	8 (8.4)	11 (10.1)	0.801	0.705	0.068	0.717
Mahalanobis Dist. ( $p95$ )	6 (6.3)	5 (4.6)	0.791	0.624	−0.174	0.162
5NN-Euclidean Dist. ( $p95$ )	8 (8.4)	13 (12.0)	0.797	0.745	0.859	1.342
5NN-CityBlock Dist. ( $p95$ )	7 (7.4)	11 (10.2)	0.799	0.741	0.034	0.944
5NN-Mahalanobis Dist. ( $p95$ )	6 (6.3)	11 (10.2)	0.801	0.735	0.908	1.183
Bounding Box	0 (0.0)	2 (1.8)	0.797	0.678	-	1.798
PCA Bounding Box	2 (2.1)	3 (2.8)	0.804	0.688	0.371	1.533
Convex Hull	22 (23.2)	31 (28.7)	0.789	0.721	−0.052	0.368
Potential Function	29 (30.5)	46 (42.6)	0.831	0.766	0.156	0.374

**Table 7.** Statistics for CAESAR Model 5 applied to CAESAR and EPI Suite test sets for different AD approaches.

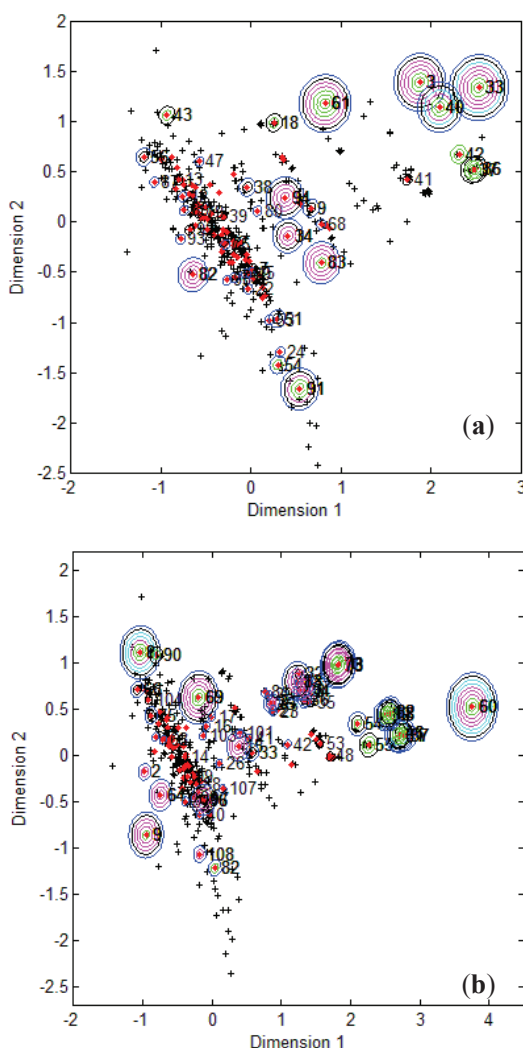
Approach	Compounds outside the AD		$Q^2$		$\Delta RMSEP$	
	CAESAR out of 95 (%)	EPI Suite out of 108 (%)	CAESAR	EPI Suite	CAESAR	EPI Suite
Euclidean Dist. ( $p95$ )	4 (4.2)	11 (10.1)	0.783	0.673	0.266	0.367
City Block Dist. ( $p95$ )	4 (4.2)	11 (10.1)	0.767	0.665	0.309	0.308
Mahalanobis Dist. ( $p95$ )	5 (5.2)	6 (5.5)	0.764	0.621	−0.327	−0.275
5NN-Euclidean Dist. ( $p95$ )	1 (1.0)	7 (6.5)	0.772	0.656	−0.331	0.126
5NN-CityBlock Dist. ( $p95$ )	2 (2.1)	8 (7.4)	0.785	0.657	0.529	0.310
5NN-Mahalanobis Dist. ( $p95$ )	2 (2.1)	6 (5.6)	0.771	0.631	−0.193	−0.043
Bounding Box	0 (0.0)	1 (0.9)	0.774	0.634	-	0.037
PCA Bounding Box	0 (0.0)	2 (1.8)	0.774	0.634	-	0.021
Convex Hull	16 (16.8)	21 (19.4)	0.780	0.643	0.049	0.051
Potential Function	28 (29.5)	47 (43.5)	0.787	0.813	0.062	0.455

To visualize where test set compounds were located with respect to the training compounds, multidimensional scaling (MDS) was performed. This enabled the representation of 5 dimensional data (the molecular descriptors defining the CAESAR models) by means of a two dimensional plot.

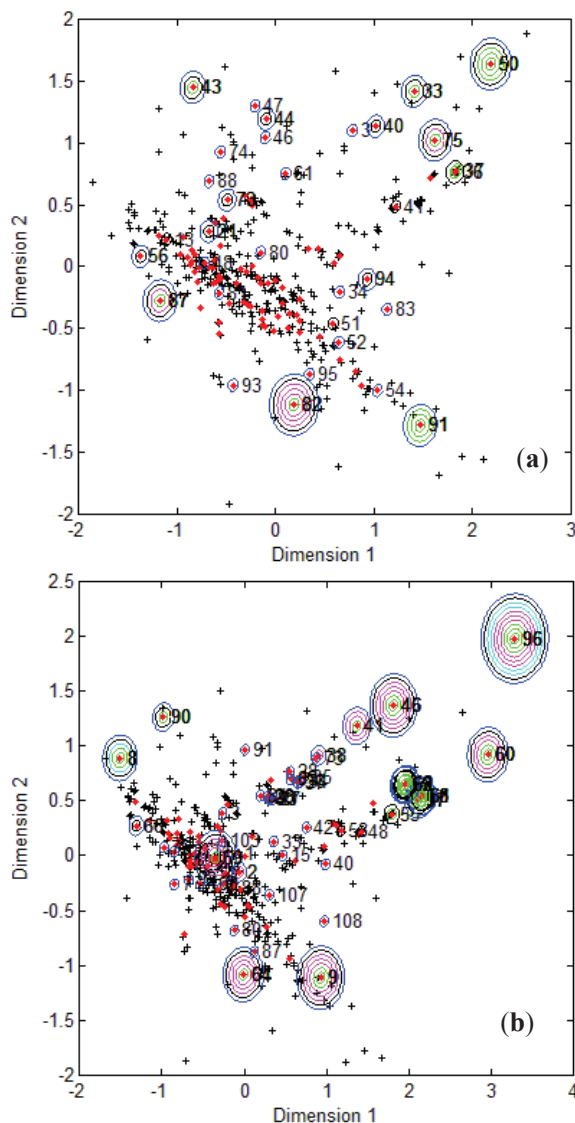
From the MDS plots in Figure 1, it is clear that several test compounds that were localized towards the extremities of training set were considered outside the AD with most of the approaches. For example, CAESAR test compound 33 and EPI Suite test compound 60 were considered outside on the basis of 7 and 9 AD approaches, respectively. However, there were several compounds that were quite close to the training space but still falling outside the AD, especially with Convex Hull and Probability Density approaches (for example, CAESAR test compound 38 and EPI Suite test compound 33). Since

the internal empty regions within chemical space cannot be easily detected and correlation between descriptors cannot be explained with Bounding Box, this approach failed to consider any test compound outside the AD. When the same approach was implemented on this dataset after PCA analysis, the correlation between descriptors was taken into account and as a result, two compounds from the test set were considered outside the AD. With respect to the EPI Suite test set, the MDS plots showed how most of test compounds outside the AD were lying in the training set extremities and were almost the same for different AD approaches. Those compounds were further more distant from training set than in the CAESAR test set. Similar results were derived for CAESAR model 5 and the corresponding plots are shown in Figure 2.

**Figure 1.** CAESAR test set (a) and Epi Suite test set (b) projected in the training space of Model 2. Training set (+); test set (♦); compounds outside the AD with different approaches; distance based  $p95$  (○), distance based 5NN (○), Bound. Box and PCA Bound. Box (○), Conv. Hull (○), Pot. Funct. (○).



**Figure 2.** CAESAR test set (a) and Epi Suite test set (b) projected in the training space of Model 5. Training set (+); test set (♦); compounds outside the AD with different approaches; distance based  $p95$  (○), distance based 5NN (○), Bound. Box and PCA Bound. Box (○), Conv. Hull (○), Pot. Funct. (○).



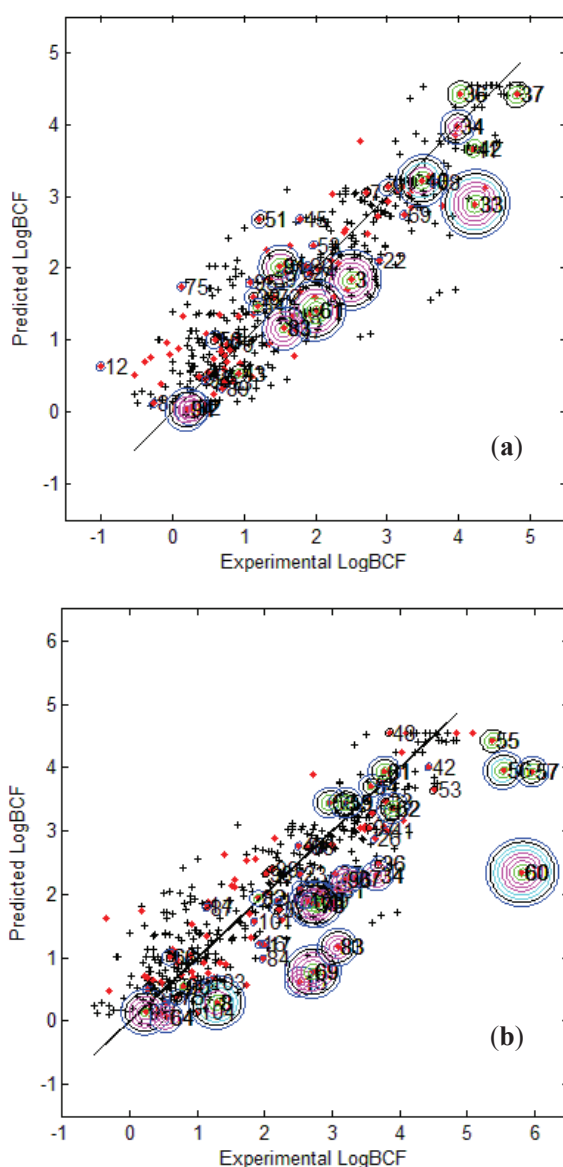
It was observed for both the CAESAR models that some compounds very close to the training compounds were considered outside the AD while others lying further were considered inside it. This could be explained by the fact that most of the implemented approaches considered only interpolation by simply excluding all test compounds in the extremities and including all those surrounded by training set compounds even if they are situated within empty regions of the chemical space.

Figure 3 provides the calculated logBCF values from the CAESAR Model 2 plotted against the experimental log BCF values (Exp logBCF). It can be noted that several test compounds not so reliably predicted were considered outside the AD. On the other hand, well predicted test compounds like 34 in



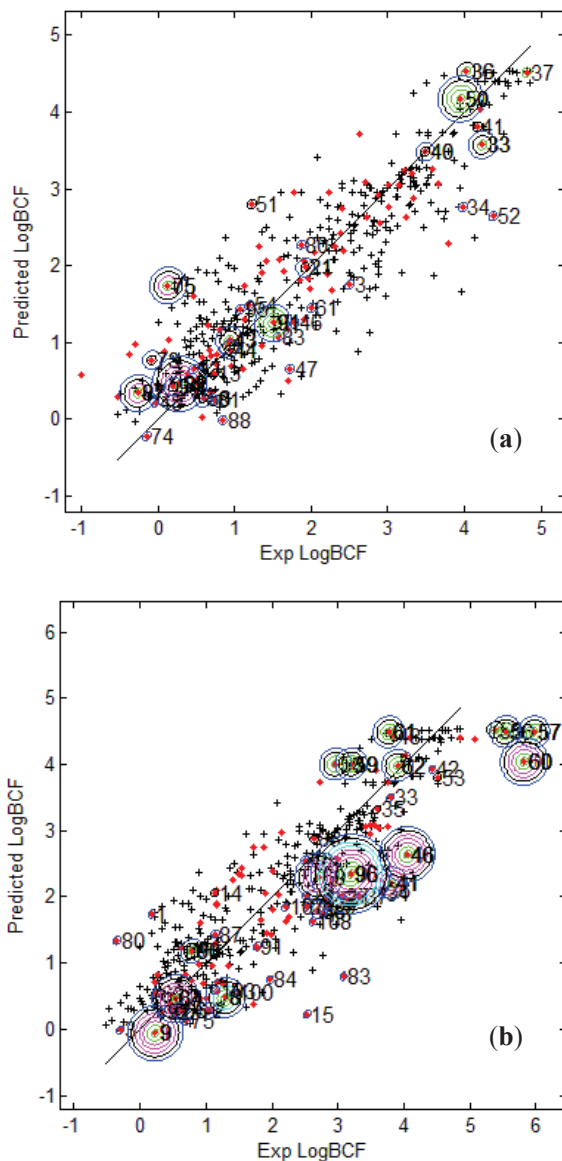
CAESAR test set and 59 in EPI Suite test set were considered outside by 2 and 5 AD approaches respectively. This indicates that the strategy used by different AD approaches might have considered some well predicted compounds outside the AD, thus affecting the model statistics. As seen earlier in Tables 6 and 7, Convex Hull and Probability Density Distribution approaches had considerable number of test compounds outside the AD; however, both the approaches differed significantly with respect to the model statistics. The results corresponding to CAESAR model 5 are plotted in Figure 4.

**Figure 3.** Predicted Vs observed log BCF values for CAESAR test set (a) and Epi Suite test set (b) with Model 2. Training set (+); test set (♦); compounds outside the AD with different approaches; distance based  $p95$  (○), distance based 5NN (○), Bound. Box and PCA Bound. Box (○), Conv. Hull (○), Pot. Funct. (○).





**Figure 4.** Predicted Vs observed log BCF values for CAESAR test set (a) and Epi Suite test set (b) with Model 5. Training set (+); test set (♦); compounds outside the AD with different approaches; distance based  $p95$  (○), distance based 5NN (○), Bound. Box and PCA Bound. Box (○), Conv. Hull (○), Pot. Funct. (○).



The plots indicate that several test compounds unreliable predicted were localized on the extremities of the training space and considered outside the AD while several well predicted test compounds were also considered outside with different approaches. This observation holds true for both the test sets however, the number of test compounds considered outside the AD were considerably higher for EPI Suite test set. Figure 3b shows that the three compounds 56, 57 and 60 considered outside the AD by several approaches were underestimated, and thus the model statistics highly improved with AD approaches not considering them within the domain of applicability.

#### 4. Conclusions

The characterization of interpolation space varied depending on the Applicability Domain approach implemented. Approaches compared in this study suffered from several limitations, some concerning the complexity of algorithm while some related to the algorithm used for defining interpolation space. Addition of PCA did not contribute significantly to the Bounding Box approach with the first test set however, with respect to the second validation set, performing PCA analysis had a significant impact on improving the model statistics. Probability Density Distribution approach and Convex Hull were associated with the highest number of test compounds outside the AD and thus allowing only a limited use of the models. Distance-based approaches considered reasonable number of test compounds outside the AD, however model statistics lowered for some distance measures. As expected, most of the test compounds considered outside the AD with most of the approaches were concentrated towards the training set extremities. It was clearly evident from the MDS plots that the distance from training space was significant in defining the model's AD. Also, several test compounds badly predicted by the model were considered as outside the AD with most of the approaches. The results from the alternative test set provided were similar; however, number of test compounds outside the AD increased. When various thresholds were subjected to distance-based approaches, it was noted, however with some exceptions, that increase in the number of test compounds outside AD also improved the model's statistics. Finally, all the implemented AD approaches had their own strengths and limitations and thus, it is up to the model builder to choose most appropriate applicability domain approach for his model. For instance, in this study, one of the aspects considered to evaluate a given AD approach was the number of test compounds outside the AD and its resulting impact on the model performance. It is important to note that the results derived with different AD approaches may vary for the same dataset and none of these approaches can be considered sufficient enough to be applied to all the cases; therefore, considering the present state of the art, it would be preferable to evaluate the results from all possible strategies before assessing a new compound set.

#### Acknowledgments

The research leading to these results has received funding from the European Community's Seventh Framework Programme [FP7/2007–2013] under Grant Agreement n. 238701 of Marie Curie ITN Environmental Chemoinformatics (ECO) project. We would like to thank Emilio Benfenati at Mario Negri Institute, Milan, Italy for providing us with the CAESAR data.

#### References and Notes

1. Netzeva, T.I.; Worth, A.; Aldenberg, T.; Benigni, R.; Cronin, M.T.D.; Gramatica, P.; Jaworska, J.S.; Kahn, S.; Klopman, G.; Marchant, C.A.; *et al.* Current status of methods for defining the applicability domain of (quantitative) structure-activity relationships. The report and recommendations of ECVAM Workshop 52. *Altern. Lab. Anim.* **2005**, *33*, 155–173.
2. Jaworska, J.; Nikolova-Jeliazkova, N.; Aldenberg, T. QSAR applicability domain estimation by projection of the training set descriptor space: A review. *Altern. Lab. Anim.* **2005**, *33*, 445–459.

3. Dimitrov, S.; Dimitrova, G.; Pavlov, T.; Dimitrova, N.; Patlewicz, G.; Niemela, J.; Mekenyan, O.A. Stepwise approach for defining the applicability domain of SAR and QSAR models. *J. Chem. Inf. Model.* **2005**, *45*, 839–849.
4. REACH. European Community Regulation on chemicals and their safe use. Available online: [http://ec.europa.eu/environment/chemicals/reach/reach\\_intro.htm](http://ec.europa.eu/environment/chemicals/reach/reach_intro.htm) (accessed on 3 February 2012).
5. Worth, A.P.; Bassan, A.; Gallegos, A.; Netzeva, T.I.; Patlewicz, G.; Pavan, M.; Tsakovska, I.; Vracko, M. *The Characterisation of (Quantitative) Structure-Activity Relationships: Preliminary Guidance*. ECB Report EUR 21866 EN, European Commission, Joint Research Centre; Ispra, Italy, 2005; p. 95.
6. OECD. Quantitative Structure-Activity Relationships Project [(Q)SARs]. Available online: [http://www.oecd.org/document/23/0,3746,en\\_2649\\_34377\\_33957015\\_1\\_1\\_1\\_1,00.html](http://www.oecd.org/document/23/0,3746,en_2649_34377_33957015_1_1_1_1,00.html) (accessed on 3 February 2012).
7. Worth, A.P.; van Leeuwen, C.J.; Hartung, T. The prospects for using (Q)SARs in a changing political environment: high expectations and a key role for the Commission's Joint Research Centre. *SAR QSAR Environ. Res.* **2004**, *15*, 331–343.
8. Nikolova-Jeliazkova, N.; Jaworska, J. An approach to determining applicability domains for QSAR group contribution models: an analysis of SRC KOWWIN. *Altern. Lab. Anim.* **2005**, *33*, 461–470.
9. Sheridan, R.; Feuston, R.P.; Maiorov, V.N.; Kearsley, S. Similarity to molecules in the training set is a good discriminator for prediction accuracy in QSAR. *J. Chem. Inf. Comp. Sci.* **2004**, *44*, 1912–1928.
10. Zhao, C.; Boriani, E.; Chana, A.; Roncaglioni, A.; Benfenati, E. A new hybrid QSAR model for predicting bioconcentration factor (BCF). *Chemosphere* **2008**, *73*, 1701–1707.
11. Lombardo, A.; Roncaglioni, A.; Boriani, E.; Milan, C.; Benfenati, E. Assessment and validation of the CAESAR predictive model for bioconcentration factor (BCF) in fish. *Chem. Cent. J.* **2010**, *4* (Suppl 1), doi:10.1186/1752-153X-4-S1-S1.
12. Meylan, W.M.; Howard, P.H.; Aronson, D.; Printup, H.; Gouchie, S. *Improved Method for Estimating Bioconcentration Factor (BCF) from Octanol-Water Partition Coefficient*, 2nd Update; SRC TR-97-006; Syracuse Research Corp., Environmental Science Center: North Syracuse, NY, USA, 1997; Prepared for: Robert S. Boethling, EPA-OPPT.
13. Meylan, W.M.; Howard, P.H.; Boethling, R.S.; Aronson, D.; Printup, H.; Gouchie, S. Improved method for estimating bioconcentration/bioaccumulation factor from octanol/water partition coefficient. *Environ. Toxicol. Chem.* **1999**, *18*, 664–672.
14. MATLAB. The Language of Technical Computing. Available online: <http://www.mathworks.com/products/matlab/> (accessed on 3 February 2012).
15. Wold, S.; Esbensen, K.; Geladi, P. Principal component analysis. *Chemometr. Intell. Lab.* **1987**, *2*, 37–52.
16. Preparata, F.P.; Shamos, M.I. Convex Hulls: Basic Algorithms. In *Computational Geometry: An Introduction*; Preparata, F.P., Shamos, M.I., Eds.; Springer-Verlag: New York, NY, USA, 1991; pp. 95–148.

17. Tropsha, A.; Gramatica, P.; Gombar, V. The importance of being earnest: validation is the absolute essential for successful application and interpretation of QSPR Models. *QSAR Comb. Sci.* **2003**, *22*, 69–77.
18. Jouan-Rimbaud, D.; Bouveresse, E.; Massart, D.L.; de Noord, O.E. Detection of prediction outliers and inliers in multivariate calibration. *Anal. Chim. Acta* **1999**, *388*, 283–301.
19. Forina, M.; Armanino, C.; Leardi, R.; Drava, G. A class-modelling technique based on potential functions. *J. Chemometr.* **1991**, *5*, 435–453.
20. Tong, W.; Hong, H.; Fang, H.; Xie, Q.; Perkins, R. Decision forest: Combining the predictions of multiple independent decision tree models. *J. Chem. Inf. Comput. Sci.* **2003**, *43*, 525–531.
21. Tong, W.; Hong, H.; Xie, Q.; Xie, L.; Fang, H.; Perkins, R. Assessing QSAR limitations: A regulatory perspective. *Curr. Comput. Aid. Drug Des.* **2004**, *1*, 65–72.
22. Wan, C.; Harrington, P.B. Self-configuring radial basis function neural networks for chemical pattern recognition. *J. Chem. Inf. Comput. Sci.* **1999**, *39*, 1049–1056.
23. DRAGON (Software for Molecular Descriptor Calculations). Talete srl, Milano, Italy. Available online: <http://www.talete.mi.it> (accessed on 3 February 2012).
24. Consonni, V.; Ballabio, D.; Todeschini, R. Comments on the definition of the  $Q^2$  parameter for QSAR validation. *J. Chem. Inf. Model.* **2009**, *49*, 1669–1678.
25. Consonni, V.; Ballabio, D.; Todeschini, R. Evaluation of model predictive ability by external validation techniques. *J. Chemometr.* **2010**, *24*, 104–201.
26. Tetko, I.V.; Sushko, I.; Pandey, A.K.; Zhu, H.; Tropsha, A.; Papa, E.; Oberg, T.; Todeschini, R.; Fourches, D.; Varnek, A. Critical assessment of QSAR models of environmental toxicity against *Tetrahymena pyriformis*: Focusing on applicability domain and overfitting by variable selection. *J. Chem. Inf. Model.* **2008**, *48*, 1733–1746.
27. Weaver, S.; Gleeson, M.P. The importance of the domain of applicability in QSAR modeling. *J. Mol. Graph. Model.* **2008**, *26*, 1315–1326.

*Sample Availability:* The CAESAR data sets used in this study can be requested directly from the CAESAR project (<http://www.caesar-project.eu>).

© 2012 by the authors; licensee MDPI, Basel, Switzerland. This article is an open access article distributed under the terms and conditions of the Creative Commons Attribution license (<http://creativecommons.org/licenses/by/3.0/>).



Contents lists available at SciVerse ScienceDirect

Analytica Chimica Acta

journal homepage: [www.elsevier.com/locate/aca](http://www.elsevier.com/locate/aca)



## Locally centred Mahalanobis distance: A new distance measure with salient features towards outlier detection

Roberto Todeschini<sup>a,\*</sup>, Davide Ballabio<sup>a</sup>, Viviana Consonni<sup>a</sup>, Faizan Sahigara<sup>a</sup>, Peter Filzmoser<sup>b</sup>

<sup>a</sup> Milano Chemometrics and QSAR Research Group, Department of Earth and Environmental Sciences, University of Milano-Bicocca, P.za della Scienza 1, 20126 Milano, Italy

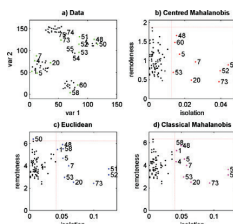
<sup>b</sup> Department of Statistics and Probability Theory, Vienna University of Technology, Vienna, Austria

### HIGHLIGHTS

- A new measure of distance is proposed.
- Two different kinds of outliers are discussed.
- Two new indices for outlier detection are defined.
- A new plot is proposed as outlier detection tool.

### GRAPHICAL ABSTRACT

The main topic of the paper is a new measure of Mahalanobis distance, centred on each sample and not on the data centroid. This new distance matrix gives interesting information for outlier detection and a new graphic tool – also useful for exploratory data analysis – is proposed.



### ARTICLE INFO

#### Article history:

Received 4 February 2013  
Received in revised form 8 April 2013  
Accepted 19 April 2013  
Available online xxx

#### Keywords:

Mahalanobis distance  
Outlier detection  
Similarity  
Isolation degree  
Remoteness  
Covariance matrix  
Data mining

### ABSTRACT

Outlier detection is a prerequisite to identify the presence of aberrant samples in a given set of data. The identification of such diverse data samples is significant particularly for multivariate data analysis where increasing data dimensionality can easily hinder the data exploration and such outliers often go undetected. This paper is aimed to introduce a novel Mahalanobis distance measure (namely, a pseudo-distance) termed as locally centred Mahalanobis distance, derived by centering the covariance matrix at each data sample rather than at the data centroid as in the classical covariance matrix. Two parameters, called as Remoteness and Isolation degree, were derived from the resulting pairwise distance matrix and their salient features facilitated a better identification of atypical samples isolated from the rest of the data, thus reflecting their potential application towards outlier detection. The Isolation degree demonstrated to be able to detect a new kind of outliers, that is, isolated samples within the data domain, thus resulting in a useful diagnostic tool to evaluate the reliability of predictions obtained by local models (e.g. k-NN models).

To better understand the role of Remoteness and Isolation degree in identification of such aberrant data samples, some simulated and published data sets from literature were considered as case studies and the results were compared with those obtained by using Euclidean distance and classical Mahalanobis distance.

© 2013 Elsevier B.V. All rights reserved.

### 1. Introduction

Outlier detection has been considered quite significant in identifying atypical observations from a given set of data [1]. In past

\* Corresponding author. Tel.: +39 0264482820.  
E-mail address: [roberto.todeschini@unimib.it](mailto:roberto.todeschini@unimib.it) (R. Todeschini).

years, several research communities addressed the detection of outliers with different terminologies, for instance, novelty detection, anomaly detection, noise detection and exception mining [2]. Usually, outliers deviate markedly from other data samples and can highly influence the predictive accuracy of several commonly used data mining algorithms [3,4]. In simple terms, outliers represent the observations that fail to follow the general pattern of the majority of data samples [5]. Thus, it is critical to detect and appropriately treat such anomalous observations, contributing to undesired performance degradation, or, alternatively, suggesting unexpected but interesting patterns.

In recent years, there had been a growing attention towards dealing with outliers since they can highly impact the variance and correlation between variables [1]. Increasing dimensionality of data adds to the complexity of detecting such outliers. Depending upon the research community performing outlier detection, aberrant observations can be either treated as noise and are usually discarded to obtain clean data, however, in other cases such outliers can themselves be a source of interest. For instance, the observations that are not well classified with a classification algorithm can be discarded to improve the accuracy of the classifier, while on the other hand, anomalous data samples can be quite informative about mineral deposits while performing geochemical exploration [4,6].

Several supervised and unsupervised-learning methods have been proposed to address outlier mining [4]. Unsupervised learning approaches do not require any prior knowledge about the data, thus processing it as static distribution and considering the remote samples as potential outliers [3]. On the other hand, supervised learning algorithms require the pre-labelled data, classified as normal or abnormal [3]. Most of the proposed techniques to deal with outliers were either diagnostic or robust approaches. Diagnostic approaches identify outliers by fitting the data with classical Least Squares methods and constructing regression diagnostics. On the other hand, robust approaches construct estimators that do justice to the majority of the data and the outliers are identified examining the residuals from this fit [7,8].

Several classical techniques performed well, provided the given set of data contained only a single outlier, however, their inefficiency emerged while dealing with multiple outliers [9]. Lacking visual perception for data with more than two dimensions, restricted the reliable use of such classical approaches only for two-dimensional data [5]. Moreover, masking and swamping considerably restricted the usefulness of such classical approaches towards detection of multiple outliers in calibration [7,8]. Many times the presence of some outliers can somehow mask the detection of other outliers. As a result, some outliers are wrongly identified as normal samples. This phenomenon is referred to as masking. On the contrary, swamping refers to the cases where the presence of a subset of observations makes normal samples being incorrectly identified as potential outliers. Several new and improved detection approaches emerged from time to time and were attempting to overcome major limitations of classical outlier detection techniques, however, this domain of data exploration perhaps may always leave a room for further improvement towards developing an approach that can tackle the increasing data complexity without comprising upon the quality of detection accuracy.

In this paper, a new distance measure, called *locally centred Mahalanobis distance*, based on the covariance matrix centred on each dataset object, is introduced and its salient properties are discussed. Two new parameters derived from the resulting pairwise distance matrix are introduced, in order to better explore the isolation of the data samples in their local and global space. The information corresponding to these new parameters when plotted can allow the analyst to better explore several interesting features of the data, particularly, in terms of detecting those samples that are quite diverse from the major pattern followed by the data samples.

The performance of this new distance measure for outlier detection is evaluated and better explained taking into account the results derived on simulated and benchmarked data sets.

## 2. Theory

Let the data matrix  $\mathbf{X}$  be comprised of  $n$  objects and  $p$  variables, defined as:  $\mathbf{X} = (\mathbf{x}_1^T, \mathbf{x}_2^T, \dots, \mathbf{x}_n^T)^T$ , where  $\mathbf{x}_i$  are column vectors representing the  $n$  observations ( $i = 1, 2, \dots, n$ ).

The data are assumed to be independently sampled from a multivariate normal distribution  $N_p(\boldsymbol{\mu}, \boldsymbol{\Sigma})$ . A general measure of squared distance from an observation  $\mathbf{x}_i$  to the centroid of the  $p$ -dimensional space  $\boldsymbol{\mu}$ , for  $i = 1, \dots, n$ , can thus be written as follows:

$$d_i^2 = (\mathbf{x}_i - \boldsymbol{\mu})^T \cdot \mathbf{M} \cdot (\mathbf{x}_i - \boldsymbol{\mu}) \quad (1)$$

where  $\mathbf{M}$  is a  $p \times p$  symmetrical matrix. It can be easily noted that formula (1) is a squared Euclidean distance if  $\mathbf{M} = \mathbf{I}$ , where  $\mathbf{I}$  is the identity matrix, and a weighted Euclidean distance if  $\mathbf{M} = \mathbf{W}$ , where  $\mathbf{W}$  is a symmetric weight matrix. Moreover, if  $\mathbf{M} = \boldsymbol{\Sigma}^{-1}$  where  $\boldsymbol{\Sigma}$  is the population covariance matrix, the squared Mahalanobis distance is obtained as:

$$d_i^2 = (\mathbf{x}_i - \boldsymbol{\mu})^T \cdot \boldsymbol{\Sigma}^{-1} \cdot (\mathbf{x}_i - \boldsymbol{\mu}) \quad (2)$$

These distances are distributed according to  $\chi_p^2$  and if the parameters  $\boldsymbol{\mu}$  and  $\boldsymbol{\Sigma}$  are estimated by the arithmetic mean  $\bar{\mathbf{x}}$  and the sample covariance matrix  $\mathbf{S} = 1/(n-1) \cdot \sum_{i=1}^n (\mathbf{x}_i - \bar{\mathbf{x}})(\mathbf{x}_i - \bar{\mathbf{x}})^T$  respectively, the (estimated) squared Mahalanobis distances are:

$$MD_i^2 = (\mathbf{x}_i - \bar{\mathbf{x}})^T \cdot \mathbf{S}^{-1} \cdot (\mathbf{x}_i - \bar{\mathbf{x}}) \quad (3)$$

The distribution is given by  $((n-1)^2/n)MD_i^2 \sim \text{Beta}(p/2, n-p-1/2)$ , (e.g., see Ref. [10]). If  $\mathbf{S}$  and  $\mathbf{x}_i$  are independent, then  $((n-p)/(n-1)p)MD_i^2 \sim F_{p,n-p}$ .

Now, if a vector  $\mathbf{v} \in \mathbb{R}^p$  is selected in the  $p$ -dimensional space, the covariance matrix, centred at  $\mathbf{v}$ , denoted by  $\mathbf{S}_{(\mathbf{v})}$ , can be calculated as:

$$\mathbf{S}_{(\mathbf{v})} = \frac{1}{n-1} \cdot \sum_{i=1}^n (\mathbf{x}_i - \mathbf{v})(\mathbf{x}_i - \mathbf{v})^T \quad (4)$$

Then, it can be easily verified that,

$$\mathbf{S}_{(\mathbf{v})} = \mathbf{S} + \frac{n}{n-1} \cdot (\bar{\mathbf{x}} - \mathbf{v})(\bar{\mathbf{x}} - \mathbf{v})^T \quad (5)$$

Finally, the squared Mahalanobis distances considering  $\mathbf{v}$  as the space centre can be derived as:

$$MD^2(i, \mathbf{v}) = (\mathbf{x}_i - \mathbf{v})^T \cdot \mathbf{S}_{(\mathbf{v})}^{-1} \cdot (\mathbf{x}_i - \mathbf{v}), \quad i = 1, \dots, n \quad (6)$$

If the above mentioned vector  $\mathbf{v}$  is now replaced by an observation  $\mathbf{x}_j$ , for  $j = 1, \dots, n$ , the new locally centred squared Mahalanobis distance between observations  $i$  and  $j$  is defined as:

$$MD_L^2(i, j) = (\mathbf{x}_i - \mathbf{x}_j)^T \cdot \mathbf{S}_{(j)}^{-1} \cdot (\mathbf{x}_i - \mathbf{x}_j) \quad (7)$$

where  $\mathbf{S}_{(j)}$  is the covariance matrix centred on the  $j$ -th observation.

It should be noted that the classical covariance matrix  $\mathbf{S}$ , being centred on the arithmetic mean vector, minimizes the data variance, while, the new defined locally centred covariance matrix encodes different information, data variance depending on the selected centre. Thus, the new distance measure is more informative than the classical Mahalanobis distance, which considers only the arithmetic mean as the data centre.

In order to obtain distances that are independent of the number of variables  $p$ , the distance values can be divided by  $p$ , thus obtaining



locally centred average squared Mahalanobis distances:

$$\begin{aligned}\overline{MD}_L^2(i, j) &= \frac{MD_L^2(i, j)}{p} \\ &= \frac{1}{p} \cdot [(\mathbf{x}_i - \mathbf{x}_j)^T \cdot \mathbf{S}_{(j)}^{-1} \cdot (\mathbf{x}_i - \mathbf{x}_j)], \quad i, j = 1, \dots, n\end{aligned}\quad (8)$$

Hereinafter these average distances will be used in all the considered case studies but, for the sake of simplicity, they will be often shortly referred to as locally centred Mahalanobis distances, still using the symbol  $MD_L^2$ .

### 2.1. Approximating the distribution of locally centred Mahalanobis distances

Generally, an  $F$ -distribution (or Hotelling's  $T^2$  distribution) is obtained by a statistic  $\mathbf{d}^T \mathbf{M}^{-1} \mathbf{d}$ , where the  $p$ -dimensional vector  $\mathbf{d}$  is normal, the  $p \times p$  matrix  $\mathbf{M}$  is a Wishart matrix, and  $\mathbf{d}$  and  $\mathbf{M}$  are independent.  $\mathbf{S}$  can be expressed by a quadratic form  $\mathbf{X}^T \mathbf{H}^{-1} \mathbf{X}$  with a matrix  $\mathbf{H}$ , however,  $\mathbf{M} = \mathbf{S}_{(v)}$  is not a Wishart matrix, since it cannot be expressed in this form.

In spite of the above considerations, the distribution of distances  $MD_L^2(\mathbf{v})$  was approximated by a  $\chi_p^2$  and Beta-distribution for an illustration with 5-dimensional normally distributed data of 100 samples and the results are shown in Fig. 1.

The approximation seems to work quite well with  $\chi_p^2$  distribution. Beta-distribution can also be used, however, it does not seem to really improve the approximation.

### 2.2. Salient features of the novel distance measure

There are two important key aspects related to this novel distance. Like the distances derived using the classical covariance matrix, the locally centred Mahalanobis distances are invariant to any sort of variable scaling. Secondly, unlike the classical Mahalanobis distance, the resulting object-centred distance is asymmetric and consequently is a pseudo-distance; indeed, the distance between two observations  $i$  and  $j$  depends on whether the selected centre is  $i$  or  $j$ :

$$MD_L^2(i, j) \neq MD_L^2(j, i) \quad (9)$$

This asymmetry is accounted due to the presence of all other observations and their resulting overall influence in deriving the distances, thus reflecting the significance of information retrieved from the locally centred covariance matrix.

The asymmetry between  $MD_L^2(i, j)$  and  $MD_L^2(j, i)$  seems to have a significant meaning. In fact, a higher value of  $MD_L^2(i, j)$  in contrast with a corresponding lower value for  $MD_L^2(j, i)$  indicates that the object  $i$  belongs to a relatively denser region with respect to the object  $j$ , which appears to be more isolated. This consideration can be further supported by the fact that, when  $j$  is isolated being the centred object, it shows a higher variance than the case when  $i$  is the centred object, which unlike the earlier, is surrounded by several objects in its vicinity. As seen from the way these locally centred Mahalanobis distances are derived, the variance is calculated as the reciprocal in the distance formula and as a result,  $j$  tends to seem closer to  $i$ , while on the contrary, object  $i$  with a lower variance tends to seem comparatively further distant from  $j$ . Usually, the objects with lower variance can be thought of being either located in a cluster or surrounded by several similar objects in their vicinity.

The variable space based on Mahalanobis distances calculated using the classical covariance matrix is estimated by an ellipsoid (or hyper-ellipsoid), while in the case of locally centred Mahalanobis distances, the variable space is defined by a family of ellipsoids (or hyper-ellipsoids) due to the multi-centred approach. Thus, a more

data-driven shaped variable space is determined using this novel distance measure.

### 2.3. Remoteness and isolation degree

It is quite easy to interpret the significance of columns and rows in the pair-wise distance matrix  $\mathbf{MD}_L^2$  resulting from the novel average locally centred squared Mahalanobis distances. In fact, each  $j$ -th column constitutes the data centre and represents how that  $j$ -th object "globally perceives" each  $i$ -th object, also taking into account the overall influence of all the other objects, while each  $i$ -th row represents how that  $i$ -th object is "globally perceived" by all the other objects.

Each  $j$ -th column of the  $\mathbf{MD}_L^2$  matrix contains information about the distances of all other  $i$  objects from the  $j$ -th centre. The minimum value of a  $j$ -th column can be taken into account to represent the squared distance of the  $j$ -th object from its nearest neighbour; this is termed as *Isolation degree* ( $Idg$ ):

$$Idg_j = \min_i ([\mathbf{MD}_L^2]_{ij}) \quad i \neq j \quad (10)$$

Similarly, each  $i$ -th row of the  $\mathbf{MD}_L^2$  matrix contains information about the squared distances of the  $i$ -th object as it is perceived from all the other objects. Thus, the average squared distance value for each  $i$ -th row is taken into account and termed as *Remoteness* ( $Rem$ ):

$$Rem_i = \frac{\sum_{j=1}^n [\mathbf{MD}_L^2]_{ij}}{n-1} \quad (11)$$

The values of remoteness can range from a minimum greater than zero and a maximum equal to  $(n-1)/p$ , while isolation degree for any given sample remains localized between 0 and 1 (see Appendix). It should be also noted that

$$\frac{\sum_{i=1}^n Rem_i}{n} = \frac{\sum_{i=1}^n \sum_{j=1}^n [\mathbf{MD}_L^2]_{ij}}{n \cdot (n-1)} = 1 \quad (12)$$

i.e., the average value of the remoteness vector or, in other words, the average value of the matrix  $\mathbf{MD}_L^2$  elements is equal to one. Then, the remoteness could be interpreted as the influence that each sample exerts over the covariance structure of the data, i.e. the values significantly larger than one identify the most influent samples.

The remoteness highlights objects which are far from the bulk of the remaining objects, i.e. they can be considered as classical outliers in the selected variable space; the Isolation degree detects a different kind of "anomalous" objects, i.e. those objects that, although located within the variable space, are isolated from the other ones or, in other words, these objects are surrounded by objects not so near. Therefore, a scatter plot of Remoteness vs. Isolation degree, called *RI plot*, for the data set in analysis can be a useful tool for exploratory purposes.

The thresholds to detect remote and isolated samples, for the two distributions of remoteness and isolation degree, are defined as the upper "fences" in the box & whisker plots:

$$threshold = Q_3 + 1.5 \cdot (Q_3 - Q_1) \quad (13)$$

where  $Q_1$  and  $Q_3$  are the first and third quartiles, respectively, and their difference is the interquartile range.

## 3. Data sets

To better evaluate the role of remoteness and isolation degree towards potential outlier detection, the following data sets were used as case studies.

As first step, in order to have a look at the behaviour of remoteness and isolation degree, two simple simulated data sets were analysed. The first data set, a two-dimensional simulated data set,

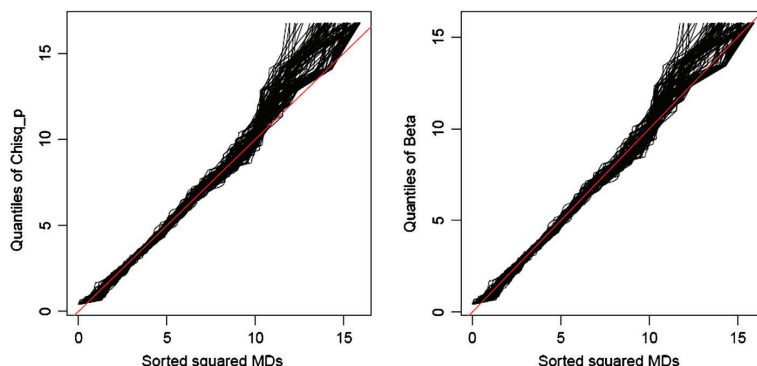


**Fig. 1.** Approximating the distribution of locally centred squared Mahalanobis distances by  $\chi_p^2$  (left) and Beta-distribution (right), with  $p/2$  and  $(n - p - 1)/2$  degrees of freedom.

consists of a cluster of 48 data samples and two additional samples (49 and 50) quite distant from each other as well as from the main sample cluster. A second two-dimensional data set was simulated with data samples roughly divided within four clusters and a single data sample localized more or less between these clusters, in the centre of the variable space.

The behaviour of the proposed two indices was also evaluated by another two-dimensional data set, taken from the literature and commonly known as Ruspini, consisted of 75 objects [11].

The other benchmark data sets were the well-known chemometric data set Iris, comprised of 150 objects and 4 variables [12],

and the Italoil data set taken from a study that was aimed to classify olive oils from different parts of Italy based on their fatty acids composition. It reports the percentage composition of 8 fatty acids (variables) within the lipid fraction for 572 Italian olive oil samples [13].

#### 4. Results and discussion

The locally centred squared Mahalanobis distances were calculated for the two simulated and three benchmarked datasets presented above. The object-oriented pair-wise distance matrix

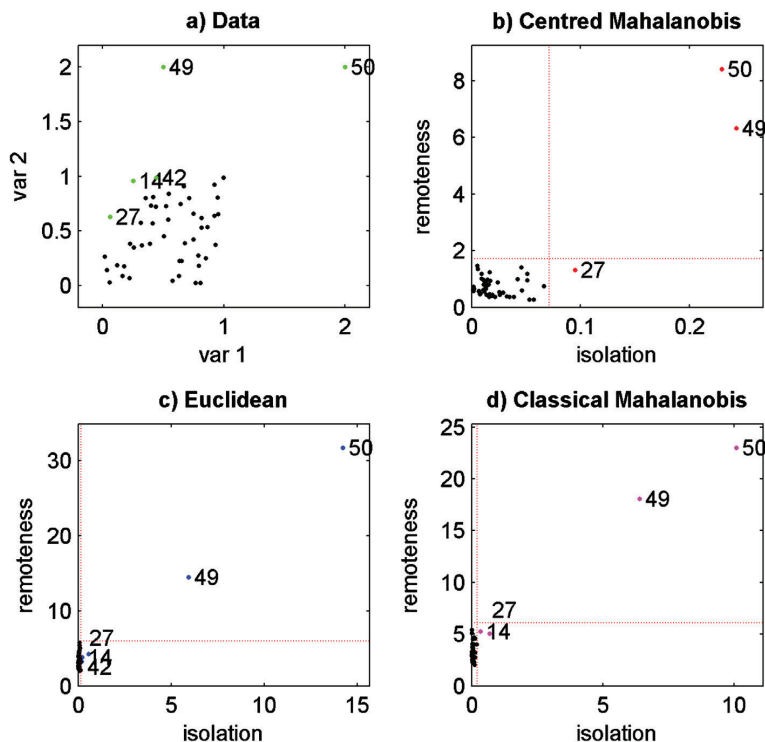


**Fig. 2.** Plots of the first simulated data set.



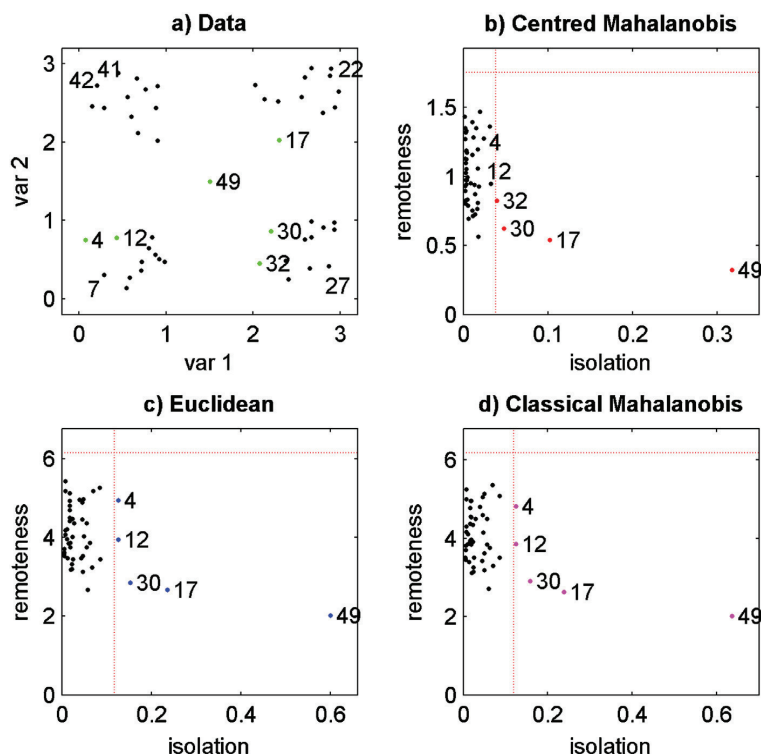


Fig. 3. Plots of the second simulated data set.

$MD_L^2$  was derived for each of them. The average distance values from each row and the minimum distance values from each column were retrieved from this distance matrix to derive the remoteness and isolation degree vectors, respectively. The values of these two parameters were used as the point coordinates of all the data samples in the *RI* plot. Thresholds for both remoteness and isolation degree were calculated according to Eq. (13) and reported in the *RI* plots by red lines. The data samples associated with very high values for remoteness were classified as outliers of first type being far from the variable space defined by the bulk of the data, i.e. remote samples; the data samples associated with high values of isolation degree were classified as outliers of second type, they being isolated from the other samples in spite of their position within the variable space, i.e. isolated samples.

To facilitate the performance evaluation of the newly proposed approach the results were compared with those derived still using the proposed definitions of remoteness and isolation degree as obtained by the Euclidean distance and the classical Mahalanobis distance. Principal component analysis (PCA) was also used to better explain the results for those cases where the number of variables exceeded two.

The scatter plot of the first simulated data set, together with the *RI* plots obtained by the locally centred Mahalanobis, Euclidean and classical Mahalanobis distances are shown in Fig. 2.

As expected, two data samples 49 and 50 were highly isolated from the cluster and far from the bulk of the data. This aspect can be easily interpreted from the *RI* plot for this simulated data set shown in Fig. 2b. Both these data samples were associated with high values for remoteness and isolation degree which clearly indicated that

they are quite isolated in their local and global spaces. Moreover, data sample 27 was associated with a higher value of isolation as compared to the other data samples in the cluster. A careful observation of the scatter plot in Fig. 2a indicates that sample 27 is within the extremities of the cluster as well as no other data samples from the cluster are very closely located in its vicinity. This indicates that the new approach is quite sensitive to the isolation of the samples.

The analogous *RI* plots obtained from the Euclidean and classical Mahalanobis distances (Fig. 2c and 2d) confirm the anomalous behaviour of samples 49, 50 and 27 but also allow to detect the samples 14 and 42 as isolated from the bulk of data, although they have a small isolation degree as for sample 27.

The second data set used as case study was a two-dimensional simulated data set with data samples roughly divided within four clusters and a single data sample (49) localized more or less between these clusters. The scatter plot of this data set in Fig. 3a indicates this isolated sample clearly being a potential outlier; however, it was also interesting to see how the outlier detection techniques were able to analyse this data.

As expected, the novel outlier detection approach was able to clearly identify sample 49 as a second type outlier based on its extreme value for isolation degree. This result was achieved with all the three metrics in analysis. Remoteness for the data samples was not extremely high for any specific data sample and then no first type outliers are detected. Samples 17, 30 and 32 that were not very closely located to their nearest of the four clusters were also identified with higher values of isolation degree (Fig. 3b). It is noteworthy that locally centred Mahalanobis distance classifies sample

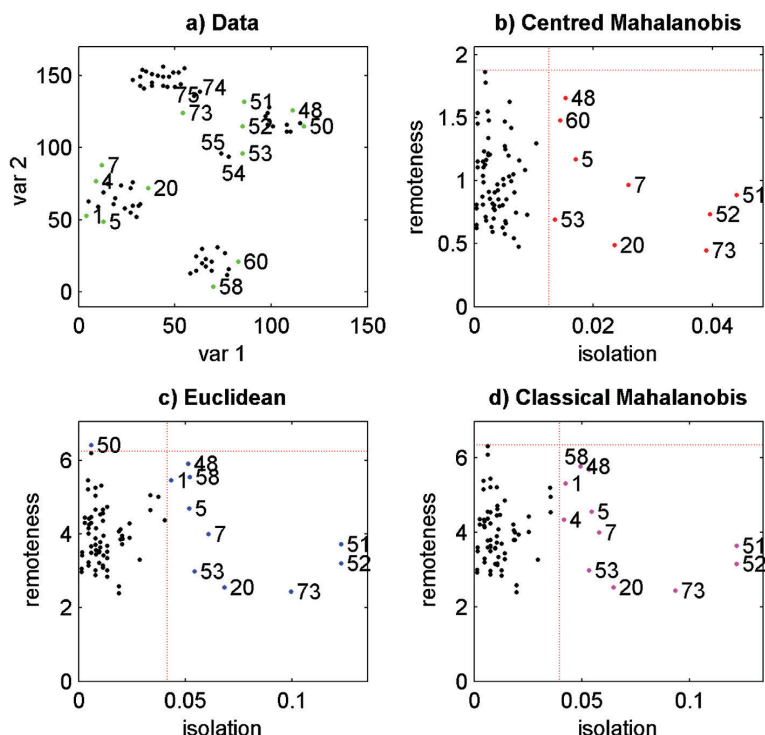


Fig. 4. Plots of the Ruspini data set.

32 as isolated sample while this is not recognized by Euclidean and classical Mahalanobis distances. The latter, on the contrary, identify 4 and 12 as isolated samples, which indeed seem quite far apart from the centre of the cluster they belong to. Being the variable space of this simulated example basically defined into a spherical space, the results obtained from the Euclidean and classical Mahalanobis distances are comparable.

The two-dimensional Ruspini data set is shown in Fig. 4a. By looking at the object disposition, it is quite apparent that no remote samples are present, while several isolated samples can be detected within the variable domain. In particular, the samples 51, 52 and 73 were associated with the highest isolation degree by all the three metrics and, to a smaller extent, the samples 7 and 20. It should be noted that the two pairs of samples 54–55 and 74–75, which are quite isolated, are not detected as isolated, they being very near to each other.

Also for this case study, the variable space being basically a spherical space, the results obtained from the three metrics are quite comparable. The most relevant differences are: (1) Euclidean distance identifies 50 as remote sample (Fig. 4c); (2) sample 60 is classified as isolated only by the method based on locally centred Mahalanobis distances (Fig. 4b); (3) 1 and 4 are identified as isolated samples by Euclidean and classical Mahalanobis even if the corresponding isolation degree values are not much larger than the threshold (Fig. 4c and 4d).

Iris data set plots are collected in Fig. 5. As the variables are four for this case study, the data set graphical visualization was achieved in the reduced space of the first two principal components (Fig. 5a).

For the Iris data set, the three *RI* plots gave very different information; Euclidean (Fig. 5c) and classical Mahalanobis (Fig. 5d)

distances provided with several isolated samples, whereas the locally centred Mahalanobis distance identified a few isolated samples (i.e., 42, 126, 118, 132), which in addition are not very distant from the threshold suggesting that they are not seen as too much isolated. Both locally centred (Fig. 5b) and the classical Mahalanobis distance (Fig. 5d) identified the same remote samples (i.e., 132, 118, 135, 142, 115, 42, 107, 16, 136, and 146), whereas the Euclidean distance seemed to be able to detect only a few of them (i.e., 132, 118, 16, 119), which are apparent anomalous samples also in the space defined by the first two principal components (Fig. 5a). To further investigate the reasons of anomalous behaviour of some samples identified by the *RI* plot based on locally centred Mahalanobis distances, the 3D plot of the Iris data set, derived from the original variables  $X_1$ ,  $X_2$ , and  $X_4$ , was analysed along with the 3D plot on PC2, PC3 and PC4 (Fig. 6).

In Fig. 6a, it can be noted that most of the detected remote samples are located near the boundary of the data space and thus are correctly identified as extreme samples. Considering this plot there are three exceptions, i.e., samples 135, 142 and 146, which seem to belong to the data bulk and, accordingly, do not appear as anomalous samples; however, if one switches to the principal component space and considers the last PC4 (Fig. 6b), then these samples clearly appear as outliers. It is also noteworthy that sample 126 is identified as isolated only by the locally centred Mahalanobis distance and looking at the plot of Fig. 6a although still belonging to the data bulk it indeed appears quite distant from its first neighbours. Only the novel locally centred Mahalanobis distance is able to clearly detect this particularity since it seems to give more emphasis to those samples that are distant from the data bulk along some direction orthogonal to the maximum variance direction; this is the case of sample 126.

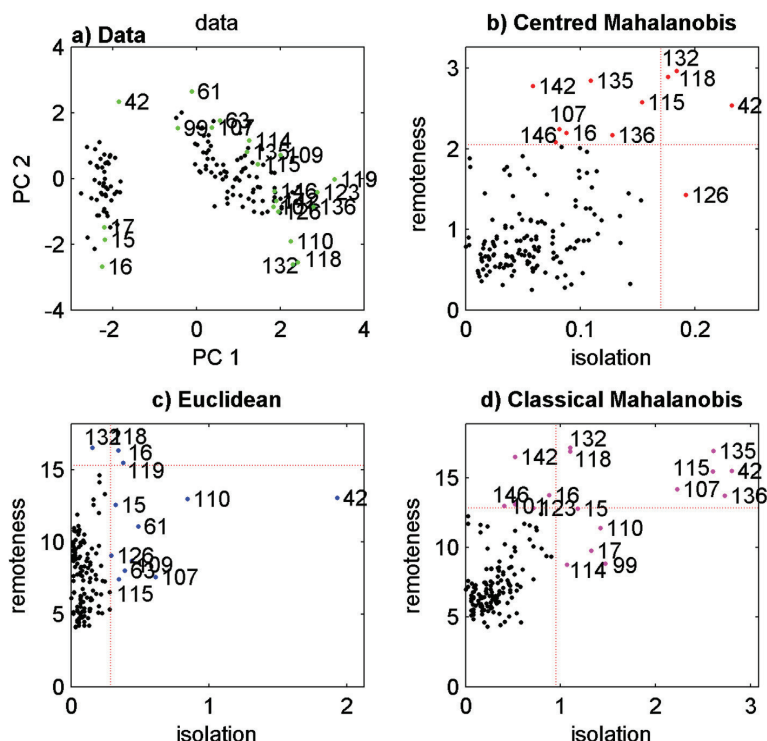


Fig. 5. Plots of the Iris data set.

Finally, the Italoil data set was considered. The corresponding plots are collected in Fig. 7, where the first plot (Fig. 7a) shows the first two principal components of this data set (explained variance 95.8%).

Also for the Italoil data set, the *RI* plots based on Euclidean (Fig. 7c) and classical Mahalanobis (Fig. 7d) distances identify a quite large number of isolated samples; on the contrary, the *RI* plot based on the centred Mahalanobis distances identifies no isolated samples. All the three *RI* plots classify several samples as remote, they being associated with remoteness values larger than the threshold. Almost all of these samples are located towards the extremities of the data space and thus are correctly identified as

anomalous, as it can be derived from the PC plot (Fig. 7a). It is noteworthy that, unlike Euclidean distance, both the locally centred and classical Mahalanobis distances do not highlight samples 263 and 317 as apparent remote sample since they are located along the directions of maximum data variance. Moreover, as shown in Fig. 7b and d, both the Mahalanobis distances identify the sample 390 as a potential outlier due to its extremely high value for remoteness. A deeper analysis of the 8 original variables for the Italoil data set did not provide any anomalous value for the sample 390; however, through PCA, it was possible to find out that considering the last two PCs (7 and 8, explained variance 1.52%, Fig. 8) the sample 390 is completely far from the data domain.

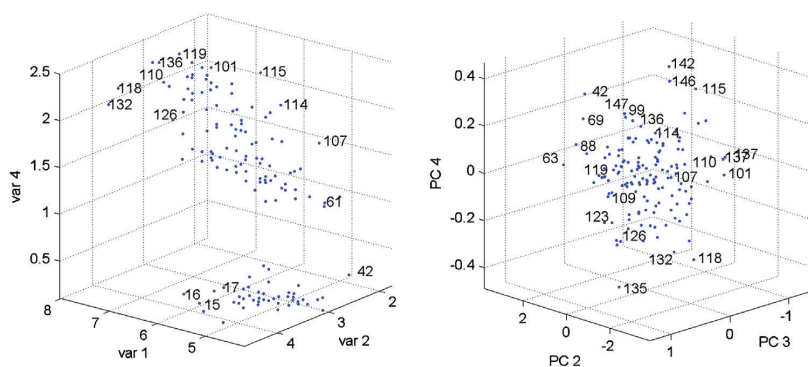


Fig. 6. 3D plots of Iris data set: (a) original variable X1, X2, and X4; (b) principal components PC2, PC3 and PC4.

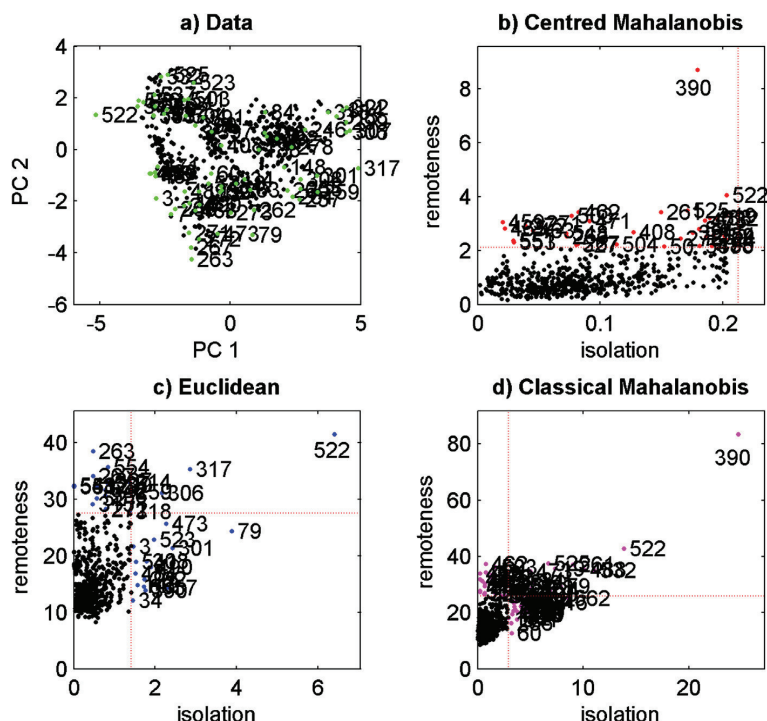


Fig. 7. Plots for the Italoil data set.

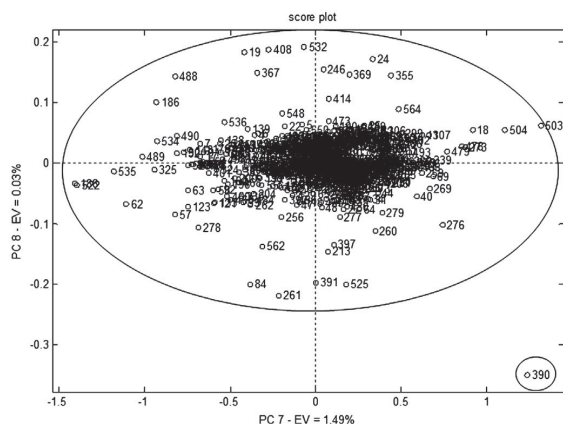


Fig. 8. Scatter plot of the last two PCs of the Italoil data set.

## 5. Conclusions

Locally centred Mahalanobis distances were derived centring the data matrix on each sample, thus obtaining an object-oriented covariance matrix. The corresponding pair-wise distance matrix for a data set was asymmetric in nature, unlike the one derived with the classical Mahalanobis distances centred on the data centroid. The significance of row and column values in this asymmetric distance matrix was discussed and later, two new parameters termed as Remoteness and Isolation degree were derived. The values corresponding to these two parameters, when plotted on the axes of a

scatter plot, represent the isolation of data samples in their global and local spaces, thus allowing to well differentiate the potential outliers that diverged from the majority pattern of the data samples. The plot derived from Remoteness and Isolation degree vectors was called *RI* plot and proposed as useful tool to data set analysis oriented towards potential outlier detection.

Considering simulated and benchmarked data sets from literature as case studies, the values corresponding to these two matrix parameters allowed identification of several diverse samples, which were highly isolated in their global and local distance space. The usefulness of these matrix parameters was more obvious while dealing with multivariate data sets, where the lack of data visualization somehow restricts the analyst to well explore the data structure or to identify structurally diverse compounds. In order to better evaluate the performance of this newly proposed approach, the results were compared with those derived from Euclidean and classical Mahalanobis distances.

Remoteness and isolation degree parameters (and the *RI* plot) can be useful to explore potential outliers from a given set of data, using all the metrics discussed in this article, although the newly proposed one appears more powerful in taking into account covariance structures of complex multivariate data sets.

In conclusion, the implementation of locally centred squared Mahalanobis distances and the *RI* plot adds something new to the existing techniques towards outlier detection and a comprehensive overview of potential outliers.

## Acknowledgments

The research leading to these results has received funding from the European Community's Seventh Framework Programme

[FP7/2007–2013] under Grant Agreement n. 238701 of Marie Curie ITN Environmental Chemoinformatics (ECO) project.

## Appendix A. Lower and upper bounds of isolation degree and remoteness

A necessary condition for the validity of the following theorems is the existence of the inverse covariance matrices  $\mathbf{S}_{(j)}$ , for  $j = 1, \dots, n$ . The inverse exists if and only if the determinant of  $\mathbf{S}_{(j)}$  is larger than zero. This implies that the number of samples  $n$  must be greater than the number of variables  $p$  and that more than  $p$  samples must be different from each other.

**Theorem 1.**  $Idg_j \in [0, 1]$

**Proof.** (a) Lower bound:  $Idg_j = 0 \Leftrightarrow \mathbf{x}_k = \mathbf{x}_j$  for  $k \neq j$ . Negative values cannot occur.

(b) Upper bound: Suppose that there exists a  $j$  with  $Idg_j > 1$ , i.e.  $\min_i (MD_L^2(i, j)) > 1$

Since

$$\begin{aligned} \sum_{i=1}^n MD_L^2(i, j) \\ = \sum_{i=1}^n \frac{1}{p} \cdot (\mathbf{x}_i - \mathbf{x}_j)^T \left[ \frac{1}{n-1} \sum_{l=1}^n (\mathbf{x}_l - \mathbf{x}_j)(\mathbf{x}_l - \mathbf{x}_j)^T \right]^{-1} (\mathbf{x}_i - \mathbf{x}_j) = n-1 \end{aligned}$$

for any  $j \in \{1, \dots, n\}$ , we have in particular:

$$MD_L^2(1, j) + \dots + MD_L^2(j-1, j) + 0 + MD_L^2(j+1, j) + \dots + MD_L^2(n, j) = n-1$$

So, these are  $n-1$  terms that have to sum up to  $n-1$ , which is in contradiction that the smallest term is already larger than 1. It follows that the minimum is not larger than 1.

**Theorem 2.**  $Rem_i \in (0, \frac{n-1}{p}]$

**Proof.** (a) Lower bound: Suppose that

$$Rem_i = 0 \Leftrightarrow MD_L^2(i, 1) = \dots = MD_L^2(i, n) = 0 \Leftrightarrow \mathbf{x}_1 = \dots = \mathbf{x}_n$$

which would lead to singularity of  $\mathbf{S}_{(j)}$ . Thus,  $Rem_i$  can be arbitrarily close to 0, but not reach 0. Negative values cannot occur.

(b) Upper bound: Consider the following property [14]:  $\max_{\mathbf{x} \neq 0} (\mathbf{x}^T \mathbf{B} \mathbf{x} / \mathbf{x}^T \mathbf{x}) = k_1$  and the maximum is attained if  $\mathbf{x} = \mathbf{e}_1$ , where  $\mathbf{e}_1$  is the normed eigenvector of  $\mathbf{B}$  to the largest eigenvalue  $k_1$ . Now consider

$$\mathbf{B} = \left[ \sum_{m=1}^n (\mathbf{x}_m - \mathbf{x}_j)(\mathbf{x}_m - \mathbf{x}_j)^T \right]^{-1}$$

Then we can find an eigenvalue decomposition of  $\mathbf{B}^{-1}$  of the form

$$\mathbf{B}^{-1} = \sum_{k=1}^p \lambda_k \mathbf{e}_k \mathbf{e}_k^T \text{ with } \lambda_1 \geq \lambda_2 \geq \dots \geq \lambda_p > 0, \text{ and normed eigenvectors } \mathbf{e}_k.$$

Then the inverse can be presented as  $\mathbf{B} = \sum_{k=1}^p \frac{1}{\lambda_k} \mathbf{e}_k \mathbf{e}_k^T$ . Now,

let  $\mathbf{e}_1 = \mathbf{x}_1 - \mathbf{x}_j \neq 0$ .

Then we have:

$$\begin{aligned} \mathbf{B}^{-1} &= (\mathbf{x}_1 - \mathbf{x}_j)(\mathbf{x}_1 - \mathbf{x}_j)^T + \sum_{m=2}^n (\mathbf{x}_m - \mathbf{x}_j)(\mathbf{x}_m - \mathbf{x}_j)^T \\ &= \lambda_1 \mathbf{e}_1 \mathbf{e}_1^T + \sum_{k=2}^p \lambda_k \mathbf{e}_k \mathbf{e}_k^T \end{aligned}$$

with  $\lambda_1 = 1$ . Now setting  $\mathbf{x} = \mathbf{e}_1$  in  $\max_{\mathbf{x} \neq 0} (\mathbf{x}^T \mathbf{B} \mathbf{x} / \mathbf{x}^T \mathbf{x})$ , attains  $k_1 = (1/\lambda_1) = 1$  as the maximum.

Note that

$$\frac{\mathbf{x}^T \mathbf{B} \mathbf{x}}{\mathbf{x}^T \mathbf{x}} = (\mathbf{x}_1 - \mathbf{x}_j)^T \left[ \sum_{m=1}^n (\mathbf{x}_m - \mathbf{x}_j)(\mathbf{x}_m - \mathbf{x}_j)^T \right]^{-1} (\mathbf{x}_1 - \mathbf{x}_j).$$

If we build the sum over all  $j = 1, \dots, n$ , the resulting maximum is  $n-1$ , because one of the terms is zero. Since

$$\begin{aligned} Rem_i &= \frac{1}{n-1} \cdot \sum_{j=1}^n MD_L^2(i, j) \\ &= \frac{1}{n-1} \cdot \sum_{j=1}^n \frac{1}{p} \cdot (\mathbf{x}_i - \mathbf{x}_j)^T \left[ \frac{1}{n-1} \sum_{m=1}^n (\mathbf{x}_m - \mathbf{x}_j)(\mathbf{x}_m - \mathbf{x}_j)^T \right]^{-1} (\mathbf{x}_i - \mathbf{x}_j) \\ &= \frac{1}{n-1} \cdot \frac{(n-1)^2}{p} \end{aligned}$$

it follows immediately that the upper bound is  $n-1/p$ .

## References

- [1] N.A. Campbell, The influence function as an aid in outlier detection in discriminant analysis, *Appl. Stat.* 27 (1978) 251–258.
- [2] A. Lazarevic, V. Kumar, Feature bagging for outlier detection, in: KDD'05 Proceedings of the Eleventh ACM SIGKDD International Conference on Knowledge Discovery in Data Mining, 2005, pp. 157–166.
- [3] V.J. Hodge, J. Austin, A Survey of outlier detection methodologies, *Artif. Intell. Rev.* 22 (2004) 85–126.
- [4] F. Angiulli, C. Pizzuti, Fast Outlier Detection in High Dimensional Spaces, *Principles of Data Mining and Knowledge Discovery*, Springer, Berlin/Heidelberg, 2002, pp. 43–78.
- [5] P.J. Rousseeuw, B.C. Van Zomeren, Unmasking multivariate outliers and leverage points, *J. Am. Stat. Assoc.* 85 (1990) 633–639.
- [6] P. Filzmoser, C. Reimann, R.G. Garrett, Multivariate outlier detection in exploration geochemistry, *Comput. Geosci.* 31 (2005) 579–587.
- [7] R.J. Pell, Multiple outlier detection for multivariate calibration using robust statistical techniques, *Chemom. Intell. Lab. Syst.* 52 (2000) 87–104.
- [8] B. Walczak, D.L. Massart, Multiple outlier detection revisited, *Chemom. Intell. Lab. Syst.* 41 (1998) 1–15.
- [9] D. Peña, F.J. Prieto, Multivariate outlier detection and robust covariance matrix estimation, *Technometrics* 43 (2001) 286–310.
- [10] J. Hardin, D. Rocke, The distribution of robust distances, *J. Comput. Graph. Stat.* 14 (2005) 1–19.
- [11] E.H. Ruspini, Numerical methods for fuzzy clustering, *Inform. Sci.* 2 (1970) 319–350.
- [12] R.A. Fisher, The use of multiple measurements in taxonomic problems, *Ann. Eugen.* 7 (1936) 179–188.
- [13] M. Forina, C. Armanino, S. Lanteri, E. Tiscornia, Classification of Olive Oils from their Fatty Acid Composition, in: H. Martens, H. Russwurm Jr. (Eds.), *Food Research and Data Analysis*, Applied Science Pub, London, 1983, pp. 189–214.
- [14] R.A. Johnson, D.W. Wichern, *Applied Multivariate Statistical Analysis*, Prentice-Hall, Englewood Cliffs (NJ), 1992.

RESEARCH ARTICLE

Open Access

# Defining a novel $k$ -nearest neighbours approach to assess the applicability domain of a QSAR model for reliable predictions

Faizan Sahigara, Davide Ballabio, Roberto Todeschini and Viviana Consonni\*

## Abstract

**Background:** With the growing popularity of using QSAR predictions towards regulatory purposes, such predictive models are now required to be strictly validated, an essential feature of which is to have the model's Applicability Domain (AD) defined clearly. Although in recent years several different approaches have been proposed to address this goal, no optimal approach to define the model's AD has yet been recognized.

**Results:** This study proposes a novel descriptor-based AD method which accounts for the data distribution and exploits  $k$ -Nearest Neighbours (kNN) principle to derive a heuristic decision rule. The proposed method is a three-stage procedure to address several key aspects relevant in judging the reliability of QSAR predictions. Inspired from the adaptive kernel method for probability density function estimation, the first stage of the approach defines a pattern of thresholds corresponding to the various training samples and these thresholds are later used to derive the decision rule. Criterion deciding if a given test sample will be retained within the AD is defined in the second stage of the approach. Finally, the last stage tries reflecting upon the reliability in derived results taking model statistics and prediction error into account.

**Conclusions:** The proposed approach addressed a novel strategy that integrated the kNN principle to define the AD of QSAR models. Relevant features that characterize the proposed AD approach include: a) adaptability to local density of samples, useful when the underlying multivariate distribution is asymmetric, with wide regions of low data density; b) unlike several kernel density estimators (KDE), effectiveness also in high-dimensional spaces; c) low sensitivity to the smoothing parameter  $k$ ; and d) versatility to implement various distances measures. The results derived on a case study provided a clear understanding of how the approach works and defines the model's AD for reliable predictions.

**Keywords:** QSAR, Applicability domain, kNN, Nearest neighbour, Model validation

## Background

The popularity of QSARs has seen a growth from time to time and was complemented by the availability of more sophisticated and efficient model development techniques. This fact was further supported by the consideration of QSAR predictions for regulatory purposes. To deal with risk assessment of chemicals for their safe use, a new European legislation – REACH (Registration, Evaluation, Authorization and restriction of Chemicals) was approved in the recent years [1]. To reduce animal testing and replacing them by cost effective methods, this law encourages

the use of QSARs as a possible alternative when enough experimental data is not available, provided that the model was strictly validated for its regulatory consideration [2].

There are several aspects that must be taken into account before considering a QSAR model reliable enough. In other words, the validity of a model has to be evaluated. Existing literature has often emphasized upon validating the QSAR models to reflect their robustness and predictive ability. In 2004, following five OECD principles for model validation were adopted to validate a QSAR model for its regulatory consideration: a) a defined end-point; b) an unambiguous algorithm; c) a defined domain of applicability d) appropriate measures for goodness-of-fit, robustness and predictivity and e) mechanistic interpretation, if possible [3].

\* Correspondence: viviana.consonni@unimib.it

Milano Chemometrics and QSAR Research Group, Department of Earth and Environmental Sciences, University of Milano-Bicocca, P.za della Scienza 1, Milano 20126, Italy



Applicability domain (AD) of a QSAR model defines the model's limitation in its structural domain and response space. In other words, this principle for model validation restricts the applicability of a model to reliably predict those test samples that are structurally similar to the training samples used to build that model [4-6]. Several approaches were proposed in the past years to define the AD of QSAR models. These approaches mainly differed in the algorithm used to characterise the AD within the descriptor space, where the model can predict reliably [7,8]. For instance, some classical approaches suggested defining the domain of applicability by a) considering the range of descriptors values; b) enclosing the training space in a convex hull; c) calculating the distance of a query compound from a defined point within the model's descriptor space and d) estimating the Probability Density Function for the given data. All these approaches were associated with their own advantages and limitations [2,7-10]. From time to time, several approaches were proposed that were aimed to be more efficient or were thought to overcome several limitations of existing approaches.

This article proposes a new heuristic approach towards defining the AD of QSAR models. The basis of this novel strategy is inspired from the *k*-Nearest Neighbours (kNN) approach and adaptive kernel methods for probability density estimation (kernel density estimators, KDE) [11]. Due to its simplicity and easy implementation, kNN had been a preferred choice for several proposed QSAR studies [6,12-18].

In the classical kNN approach for AD evaluation [6,18], average distances of all the training samples from their *k* nearest neighbours are calculated and used to define a unique threshold to decide if a test sample is inside or outside the model's AD (for example, 95th percentile). Moreover, in the framework of the probability density function estimation, the nearest neighbour method provides density estimates depending on the Euclidean distance to the *k*-th nearest data point [19]. Following the same concept, the proposed method tries to integrate the kNN principle with the salient features of adaptive kernel methods [11], which define local bandwidth factors corresponding to the training data points and use them to build the density estimate at a given point.

The novelty of the kNN based AD approach proposed in this article lies in the overall strategy that is properly executed in a three-stage procedure to encapsulate and reflect upon several significant aspects towards model validation. Moreover, some features common to most of the AD approaches were dealt differently with this approach; for instance, rather than defining a general threshold as in all the distance-based approaches, each training sample in this approach was associated with its individual threshold; in order to find an optimal smoothing parameter *k*, this

approach performed a *k*-optimization procedure based on Monte Carlo validation; additionally, model's statistical parameters and other relevant aspects were dealt simultaneously to reflect upon the reliability in the derived results.

To better understand the strategy behind this approach, it was implemented on a dataset from the literature. The dataset was chosen from the CAESAR project to predict the bioconcentration factor (BCF) [20,21]. The derived results were discussed in comparison with those derived from other literature AD approaches.

## Methods

### *k*-Nearest Neighbours principle from AD perspective

The kNN principle basically reflects upon the structural similarity of a test sample to the training samples used to build that model. In theory, the distance of a query sample is considered from its *k* closest data points in the chemical space. Lower distance values correspond to a higher similarity, while the increasing distances signify higher levels of structural mismatch. The *k* value plays a significant role in defining how constraint the approach will be and thus, it can be referred to as the smoothing parameter.

A stepwise execution of the following three stages characterises the workflow of this approach:

- 1) defining thresholds for training samples
- 2) evaluating AD for new/test samples
- 3) optimizing the smoothing parameter *k*

To allow a better interpretation of the proposed approach, results on a two-dimensional simulated dataset will be considered throughout the major part of this discussion and wherever applicable. As shown in Figure 1, this dataset has a cluster of 48 training samples and the remaining two training samples (49 and 50) are located quite in the extremities of the space with respect to these clustered samples.

### Defining thresholds for training samples

Thresholds have a great influence in characterising the AD for reliable predictions; a test sample that exceeds the threshold condition is associated with an unreliable prediction.

Like the adaptive kernel methods, instead of defining a general unique threshold as seen with several classical AD approaches, the proposed approach allocates a set of thresholds corresponding to the various training samples.

For a given value of *k*, threshold allocation process can be summarised as follows:

- a) First of all, the distances of each training sample from the remaining  $n - 1$  samples are calculated and ranked in increasing order, *n* being the total number of training samples. This will result in a  $n \times (n - 1)$

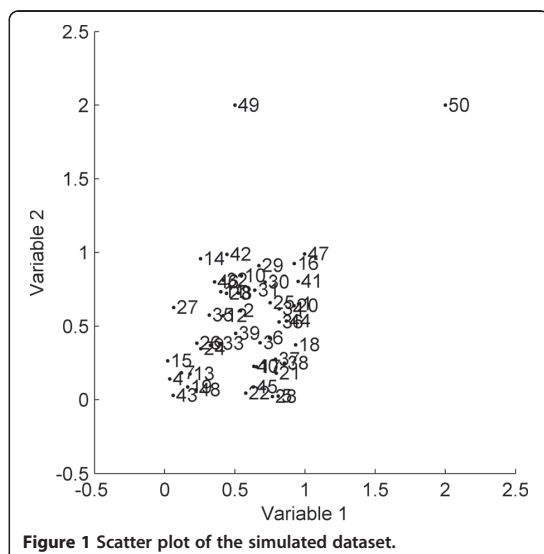


**Figure 1** Scatter plot of the simulated dataset.

neighbour table **D**; an entry  $D_{ij}$  of the table corresponds to the distance of the  $i$ -th sample from its  $j$ -th nearest neighbour:

$$D_{i1} \leq D_{i2} \leq \dots \leq D_{i,n-1}$$

- b) The average distance of each  $i$ -th sample from its  $k$  nearest neighbours is calculated considering the first  $k$  entries in  $i$ -th row of the neighbour table:

$$\bar{d}_i(k) = \frac{\sum_{j=1}^k D_{ij}}{k}$$

where,  $1 \leq k \leq n-1$  and  $\bar{d}_i(k) \leq \bar{d}_i(k+1)$  (1)

A vector  $\bar{\mathbf{d}}(k)$  of average distance values is then derived considering all the samples in the training set.

- c) Next, a reference value (from now on referred as *Ref Val*),  $\bar{d}(k)$  is determined as follows:

$$\bar{d}(k) = Q3(\bar{\mathbf{d}}(k)) + 1.5[Q3(\bar{\mathbf{d}}(k)) - Q1(\bar{\mathbf{d}}(k))] \quad (2)$$

where,  $Q1(\bar{\mathbf{d}}(k))$  and  $Q3(\bar{\mathbf{d}}(k))$  are the values corresponding to the 25th and 75th percentiles in the vector  $\bar{\mathbf{d}}(k)$ , respectively [22].

- d) Next, the ordered distances of each  $i$ -th training sample from all other  $n-1$  training samples are compared with the *Ref Val*. If the distance value of the  $i$ -th sample from its given  $j$ -th training neighbour (where  $1 \leq j \leq n-1$ ) is less than or equal to the *Ref Val*, then that distance value is retained, otherwise is discarded. The number  $K_i$  of neighbours

satisfying this condition, minimum zero and maximum being  $n-1$ , defines the density of the  $i$ -th sample neighbourhood:

$$K_i: \{D_{ij} \leq \bar{d}(k)\} \quad \forall j: 1, n-1 \quad (3)$$

- e) Finally, each  $i$ -th training sample is associated with a threshold  $t_i$  which defines the width of its neighbourhood as:

$$t_i = \frac{\sum_{j=1}^{K_i} D_{ij}}{K_i} \quad (4)$$

If no distance value was retained for a given  $i$ -th training sample ( $K_i = 0$ ), then its threshold  $t_i$  would be theoretically settled to 0, but a pragmatic solution is to set it equal to the smallest threshold of the training set.

The plot in Figure 2 provides with an overview of the thresholds for all the 50 samples in the simulated dataset. As expected, most of the training samples within the cluster (for instance, samples 2, 33 and 39) were associated with higher  $K_i$  values. On the other hand, obvious potential outliers (samples 49 and 50) had their thresholds equal to 0 since they couldn't satisfy the threshold criterion even for a single training neighbour (i.e.  $K_i = 0$ ), thus no distance values contributed to their threshold calculation. Nevertheless, they were associated with the minimum threshold equal to 0.42, i.e. the threshold of sample 43.

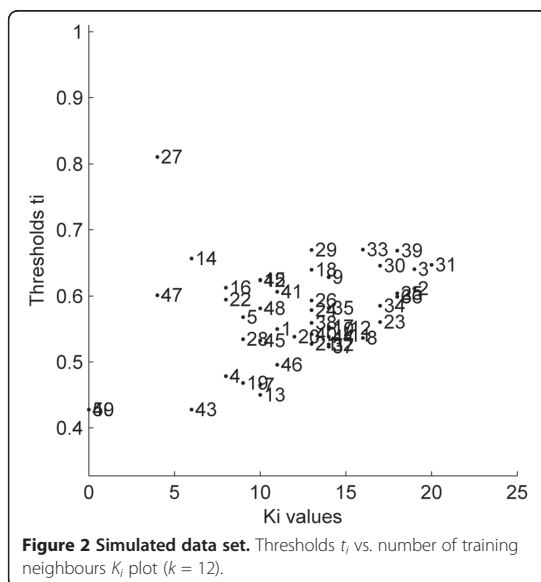


**Figure 2** Simulated data set. Thresholds  $t_i$  vs. number of training neighbours  $K_i$  plot ( $k = 12$ ).



### Evaluating AD for new/test samples

Until this point, each training sample was associated with its individual threshold. The next step will be to characterise the AD which usually relies upon a set of conditions that will decide if a given test sample can be associated with a reliable prediction or not.

The criterion used by this approach to associate a given test sample to be within the domain of applicability can be summarised below.

Given a test sample, its distance from all the  $n$  training samples is calculated and simultaneously, compared to be less than or equal to the thresholds associated with those training samples. If this condition holds true with at least one training sample, the test sample will be considered inside the domain of applicability for that model. Otherwise, the prediction for that test sample will be rendered unreliable.

More formally, given the training set  $TR$ , for each test sample  $j$ , the AD decision rule is:

$$j \in AD \quad \text{iff} \quad \exists i \in TR : D_{ij} \leq t_i \quad (5)$$

where  $D_{ij}$  is the distance between the  $j$ -th test sample and the  $i$ -th training sample and  $t_i$  is the individual threshold of the latter. In addition, each test/new sample will be associated with the number  $K_j$  of nearest training neighbours for which the previous condition holds true. This number can be assumed as a measure of prediction reliability; indeed, high values of  $K_j$  indicate that the new sample falls within a dense training region of the model's space, while low values of  $K_j$  denote that the new sample still belongs to the model's space, but located in sparse training regions.  $K_j$  equal to zero rejects the sample as it being outside the model's AD since no training neighbours are identified.

Figure 3 provides with the contour plot for the simulated dataset derived projecting several data points enough to fill the training space. Thresholds were calculated using 12 nearest neighbours and Euclidean distance. This choice of  $k = 12$  nearest neighbours was based on the results derived performing an internal  $k$ -optimization, discussed later in this article. The space enclosed around the cluster represented as black line indicates that all the data points within this enclosed region were inside the AD. Thus, this region reflects in a way how the AD was characterised for this two-dimensional dataset. Area of this enclosed region tends to expand or shrink depending upon the number of nearest neighbours used for threshold calculation.

As explained earlier, the extreme outliers in the training space will be associated with the number  $K_i$  of neighbours equal to zero and the lowest possible threshold in the training set. Consider the sample 49 from the simulated dataset which is an extreme outlier with its threshold equal to 0.42. If there is a test sample that seems to

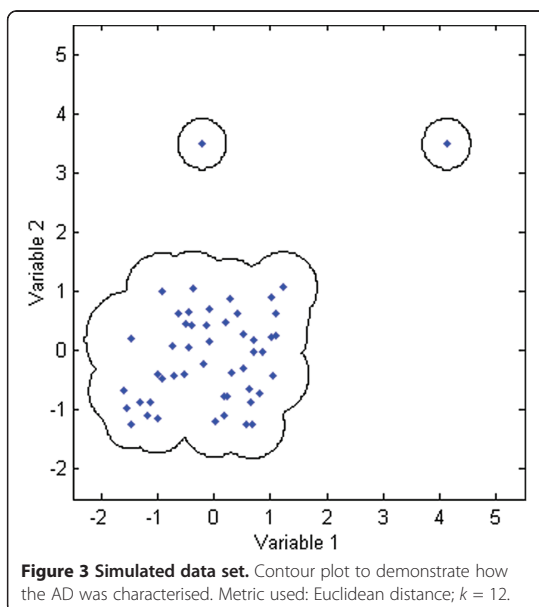


**Figure 3 Simulated data set.** Contour plot to demonstrate how the AD was characterised. Metric used: Euclidean distance;  $k = 12$ .

be quite in the vicinity of this potential outlier within the descriptor space, the test sample will be associated with an unreliable prediction since its distance from sample 49 will likely exceed the small threshold. Now, consider a case, where the descriptor values for another test sample exactly overlap or are very similar to those for this potential outlier. In this situation, the distance of that sample from the outlier will be less than the threshold and thus it will be considered within the domain of applicability. In theory, this is not wrong because the potential outlier is still a part of the training space. Practically, the approach retains all the training samples to characterize the AD but minimizing the role of potential outliers in doing so. That's the reason why the first test sample was excluded from being reliably predicted while the second sample was not. However, for the latter the number  $K_j$  of nearest training neighbours will likely be equal to one indicating that its prediction has some degree of uncertainty. In conclusion, there exists a relation between the defined AD and the impact of training samples in characterising it based on their threshold values.

### Optimizing the smoothing parameter $k$

Another important aspect is concerning the choice of an appropriate smoothing parameter  $k$ , whose theoretical range is between 1 and  $n-1$ .

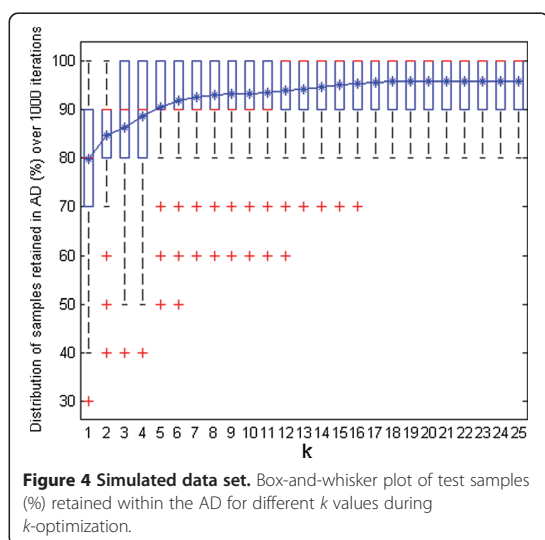
Very low  $k$  values will restrict the domain of applicability in a very strict manner as compared to the AD derived opting for larger  $k$  values. This is because, an opted  $k$  value will have a direct impact on the threshold calculations which in turn can make it more rigid or easier

for test samples to satisfy the threshold criterion. The strategy implemented in this article to select an appropriate  $k$  value was performed by Monte Carlo validation, maximizing the percentage of the test samples considered within the AD, i.e. satisfying AD criterion (Equation 5).

Box-and-whisker plots (box plots) were produced to get an overview of all these derived results. For instance, consider the plot in Figure 4 derived for the simulated dataset showing percentage of test samples retained within the AD with different  $k$  values (optimization carried out with 20% of samples in the test set and 1000 iterations).

Median quartile in the middle of the box (marked in red) can be referred for all the  $k$  values to get a hint about how many test samples were retained on average during the optimization process for a given  $k$  value. The top and bottom edges of each box plot (quartiles Q3 and Q1) correspond to 75th and 25th percentile, respectively. The whisker can extend further from  $Q1 - w(Q3 - Q1)$  until  $Q3 + w(Q3 - Q1)$ , of 1.5 [23]. The test samples falling outside this coverage are considered as outliers and are highlighted as '+' in red. About their usefulness in the proposed AD approach, box plots showing limited spread and allowing majority of test samples to be retained within the AD can be favoured and their corresponding range of  $k$  values can be considered to finally opt for the most appropriate  $k$ . Additionally, a line plot is integrated in the same figure indicating the mean percentage of test samples that were considered within the AD for each  $k$  value. A simultaneous interpretation of both these plots can make it easier for a user to decide upon an appropriate  $k$  value.

Figure 4 shows that the spread of the box plots for initial  $k$  values is quite large. This may have resulted due to



the impact of restricted training thresholds that excluded several test samples from the AD. With an increase in  $k$  values, the spread narrowed, however the outliers were still present until  $k = 17$ . After this point, the box plots remained unchanged throughout the plot with no outliers. Similar observations were derived from the mean line plot which showed a significant rise initially followed by a stable curve until the first half of the  $k$  values. The plot didn't show any major changes for the second half of the  $k$  values. In order to avoid very high  $k$  values good enough to unnecessarily expand the defined AD, a  $k$  value of 12 was opted as appropriate  $k$  for this dataset. The plots dealt earlier (Figures 2 and 3) for this dataset were thus derived using this opted  $k$  value.

We also performed an extended analysis on several diverse data sets (results not reported in this paper), to study the influence of the smoothing parameter  $k$  on model's AD definition. It was concluded that optimization of  $k$  can be a time-demanding procedure especially in the case of a huge number of samples, but it was also observed that this approach is quite insensitive to the smoothing parameter  $k$ , except for very small  $k$  values which led to the results influenced by local noise. Therefore, for many applications the optimization of the smoothing parameter can be avoided and reasonable results can instead be obtained by a fixed  $k$  value empirically calculated as  $n^{1/3}$ .

#### Reflecting the reliability in derived results

After the AD approach has been applied to the model of interest, several features will be taken into account to reflect upon the derived results. Moreover, as stated earlier the response domain will be taken into account to address the reliability in the results derived by characterising the AD of a model in its descriptor space.

In order to reflect upon a model's predictive ability, the predictive squared correlation coefficient ( $Q^2$ ) was used. Since the test samples excluded from the model's AD are unreliably predicted, in theory they should not be accounted for to calculate the model's statistics ( $Q^2$ ).

The following key parameters were evaluated:

- Number of test samples retained within the AD.
- $Q^2$  calculated from the test samples retained within the AD [24,25]:

$$Q^2 = 1 - \frac{\left[ \sum_{j=1}^{n_{TS}} (\hat{y}_j - y_j)^2 \right] / n_{TS}}{\left[ \sum_{i=1}^{n_{TR}} (y_i - \bar{y}_{TR})^2 \right] / n_{TR}} \quad (6)$$

where,  $y_j$  is the measured response value for the  $j$ -th sample and  $\hat{y}_j$  its predicted value;  $n_{TR}$  and  $n_{TS}$  represent the total number of training and test

samples, respectively, and  $\bar{y}_{TR}$  is the mean response of the training set.

- c) List of all the test samples considered outside the AD.
- d) For each  $j$ -th test sample, the absolute standardized error calculated as:

$$SE_j = \frac{|y_j - \hat{y}_j|}{s_Y} \quad (7)$$

where,  $y_j$  is the measured value for the  $j$ -th sample and  $\hat{y}_j$  its predicted value;  $s_Y$  the standard error of estimate derived from the training set.

- e) The information about how many times the threshold criterion (Equation 5) is satisfied by each test sample, that is, how many training neighbours (i.e.  $K_j$ ) are located at a distance less than or equal to their threshold values, from a given test sample.

In theory, a test sample satisfying the threshold criterion several times (i.e. having high  $K_j$ ) is expected to be predicted with higher accuracy. This can be desired since less distant training neighbours indicate a higher structural similarity of the test sample. On the contrary, a test sample satisfying the threshold criterion for no training neighbours ( $K_j = 0$ ) indicates that there wasn't any training sample similar enough to reliably predict that test sample.

## Results and discussion

As the case study to derive results with the proposed strategy, the CAESAR Model 2 to predict bioconcentration factor (BCF), which was developed under the EU project CAESAR following the REACH requirements, was selected. It is a Radial Basis Function Neural Network (RBFNN) model derived from 378 training and 95 test samples [20,21]. The five descriptors used to develop this model were calculated using Dragon 5.5 [26].

The statistics for this model are summarized in Table 1.

For comparison purposes, some AD approaches taken from literature [2,7-10] were implemented on the selected case study. Among them, the classical kNN-based AD approach [6,18] was implemented by calculating average distances of all the training samples from their 5 nearest neighbours (i.e.  $k = 5$ ); since the choice of

thresholds didn't follow any strict rules in the existing literature, the value corresponding to 95th percentile in this vector of average distances was considered as general threshold. If the average distance of a test sample was lesser than or equal to the threshold value, the test sample was retained within the AD.

In addition to the classical kNN-based AD approach, the following methodologies were considered [2,7-10]: the Bounding Box, which is based on the ranges of model variables; its variant based on principal components instead of the original variables (PCA-Bounding Box); the Convex Hull, which is the smallest convex area that contains the original set; two distance-based methods, which calculate the distance (Euclidean and Mahalanobis) of a test sample from the data centroid and use the 95th percentile of the training sample distances as threshold.

Finally, some methods for probability density function estimation were also considered. Among the multivariate kernel density methods, four variants of Gaussian kernel estimators were implemented [19]: fixed Gaussian kernel with bandwidth equal to 0.462 (for the studied data set); optimized Gaussian kernel with a smoothing parameter equal to 0.237 obtained by leave-one-out cross-validation [27]; variable Gaussian kernel with bandwidth calculated as the inverse function of the Euclidean distance to  $k$ -th neighbour ( $k = 15$ ) [27]; adaptive Gaussian kernel, with fixed Gaussian kernel as the pilot estimate and sensitivity parameter  $\alpha$  equal to 0.5. Finally, Epanechnikov kernel with a fixed bandwidth equal to 1.961 and the nearest neighbour density estimator with smoothing parameter  $k$  equal to 15, were also considered [19].

For all the implemented methods, except for Bounding Box and Convex Hull, autoscaling was adopted as data pretreatment.

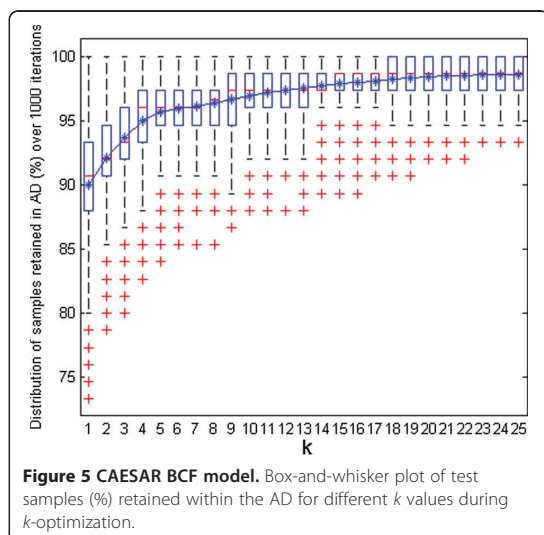
The proposed AD strategy was implemented in MATLAB [28] using autoscaled Euclidean distances. The  $k$ -optimization procedure was carried out initially to decide upon an optimal  $k$  value; the training set of 378 samples was randomly partitioned 1000 times selecting 20% of samples in the test set (i.e. 75 samples). The box plots in Figure 5 summarize the percentage of test samples retained within the AD for different  $k$  values (up to 25).

As expected, the first lower  $k$  values were associated with box plots having highest spread. This degree of dispersion lowered gradually with increase in number of neighbours considered. The line plot of the mean showed an increase in the number of samples throughout the plot, however, this increment after initial  $k$  values was gradual. Based on their lower spread and preference to retain reasonably higher number of samples within the AD (as reflected from their median), the  $k$  values in the range of 15–19 were considered further to decide upon an optimal  $k$ . Finally, to avoid unnecessarily higher training thresholds and their resulting impact on the defined AD,  $k = 15$  was

**Table 1 Summary of model statistics for the case study**

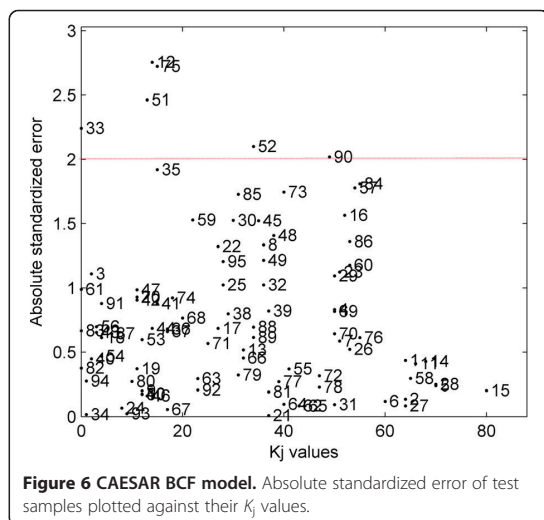
Model	Training set			Test set		
	$n_{TR}$	$R^2$	RMSE	$n_{TS}$	$Q^2$	RMSEP
CAESAR Model 2	378	0.804	0.591	95	0.797	0.600

$R^2$  Determination coefficient; RMSE Root-mean-square error;  $Q^2$  Predictive squared correlation coefficient; and RMSEP Root-mean-square error of prediction.



considered as an optimal choice for this case study. Considering the selected  $k$  value of 15, the novel AD approach identified four test samples (33, 61, 82 and 83) being outside the model's AD.

To reflect upon the reliability in the results derived with this approach, absolute standardized error of all the test samples was plotted against their corresponding  $K_j$  values. As shown in Figure 6, four test samples considered outside the AD with this approach were associated with a value of  $K_j = 0$ . The absolute standardized error for sample 33 was quite higher as compared to the remaining three samples. As seen clearly from the plot,



there had been a sharp decrease in the prediction error of test samples with an increase in  $K_j$ . However, it can't be denied that this pattern wasn't rigidly followed in the results. There had been test samples with very low  $K_j$  values but extremely low or negligible absolute standardized error, meaning that even less reliable predictions can have good accuracy. In any case, this plot somehow tried to interpret the AD results derived in model's descriptor space taking into account the response domain, and clearly informed about both, reliability and accuracy in the predictions of the test samples. Most of the predictions had good accuracy, them being within two units of standardized error and high reliability. The samples corresponding to these reliable predictions were associated with higher  $K_j$  values, thus being well represented by several training samples.

Generally, a standardized error of two/three units is usually considered as a warning value for outliers detection. In Figure 6, six test samples (12, 33, 51, 52, 75 and 90) exceeded a two-unit threshold for the absolute standardized error indicating them as outliers in the model's response domain. It can be interesting to further evaluate the reasons behind categorising them as outliers; however, this is beyond the scope of this article as the proposed AD approach is defined within the model's descriptor space. Nevertheless, this evaluation identifies sample 33 as an outlier in model's descriptor's space as well as its response domain which further supports the results derived from the proposed approach to exclude this sample from the model's AD.

Finally, the results derived by this approach were compared with those derived from classical AD approaches. Table 2 reports these results; the first row shows results when no AD approach has been applied to bound the model's descriptor space.

The number  $k$  of nearest neighbours considered with the proposed approach (i.e. 15) was comparatively higher than the one considered with classical kNN (i.e. 5); however, the impact on model statistics was not so obvious on the resulting  $Q^2$ , while the number of retained samples increased from 87 (classical kNN) to 91 (proposed approach). Discussing the results derived with classical approaches, number of samples retained within the AD varied significantly depending on what strategy was used. Convex hull, optimized and variable Gaussian kernel methods retained the least number of samples while the Bounding Box considered none of the test samples outside the AD. Overall, the proposed approach worked quite well on the CAESAR model, trying to define an AD with maximum retained test samples within the domain and positive impact on the model statistics.

The last column of Table 2 reports the list of samples considered outside the AD with all the approaches. Irrespective of total number of samples considered outside

**Table 2 Comparison of AD methods applied to the test set of CAESAR BCF model**

Approach	IN AD	Q <sup>2</sup>	OUTSIDE AD
All samples inside (no AD approach)	95	0.797	None
Proposed approach (Euclidean dist., $k = 15$ )	91	0.803	33 61 82 83
Bounding box	95	0.797	None
PCA bounding box	93	0.804	33 40
Convex hull	73	0.789	3 7 9 13 18 33 34 36 37 38 39 40 41 43 51 56 61 72 79 91 92 94
Euclidean dist (95 percentile)	88	0.802	3 33 36 37 40 42 61
Mahalanobis dist (95 percentile)	89	0.791	18 43 54 61 83 91
Classical kNN (Euclidean dist., $k = 5$ )	87	0.797	3 33 34 40 61 82 83 94
Fixed Gaussian kernel	85	0.794	3 24 33 34 40 61 82 83 91 94
Optimized Gaussian kernel	66	0.831	3 912 22 24 33 34 38 40 45 47 51 53 54 56 61 68 69 75 76 80 82 83 87 89 91 93 94 95
Variable Gaussian kernel ( $k = 15$ )	81	0.790	3 24 33 34 40 43 61 80 82 83 89 91 94 95
Adaptive Gaussian kernel	88	0.801	3 33 43 61 82 83 91
Fixed Epanechnikov kernel	87	0.799	3 33 40 43 61 83 91 94
Nearest neighbour density estimator ( $k = 15$ )	91	0.806	3 33 61 91

the AD, all the methods converged significantly identifying a subset of common samples that were always excluded from the model's AD.

## Conclusions

A novel kNN-based approach to define the AD of QSAR models was proposed. The overall execution of this approach was performed in three different phases that efficiently used the salient features of kNN principle to define a model's AD in its descriptor space. Significant features that distinguished the proposed AD approach include defining individual threshold for each training sample, optimizing the smoothing parameter  $k$  to be considered and taking into account the model's response domain to reflect upon the reliability of results derived in its descriptor space.

In the proposed AD method, the appropriate number  $k$  of neighbours can be chosen on the basis of the plot with retained samples vs.  $k$  values obtained by Monte Carlo validation; it allowed to identify a smoothed region of the  $k$  values where the results remained unchanged, ensuring high robustness in the AD definition.

The results on the selected case study defined an AD with a positive impact on model statistics retaining maximum possible samples that were reliably predicted. Comparison of the derived results with those from the classical approaches by no means intended to project the pitfalls of existing approaches but it was aimed to have a performance evaluation of this novel strategy to understand how its implementation could lead to obtain similar or different results as compared to the classical

ways of defining the AD. An extended comparison of the different AD approaches on several diverse data sets have indicated the following relevant features that characterize the proposed AD approach: a) adaptability to local density of samples, useful when the underlying multivariate distribution is asymmetric, with wide regions of low data density; b) unlike several kernel density estimators, effectiveness also in high-dimensional spaces; d) low sensitivity to the smoothing parameter  $k$ ; d) versatility to implement various distances measures other than Euclidean distance, such as Manhattan distance, Mahalanobis distance and the recently proposed locally-centred Mahalanobis distance [29], depending on the data set in analysis.

A MATLAB module for the model's AD estimate by different approaches will be soon available at <http://michem.disat.unimib.it/chm/>.

## Competing interests

The authors declare that they have no competing interests.

## Authors' contributions

All the authors listed on the title page of this article contributed equally to this work. The final version of this manuscript was revised and approved by all the authors.

## Acknowledgements

The research leading to these results has received funding from the European Community's Seventh Framework Programme [FP7/2007–2013] under Grant Agreement n. 238701 of Marie Curie ITN Environmental Chemoinformatics (ECO) project.

Received: 13 February 2013 Accepted: 23 May 2013

Published: 30 May 2013



## References

1. REACH. European Community Regulation on chemicals and their safe use. [http://ec.europa.eu/environment/chemicals/reach/reach\\_intro.htm](http://ec.europa.eu/environment/chemicals/reach/reach_intro.htm).
2. Worth AP, Bassan A, Gallegos A, Netzeva TI, Patlewicz G, Pavan M, Tsakovska I, Vracko M: *The Characterisation of (Quantitative) Structure-Activity Relationships: Preliminary Guidance*. ECB Report EUR 21866 EN, 95pp. Ispra, Italy: European Commission, Joint Research Centre; 2005.
3. OECD. *Quantitative Structure-Activity Relationships Project*. [http://www.oecd.org/document/23/0,3746,en\\_2649\\_34377\\_33957015\\_1\\_1\\_1\\_1,00.html](http://www.oecd.org/document/23/0,3746,en_2649_34377_33957015_1_1_1_1,00.html).
4. Worth AP, van Leeuwen CJ, Hartung T: **The prospects for using (Q)SARs in a changing political environment: high expectations and a key role for the Commission's Joint Research Centre**. *SAR QSAR Environ Res* 2004, **15**:331–343.
5. Nikolova-Jeliazkova N, Jaworska J: **An approach to determining applicability domains for QSAR group contribution models: an analysis of SRC KOWWIN**. *Altern Lab Anim* 2005, **33**:461–470.
6. Sheridan RP, Feuston BP, Maiorov VN, Kearsley S: **Similarity to molecules in the training set is a good discriminator for prediction accuracy in QSAR**. *J Chem Inf Comput Sci* 2004, **44**:1912–1928.
7. Sahigara F, Mansouri K, Ballabio D, Mauri A, Consonni V, Todeschini R: **Comparison of different approaches to define the applicability domain of QSAR models**. *Molecules* 2012, **17**:4791–4810.
8. Netzeva TI, Worth A, Aldenberg T, Benigni R, Cronin MT, Gramatica P, Jaworska JS, Kahn S, Klopman G, Marchant CA, Myatt G, Nikolova-Jeliazkova N, Patlewicz GY, Perkins R, Roberts D, Schultz T, Stanton DW, van de Sandt JJ, Tong W, Veith G, Yang C: **Current status of methods for defining the applicability domain of (quantitative) structure-activity relationships. The report and recommendations of ECVAM Workshop 52**. *Altern Lab Anim* 2005, **33**:155–173.
9. Jaworska J, Nikolova-Jeliazkova N, Aldenberg T: **QSAR applicability domain estimation by projection of the training set descriptor space: A review**. *Altern Lab Anim* 2005, **33**:445–459.
10. Dimitrov S, Dimitrova G, Pavlov T, Dimitrova N, Patlewicz G, Niemela J, Mekenyan OA: **Stepwise approach for defining the applicability domain of SAR and QSAR models**. *J Chem Inf Model* 2005, **45**:839–849.
11. Breiman L, Meisel W, Purcell E: **Variable kernel estimates of multivariate densities**. *Technometrics* 1977, **19**:135–144.
12. Asikainen AH, Ruuskanen J, Tuppurainen KA: **Consensus kNN QSAR: a versatile method for predicting the estrogenic activity of organic compounds in silico. A comparative study with five estrogen receptors and a large, diverse set of ligands**. *Environ Sci Technol* 2004, **38**:6724–6729.
13. Tropsha A: **Best practices for QSAR model development, validation, and exploitation**. *Mol Inf* 2010, **29**:476–488.
14. Cedeño W, Agrafiotis DK: **Using particle swarms for the development of QSAR models based on K-nearest neighbor and kernel regression**. *J Comput Aided Mol Des* 2003, **17**:255–263.
15. Golbraikh A, Shen M, Xiao Z, Xiao YD, Lee KH, Tropsha A: **Rational selection of training and test sets for the development of validated QSAR models**. *J Comput Aided Mol Des* 2003, **17**:241–253.
16. Itskowitz P, Tropsha A: **k nearest neighbors QSAR modeling as a variational problem: theory and applications**. *J Chem Inf Model* 2005, **45**:777–785.
17. Nigsch F, Bender A, van Buuren B, Tissen J, Nigsch E, Mitchell JB: **Melting point prediction employing k-nearest neighbor algorithms and genetic parameter optimization**. *J Chem Inf Model* 2006, **46**:2412–2422.
18. Tetko IV, Sushko I, Pandey AK, Zhu H, Tropsha A, Papa E, Oberg T, Todeschini R, Fourches D, Varnek A: **Critical assessment of QSAR models of environmental toxicity against Tetrahymena pyriformis: Focusing on applicability domain and overfitting by variable selection**. *J Chem Inf Model* 2008, **48**:1733–1746.
19. Silverman BW: *Density Estimation for Statistics and Data Analysis*. London, UK: Chapman and Hall; 1986.
20. Zhao C, Boriani E, Chana A, Roncaglioni A, Benfenati E: **A new hybrid system of QSAR models for predicting bioconcentration factors (BCF)**. *Chemosphere* 2008, **73**:1701–1707.
21. Lombardo A, Roncaglioni A, Boriani E, Milan C, Benfenati E: **Assessment and validation of the CAESAR predictive model for bioconcentration factor (BCF) in fish**. *Chem Cent J* 2010, **4**(Suppl 1):S1. doi:10.1186/1752-153X-4-S1-S1.
22. Chambers JM, Cleveland WS, Kleiner B, Tukey PA: *Graphical methods for Data Analysis*. Pacific Grove, CA: Wadsworth & Brooks/Cole; 1983.
23. *Box plot* – MATLAB. <http://www.mathworks.it/it/help/stats/boxplot.html>.
24. Consonni V, Ballabio D, Todeschini R: **Comments on the definition of the Q2 parameter for QSAR validation**. *J Chem Inf Model* 2009, **49**:1669–1678.
25. Consonni V, Ballabio D, Todeschini R: **Evaluation of model predictive ability by external validation techniques**. *J Chemometr* 2010, **24**:194–201.
26. DRAGON (Software for Molecular Descriptor Calculations). Talete srl, Milano, Italy. <http://www.talete.mi.it>.
27. Forina M, Lanteri S, Armanino C, Cerrato Oliveros C, Casolino C: *V-PARVUS software, User manual*. 2004 <http://parvus@difar.unige.it>.
28. MATLAB. *The Language of Technical Computing*. <http://www.mathworks.com/products/matlab/>.
29. Todeschini R, Ballabio D, Consonni V, Sahigara F, Filzmoser P: **Locally-centred Mahalanobis distance: a new distance measure with salient features towards outlier detection**. *Anal Chim Acta* 2013. doi:10.1016/j.aca.2013.04.034.

doi:10.1186/1758-2946-5-27

**Cite this article as:** Sahigara et al.: Defining a novel k-nearest neighbours approach to assess the applicability domain of a QSAR model for reliable predictions. *Journal of Cheminformatics* 2013 **5**:27.

Publish with **ChemistryCentral** and every scientist can read your work free of charge

“Open access provides opportunities to our colleagues in other parts of the globe, by allowing anyone to view the content free of charge.”

W. Jeffery Hurst, The Hershey Company.

- available free of charge to the entire scientific community
- peer reviewed and published immediately upon acceptance
- cited in PubMed and archived on PubMed Central
- yours — you keep the copyright

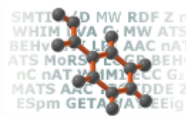


Submit your manuscript here:  
<http://www.chemistrycentral.com/manuscript/>

**ChemistryCentral**

# Molecular Descriptors

the free online resource



## **Defining the Applicability Domain of QSAR models:** **An overview**

**Faizan Sahigara**

Milano Chemometrics and QSAR Research Group, Department of Environmental Sciences, University of Milano-Bicocca, P.za della Scienza 1-20126 Milano, Italy.

This tutorial has been retrieved from the following web link:

[http://www.molecularDescriptors.eu/tutorials/T7\\_molecularDescriptors\\_ad.pdf](http://www.molecularDescriptors.eu/tutorials/T7_molecularDescriptors_ad.pdf)

### **What is Applicability Domain ?**

QSARs establish a quantitative relationship between chemical structures and their properties [1]. In theory, QSAR models can be used to predict the properties of chemical structures, provided their structural information is available. In the recent years, there had been a growing awareness about QSARs and their applications. This is quite evident from their use for regulatory purposes. A new European legislation on chemicals – REACH (Registration, Evaluation, Authorization and restriction of Chemicals) came into force in 2007, allows and encourages the use of QSAR model predictions when the experimental data are not sufficiently available or as supplementary information, provided validity of the model is justified [2,3].

However, this rising popularity of QSAR models is also accompanied by a question over their reliable predictions [4]. In theory, derivation of QSAR models is based primarily on training sets which are structurally limited and thus, their applicability to the query chemicals is limited [5]. Thus, their applicability towards reliable predictions is restricted in a chemical space to some specific chemical categories. Such reliable predictions are usually confined to those chemicals, that are structurally similar to the training compounds used to build the model [6-8].

The principle of Applicability Domain obliges the users to specify the scope of their proposed models thus, defining the model limitations with respect to its structural domain and response space. If an external compound is beyond the defined scope of a given model, it is considered outside that model's Applicability Domain (AD) and cannot be associated with a reliable prediction.

### **What are the key aspects in defining the AD of QSAR models ?**

1) Identification of the subspace of chemical structures that can be predicted reliably.

- 2) Defined AD determines the degree of generalization of a given predictive model. Thus, if the AD is too restricted, it implies the model can provide reliable predictions for very limited chemical categories.
- 3) A well defined AD indicates if the endpoint for the chemical structures under evaluation can be reliably predicted.
- 4) Characterization of the interpolation space is very significant to define the AD for a given QSAR model.

### How can the AD of a model be defined ?

Several strategies towards defining the Applicability Domain of QSAR models have been proposed in literature. This section of the tutorial aims to provide an overview of some major AD approaches.

#### 1) Range-based Methods

##### a) Bounding Box

Considering the range of individual descriptors used to build the model, this approach defines the AD as a Bounding Box which is a  $p$ -dimensional hyper-rectangle defined on the basis of maximum and minimum values of each descriptor used to build the model.

*Drawbacks:* Empty regions in the interpolation space cannot be identified and also the correlation between descriptors cannot be taken into account [1,4].

##### b) PCA Bounding Box

Similar to the earlier approach, however, the AD is defined considering the projection of the molecules in the principal component space and taking into account the maximum and minimum values for the PC scores. This approach resolves the problem of correlation between descriptors.

*Drawbacks:* Empty regions within the interpolation space still cannot be identified [1,3-4].

#### 2) Geometric Method

This approach characterizes the interpolation space by defining a smallest convex area containing the entire training set.

*Drawbacks:* Increasing data complexity highly affects the implementation of a convex hull. For a data with two or three dimensions, the method works efficiently however, with further increase in dimensions, the implementation adds to the complexity of the algorithm [1,9]. Set boundaries are analyzed without considering the actual data distribution. Convex Hull cannot identify the potential internal empty regions within the interpolation space [1,2].

#### 3) Distance-based Methods



These approaches define the AD by calculating distances of a query compound from a defined point within the descriptor space of the training data. This measured distance between defined point and the dataset is then compared with a pre-defined threshold. However, no strict rules are evident from the literature about this pre-defined threshold and thus, it is up to the user to take an appropriate decision towards defining the thresholds [1-5].

Some commonly used and most useful distance measures in QSAR studies include Mahalanobis, Euclidean and City Block distances. Leverage is another measure that is recommended in defining model's AD [10]. In theory, Leverage is proportional to Hotellings  $T^2$  statistic and Mahalanobis distance measure from the centroid of the training set [4]. Usually, a warning threshold is set to three times the average of the leverage  $p/n$ , where  $p$  is the number of model parameters while  $n$  is the number of training compounds. Query compounds with leverage higher than this defined threshold of  $3 * p/n$  are considered to be unreliably predicted.

*Drawbacks:* Lack of strict rules in literature towards defining the thresholds can lead to ambiguous results. Correlated descriptors can be handled using Mahalanobis distance or Leverage, since they use co-variance matrix for their calculations, however, an additional treatment like PC rotation is required for other distance measures.

#### **4) Probability Density Distribution based Methods**

These approaches defines a model's AD by estimating the Probability Density Function for the given data. The estimation of Probability Density Function is feasible by both, parametric methods that assume standard distribution and non parametric methods which do not have any such assumptions concerning the data distribution. These approaches are considered to be efficient due to their ability to identify the internal empty regions and reflecting actual data distribution by generating concave regions around the extremities of the interpolation space [1,4].

Potential function is calculated for all the training compounds, followed by which a global potential is obtained by adding the individual potentials, thus indicating the potential density [11,12]. A percentile value for the probability density is opted and a threshold value is defined. Finally, those query compounds having potential function values lower than this threshold are considered to be outside the AD.

#### **5) K Nearest Neighbours Approach**

This approach defines the model's AD by assessing the similarity between training and test compounds. Distance of a query compound from its nearest training neighbour or its average distance from k nearest training neighbours is calculated. The calculated distances for test compounds are then compared with a pre-defined threshold. The test compounds with low distance to the training set is associated with higher number of training compounds and thus, is considered to be reliably predicted [8].

#### **6) Decision Trees and Decision Forests Approach**

This approach defines the AD for a consensus prediction of Decision Trees, in terms of prediction confidence and domain extrapolation. Decision Trees are combined and the distance between them are kept to maximum possible, thus to minimize the overfitting. Prediction confidence for a given compound is determined by averaging the predictions derived from all combined Decision Trees while, its prediction accuracy outside the training space is represented by the domain extrapolation [1,13,14].

## 7) Stepwise Approach to Determine Model's AD

With the Stepwise approach, AD of a QSAR model is better assessed executing four stages in a sequential manner. First stage checks if a test compound is within the variation range of physicochemical properties of the training compounds. Next, a structural similarity check is made for those compounds that were reliably predicted by the model. A mechanistic check is made in the third stage while, the last stage takes into account the reliability of simulated metabolism [3,5].

## 8) Distance to Model Approach

Distance to Model (DM) approach [15] estimates the prediction quality by using the information about the target property. Thus, the information about prediction itself is used for AD evaluation.

Standard Deviation (STD) DM: This method uses the standard deviation of predictions vector as the DM, since for given predictions from different set of models based on the same data, significant discrepancy in values indicates unreliability of a prediction.

CORREL: This method is derived from ensemble of models and is based on correlation of vectors of ensemble's predictions for the target and training set compounds. Compounds are considered to be 'near to the model' if they have a higher value for correlation coefficient.

CLASS-LAG: Prediction accuracy for classification models is provided by the CLASS-LAG measure that signals the confidence in prediction based on the idea that values closest to the classification label  $\{+1, -1\}$  are more reliably predicted and those that are nearer to 0 can be associated with 'uncertainty area' indicating an unreliable prediction [16].

PROB-STD: This DM combines the information from STD and CLASS-LAG. Lowering of STD value and approach towards the classification label  $\{+1, -1\}$  results in lower value for PROB-STD, indicating a reliable prediction.

## 9) Virtual models for property Evaluation of chemicals within a Global Architecture (VEGA)

VEGA [17] uses Applicability Domain Index (ADI) as a major criterion in defining Applicability Domain of predictions. The values for this Index ranges from 0 (worst case) to 1 (best case). In theory, this index is derived evaluating several other

indices, each of which focuses on a specific aspect relevant in defining the AD. The values for each index including the main ADI is categorised into three different intervals to indicate if the evaluation was positive, suspicious or negative.

Following are the components reported in VEGA platform for AD assessment:

- 1) Similar molecules with known experimental value
- 2) Accuracy (average error) of prediction for similar molecules
- 3) Concordance with similar molecules (average difference between target compound prediction and experimental values of similar molecules)
- 4) Maximum error of prediction among similar molecules
- 5) Atom Centered Fragments similarity check
- 6) Descriptors noise sensitivity analysis
- 7) Model descriptors range check and
- 8) Global AD Index.

### Further Reading

Recently, following publication was made available online discussing the results derived from several classical descriptor-based AD approaches on existing validated datasets from the literature:

Sahigara, F.; Mansouri, K.; Ballabio, D.; Mauri, A.; Consonni, V.; Todeschini, R. Comparison of Different Approaches to Define the Applicability Domain of QSAR Models. *Molecules* **2012**, *17*, 4791-4810.

### References

1. Netzeva, T.I.; Worth, A.; Aldenberg, T.; Benigni, R.; Cronin, M.T.D.; Gramatica, P.; Jaworska, J.S.; Kahn, S.; Klopman, G.; Marchant, C.A.; *et al.* Current status of methods for defining the applicability domain of (quantitative) structure-activity relationships. The report and recommendations of ECVAM Workshop 52. *Altern. Lab. Anim.* **2005**, *33*, 155-173.

2. REACH - European Community Regulation on chemicals and their safe use. Available online: [http://ec.europa.eu/environment/chemicals/reach/reach\\_intro.htm](http://ec.europa.eu/environment/chemicals/reach/reach_intro.htm)

3. Worth, A.P.; Bassan, A.; Gallegos, A.; Netzeva, T.I.; Patlewicz, G.; Pavan, M.; Tsakovska, I.; Vracko, M. *The Characterisation of (Quantitative) Structure-Activity Relationships: Preliminary Guidance*. ECB Report EUR 21866 EN, European Commission, Joint Research Centre; Ispra, Italy, 2005; p. 95.

4. Jaworska, J.; Nikolova-Jeliazkova, N.; Aldenberg, T. QSAR applicability domain estimation by projection of the training set descriptor space: A review. *Altern. Lab. Anim.* **2005**, *33*, 445-459.

5. Dimitrov, S.; Dimitrova, G.; Pavlov, T.; Dimitrova, N.; Patlewicz, G.; Niemela, J.; Mekenyan, O.A. Stepwise approach for defining the applicability domain of SAR and QSAR models. *J. Chem. Inf. Model.* **2005**, *45*, 839-49.

6. Worth, A.P.; van Leeuwen, C.J.; Hartung, T. The prospects for using (Q)SARs in a changing political environment: high expectations and a key role for the Commission's Joint Research Centre. *SAR QSAR Environ. Res.* **2004**, *15*, 331–343.
7. Nikolova-Jeliazkova, N.; Jaworska, J. An approach to determining applicability domains for QSAR group contribution models: an analysis of SRC KOWWIN. *Altern. Lab. Anim.* **2005**, *33*, 461–470.
8. Sheridan, R.; Feuston, R.P.; Maiorov, V.N.; Kearsley, S. Similarity to molecules in the training set is a good discriminator for prediction accuracy in QSAR. *J. Chem. Inf. Comp. Sci.* **2004**, *44*, 1912–1928.
9. Preparata, F.P.; Shamos, M.I. Convex hulls: Basic Algorithms. In *Computational Geometry: An Introduction*; Preparata, F.P., Shamos, M.I., Eds.; Springer-Verlag: New York, NY, USA, 1991; pp. 95–148.
10. Tropsha, A.; Gramatica, P.; Gombar, V. The importance of being earnest: validation is the absolute essential for successful application and interpretation of QSPR Models. *QSAR & Comb. Sci.* **2003**, *22*, 69–77.
11. Jouan-Rimbaud, D.; Bouveresse, E.; Massart, D.L.; de Noord O.E. Detection of prediction outliers and inliers in multivariate calibration. *Anal. Chim. Acta* **1999**, *388*, 283–301.
12. Forina, M.; Armanino, C.; Leardi R.; Drava, G. A class-modelling technique based on potential functions. *J. Chemometr.* **1991**, *5*, 435–453.
13. Tong, W.; Hong, H.; Fang, H.; Xie, Q. Perkins, R. Decision forest: Combining the predictions of multiple independent decision tree models. *J. Chem. Inf. Comput. Sci.* **2003**, *43*, 525–531.
14. Tong, W.; Hong, H.; Xie, Q.; Xie, L.; Fang, H.; Perkins, R. Assessing QSAR limitations: A regulatory perspective. *Curr. Comput. Aid. Drug.* **2004**, *1*, 65–72.
15. Sushko, I.; Novotarskyi, S.; Körner, R.; Pandey, A.K.; Kovalishyn, V.V.; Prokopenko, V.V.; Tetko, I.V. Applicability domain for in silico models to achieve accuracy of experimental measurements *J. Chemometrics.*, 2010, *24*(3-4), 202-208.
16. Manallack DT, Tehan BG, Gancia E, Hudson BD, Ford MG, Livingstone DJ, Whitley DC, Pitt WR. A consensus neural network-based technique for discriminating soluble and poorly soluble compounds. *J. Chem. Inf. Comput. Sci.* 2003; *43*(2): 674–679.
17. <http://www.vega-qsar.eu/index.php>